Electric discharges– Paschen law shortened second lecture

Doporučená literatura:

Professor Dr. Yuri P. Raizer

This edition is based on the original second Russian edition: *Fizika gazovogo razryad*

1st Edition 1991
Corrected 2nd Printing 1997

ISBN 3-540-19462-2 Springer-Verlag Berlin Heidelberg New York

Viktor Martišovič
ZÁKLADY FYZIKY PLAZMY
Bratislava 2004
Učebný text pre 3. ročník magisterského štúdia
FAKULTA MATEMATIKY, FYZIKY A INFORMATIKY
UNIVERZITA KOMENSKÉHO

Úvod do fyziky plazmatu
ČSAV, Academia Praha 1984
Francis F. Chen

The voltage of Nicola Tesla's man-made lightning can be calculated from altitude and gap

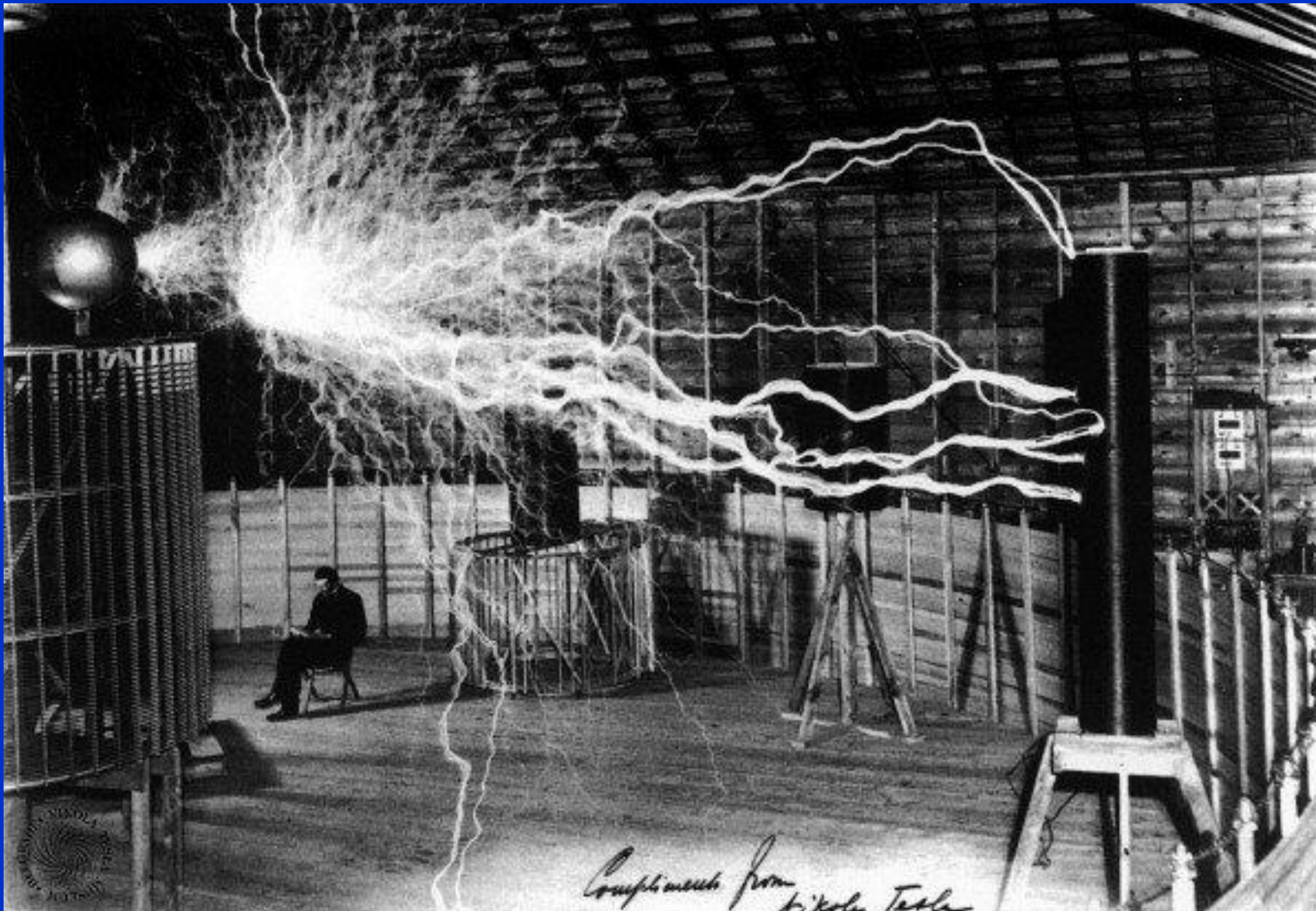

Plazmatické světelné zdroje

Nízkotlaké světelné zdroje, zářivky, sodíkové nízkotlaké výbojky, Vysokotlaké plazmatické světelné zdroje, konstrukce a provoz, plazmové zobrazovače

Fachhochschule
Münster University of
Applied Sciences

Gas Discharge Light Sources

Marco Miebach
Presentation incoherent light sources

Historical overview

- 1675: Phenomenon of glowing vacant space in a Barometer while moving it, discovered by Jean-Felix Picard
- 1705: First Demonstration of gas discharge lamp by Francis Hauksbee
- 1857: Development of Geissler Tubes (low-pressure gas discharge tubes) by Heinrich Geissler
- 1898: Discovery of Neon by William Ramsay and Morris W. Travers
- 1910: Commercialization of Geissler Tubes as neon lighting, used in neon signs

Jean Picard (1620-1682)
Astronom
Zodpovědný za první přesné měření poloměru Země

Jean Picard si všiml, že prázdný prostor v jeho rtuťovém barometru zářil, jak se rtuť chvěla, když nesl barometr. Francis Hauksbee poprvé předvedl plynovou výbojku v roce 1705. Ukázal, že evakuovaná nebo částečně evakuovaná skleněná koule, do které umístil malé množství rtuti, nabíjená statickou elektřinou, může produkovat světlo dostatečně jasné, aby se dalo číst.

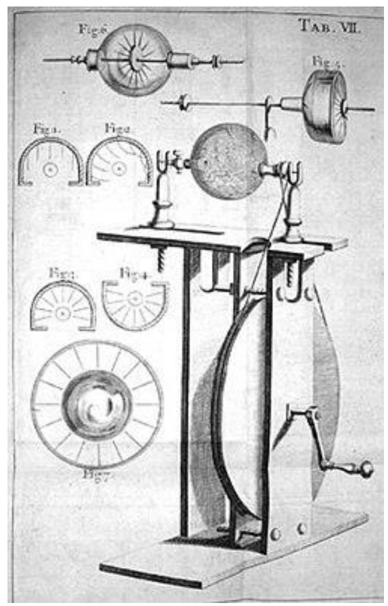

Generator built by Francis Hauksbee. From Physico-Mechanical Experiments, 2nd Ed., London 1719

Geisslerovy trubice

Heinrich Geisler (1814-1879)

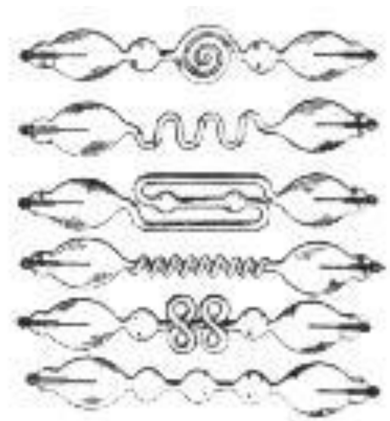

Dvě elektrody v trubici s plynem (neon, argon, krypron, xenon, vodík, CO_2) o nízkém tlaku, doutnavý výboj

Neonové výbojky

Komerčně produkoval Georges Claude od roku 1910

0.4 – 3 kPa, doutnavý výboj (hlavně pozitivní sloupec)

Oranžová barva (neon)

Další barvy s využitím jiných plynů (vodík – červená, helium – žlutá, CO_2 – bílá, rtuť – modrá) a luminoforů

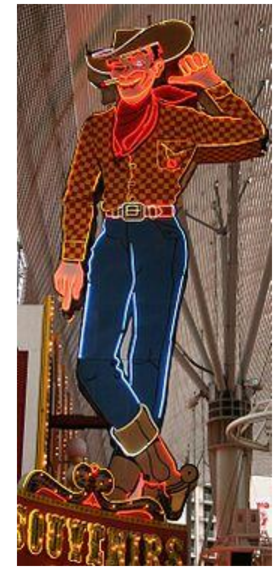

Neon glow lamp (doutnavka)

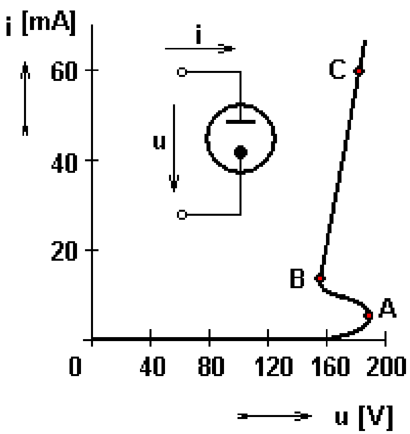

Tlak řádově stovky Pa
Dvě elektrody blízko sebe, doutnavý výboj

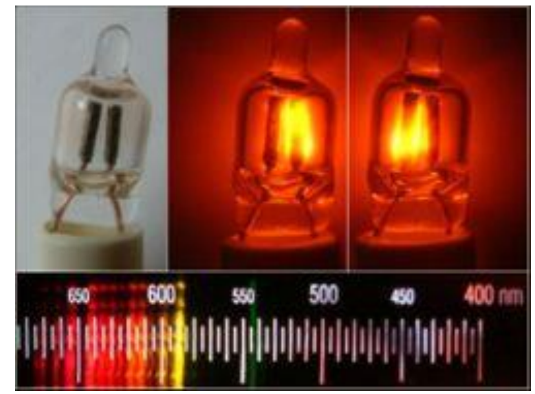

Vypínače, indikátory, ochrana proti přepětí, stabilizátory napětí atd.

Zkoušečka

Fachhochschule Münster University of Applied Sciences

Overview:

- Low pressure gas discharge lamps
- High pressure gas discharge lamps
- Excimer lamp

Rtuťová výbojka (za atmosférického tlaku)

Wavelength (nm)	Name (see photoresist)	Color
184.45		ultraviolet (UVC)
253.7		ultraviolet (UVC)
365.4	I-line	ultraviolet (UVA)
404.7	H-line	violet
435.8	G-line	blue
546.1		green
578.2		yellow-orange
650		red

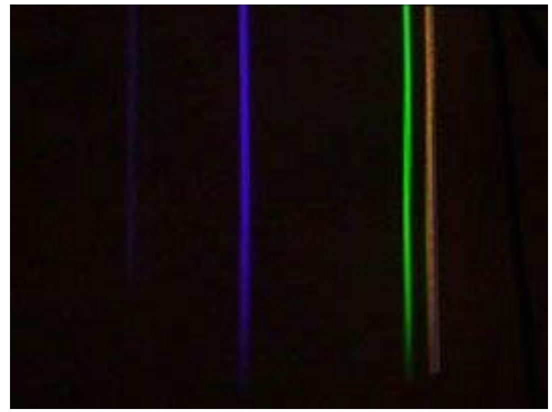

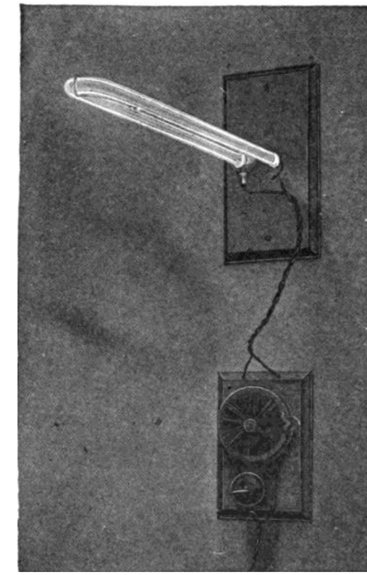

Výbojem v argonu se začne vypařovat rtuť a tlak vzroste na 2 – 18 atmosfér -> výboj v parách rtuti, tato nástupní fáze trvá několik minut během nichž lampa svítí čím dál tím více. Luminofor kolem výbojky se používá, aby bylo záření příjemnější pro oči).

Přítomnost silného ultrafialového záření se využívala k desinfekci.

Dnes se většinou k osvětlení nepoužívají (příliš mnoho rtuti)

Types of gas light sources

Low pressure gas discharge lamp

Fachhochschule Münster University of Applied Sciences

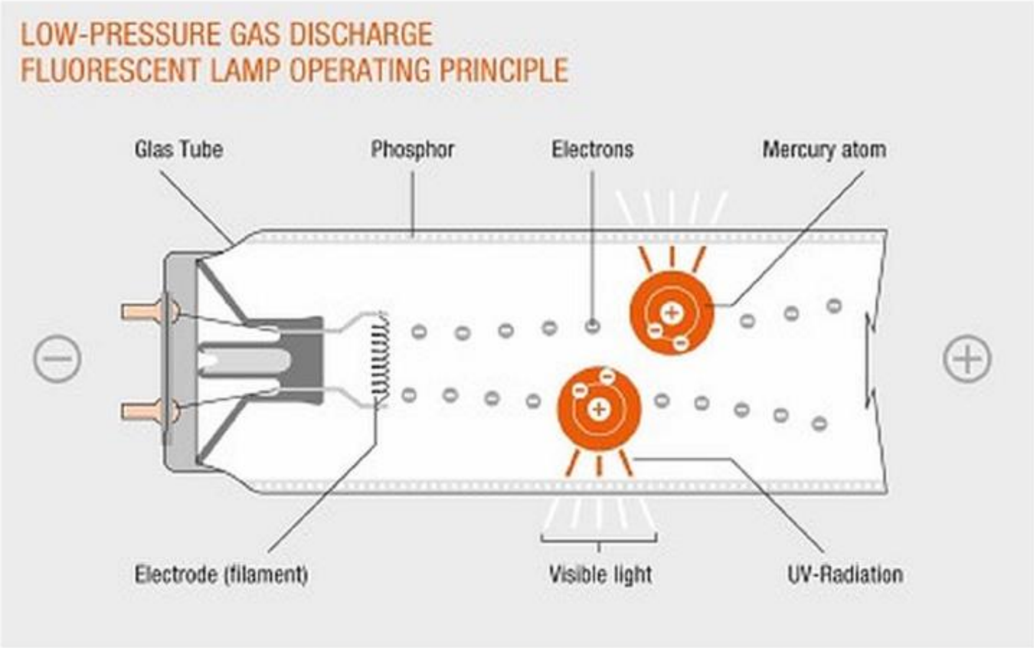

Sketch of a low pressure mercury vapour gas discharge fluorescent lamp.

Obloukový výboj v parách rtuti

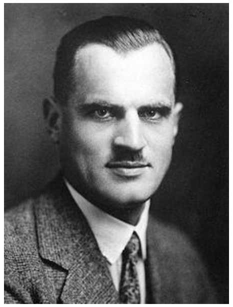

Komerční vývoj zářivek byl inicializován výzkumy Arthura Comptona (Nobel prize 1927) ve třicátých letech.

Zářivky (Low pressure fluorescent lamp)

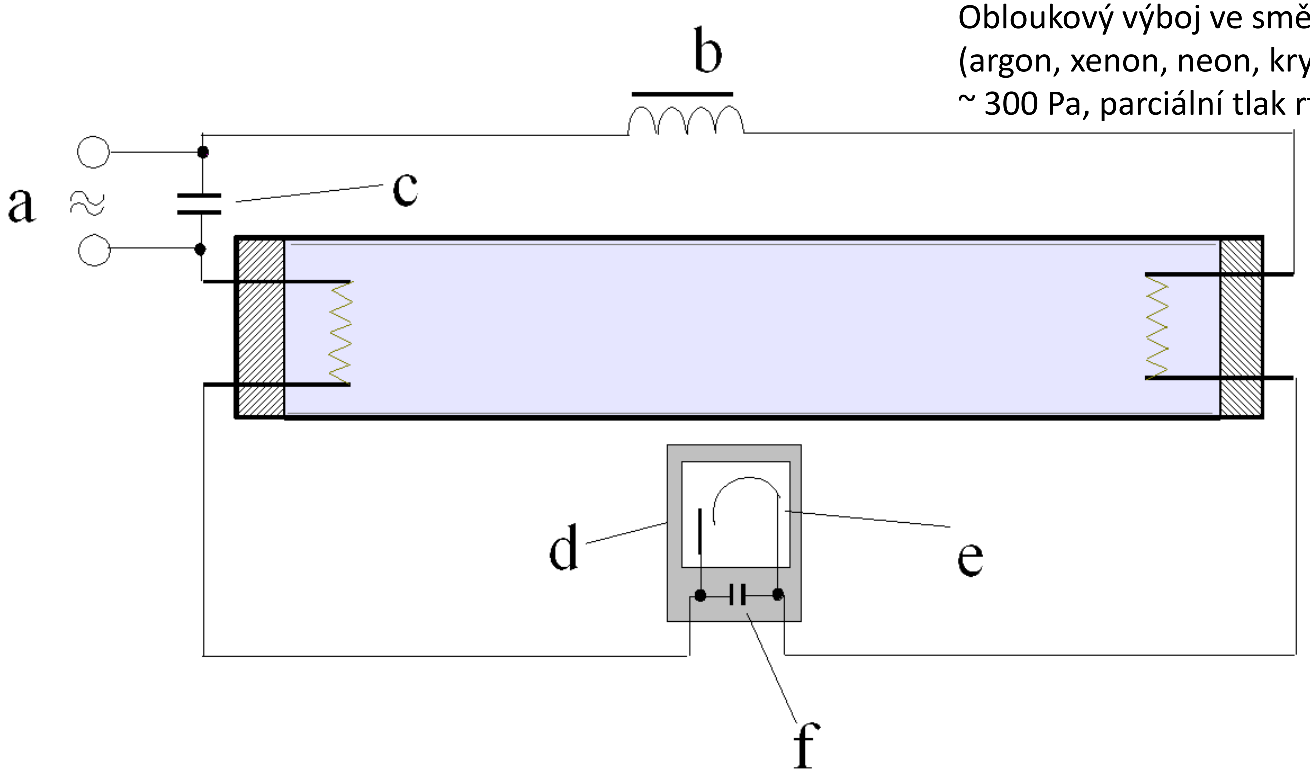

Obloukový výboj ve směsi vzácného/ných plynů (argon, xenon, neon, krypton) a rtuti. Celkový tlak ~ 300 Pa, parciální tlak rtuti ~ 0.8 Pa

Zapojení startéru a tlumivky k zářivkové trubici.
a - vstup, b - tlumivka, c - kompenzační kondenzátor, d - startér, e - bimetalová elektroda, f - odrušovací kondenzátor

Vyzařuje převážně na 185 a 254 nm (UV), proto musí být luminofor.

Zářivky (Low pressure fluorescent lamp)

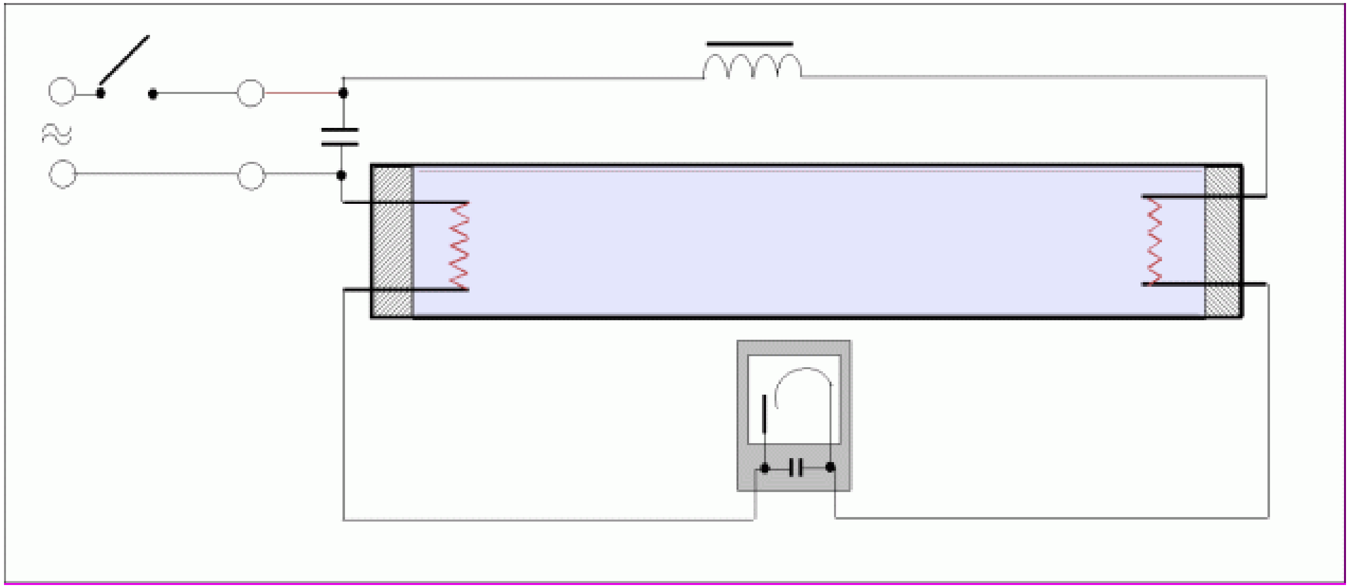

Phosphor composition:

- „Old“ Halophosphate-type Phosphor:
  - Mainly emits yellow and blue light
  - Weak emission of red and green light
  - Appears white to the eye
  - Has incomplete Spectrum => CRI ~ 60
- „New“ Triphosphor mixture (since 1990s):
  - Based on Eu and Tb
  - More evenly distributed VIS spectrum
  - CRI typically 82-100

CRI – color rendering index (100 sun black body radiation)

Types of gas light sources

Low pressure gas discharge lamp

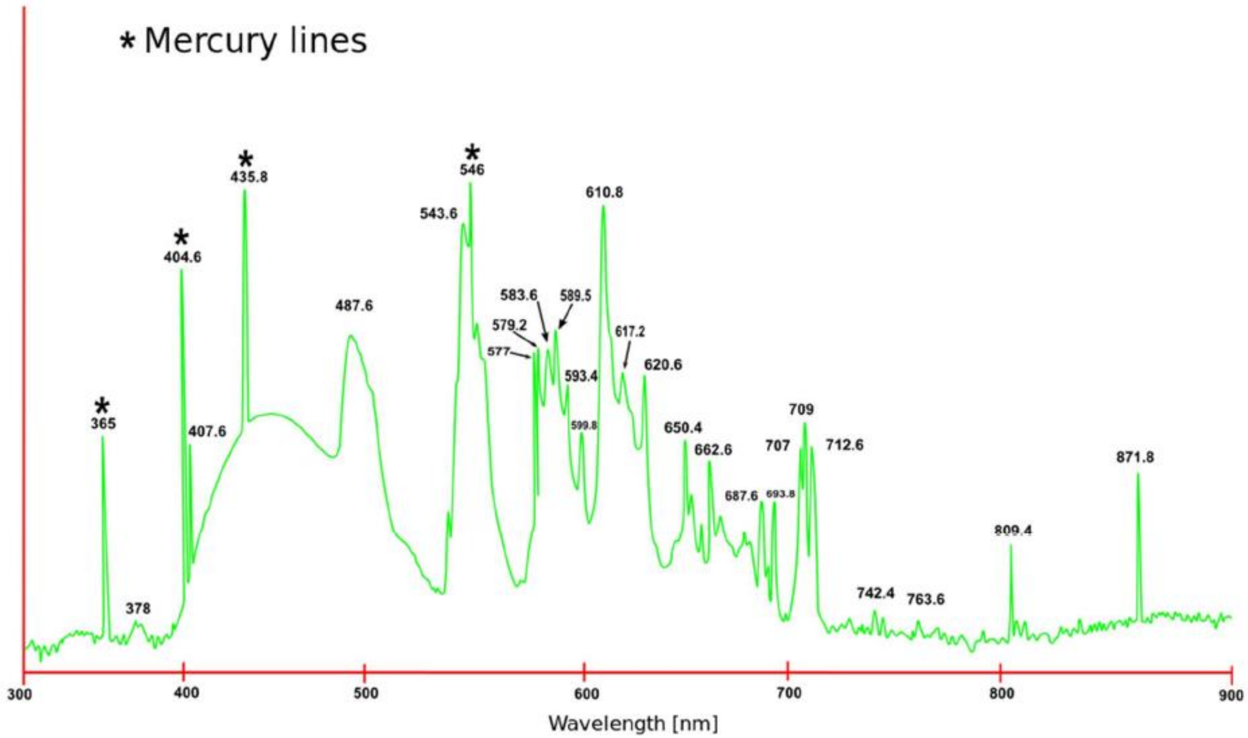

Spectrum from a 48" Philips F32T8 natural sunshine fluorescent light

Plazmové zobrazovače

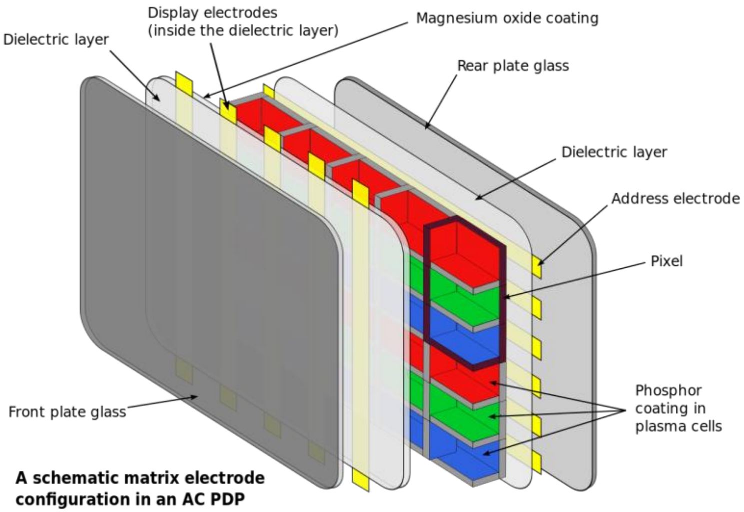

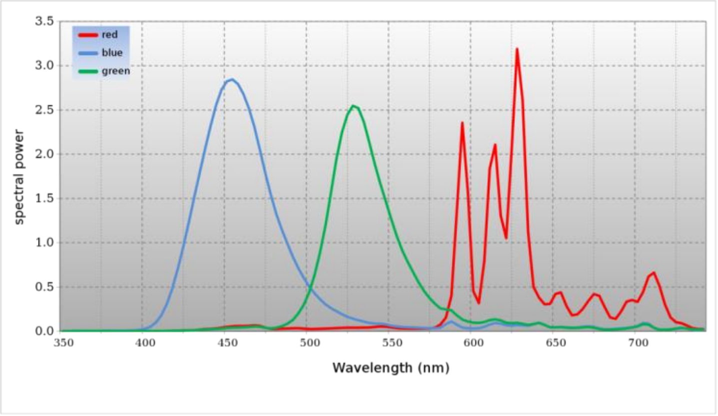

Spektralni charakteristiky typicky používaných luminoforů

Plazmové zobrazovače

Plasma displays were first used in PLATO computer terminals. This PLATO V model illustrates the display's monochromatic orange glow seen in 1981

Lepší kontrast než LCD, velmi dobrá reprodukce barev

Velmi široký úhel, ze kterého je možné se na televizi dívat

Vysoká obnovovací frekvence a odezva

Relativně velká spotřeba elektřiny

„Vypalování obrazu“ – přehřátí luminoforu

Dnes už komerčně nahrazeny LCD a OLED

Větší hmotnost než LCD obrazovky

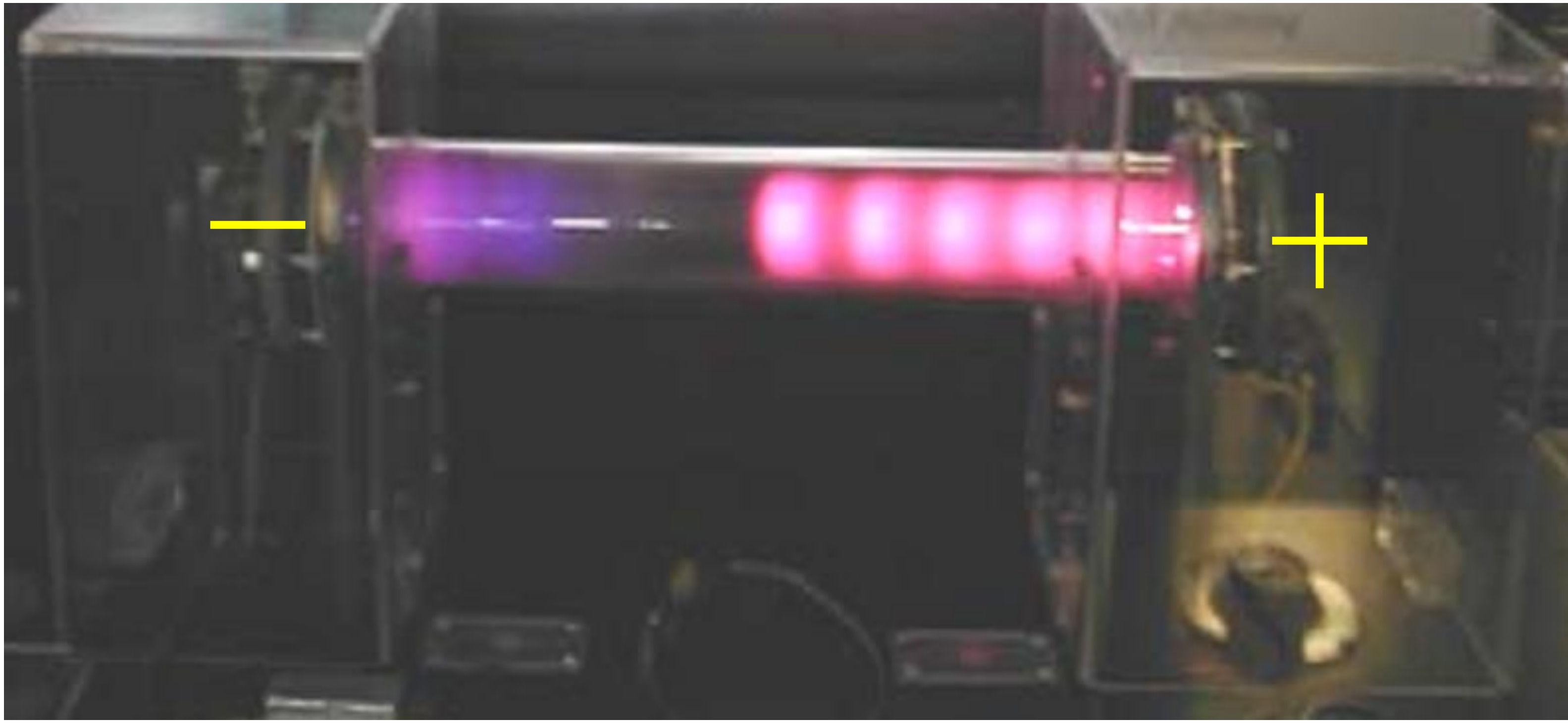

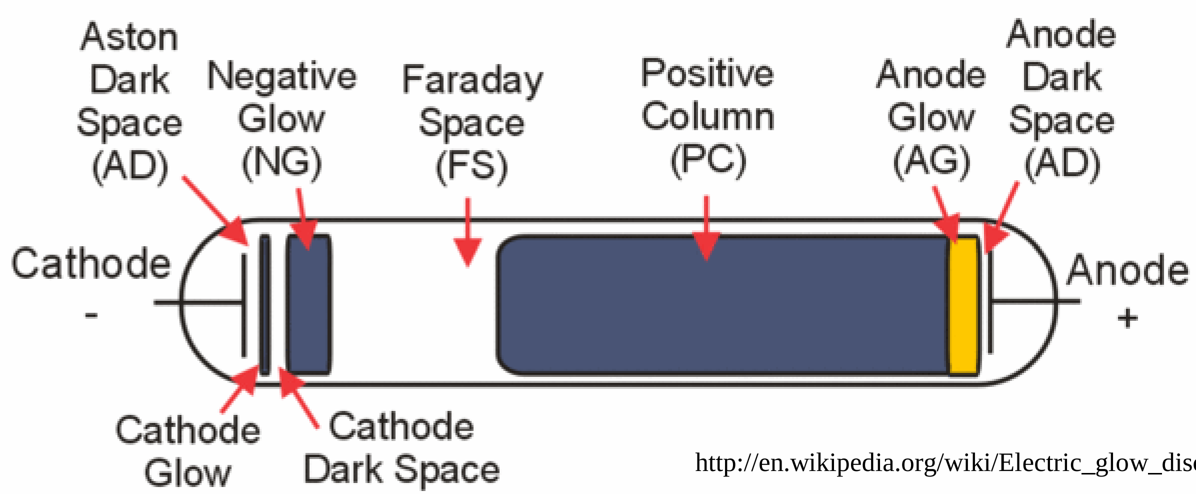

http://en.wikipedia.org/wiki/Electric_glow_discharge

http://www.exo.net/~pauld/origins/glowdisharge.html

Louis Carl Heinrich Friedrich Paschen (22 January 1865 - 25 February 1947)

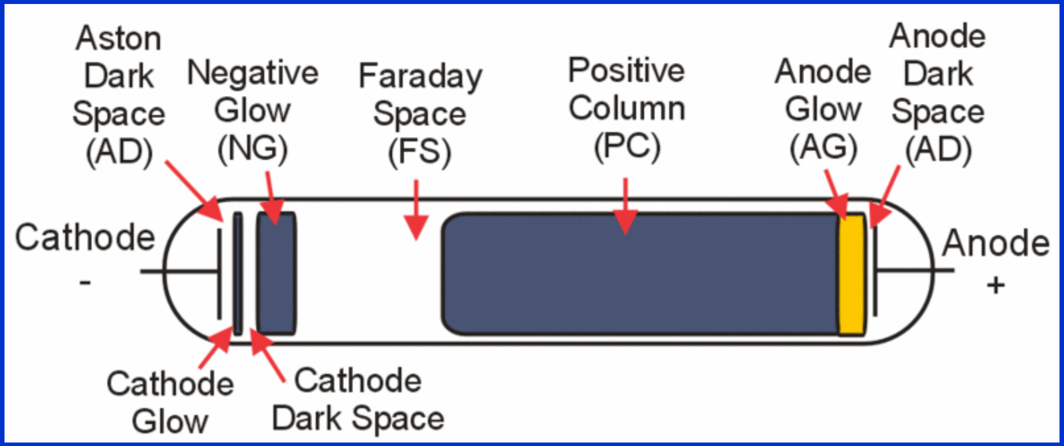

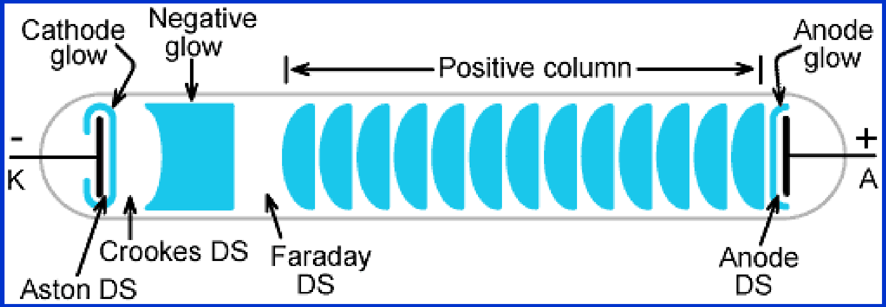

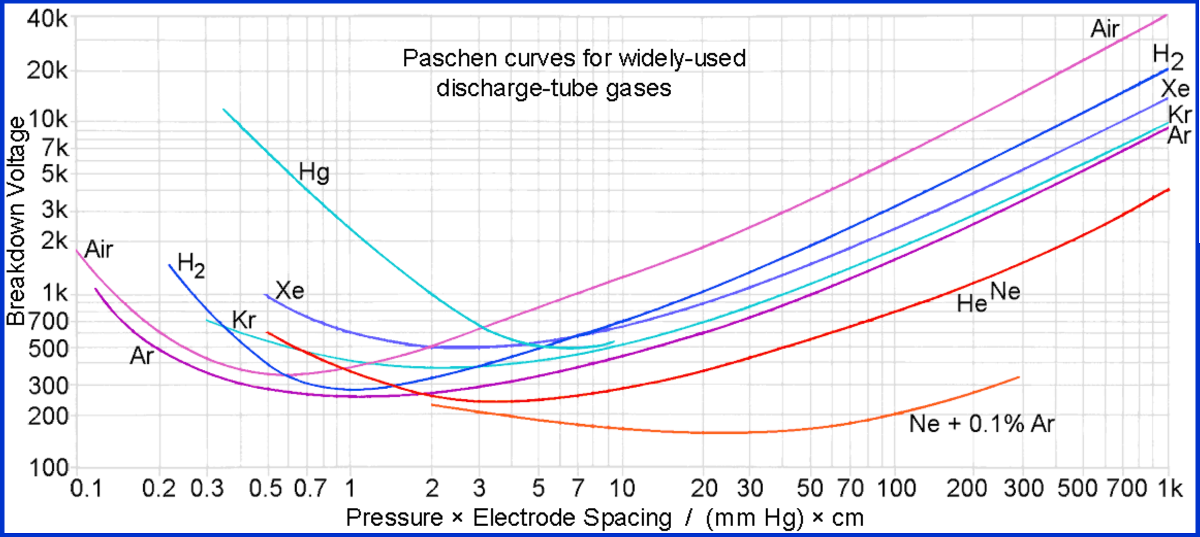

He is also known for the Paschen series, a series of hydrogen spectral lines in the infrared region that he first observed in 1908. He established the now widely used Paschen curve in his article *"Über die zum Funkenübergang in Luft, Wasserstoff und Kohlensäure bei verschiedenen Drücken erforderliche Potentialdifferenz"*.[1]

Louis Carl Heinrich Friedrich Paschen (22 January 1865 - 25 February 1947)

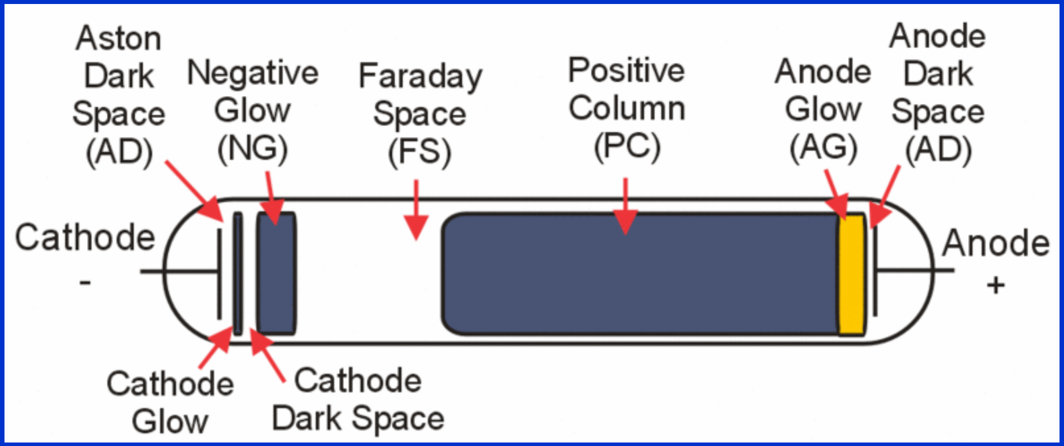

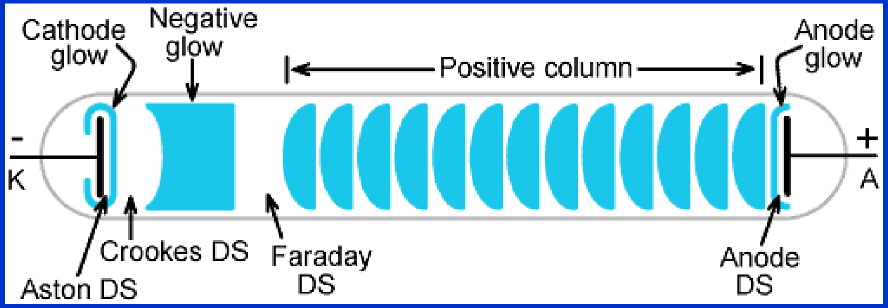

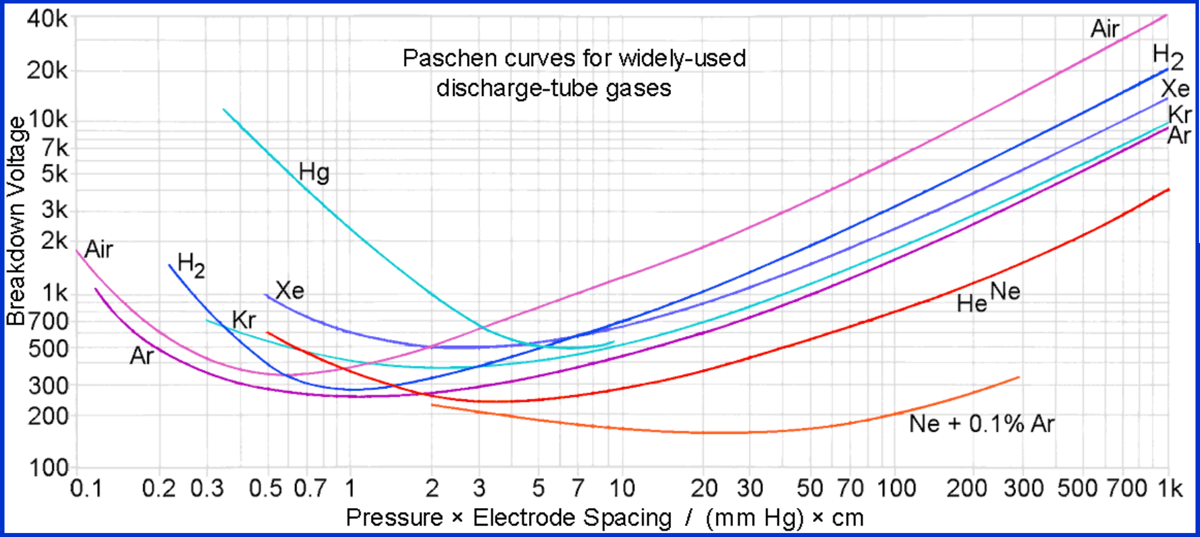

He is also known for the Paschen series, a series of hydrogen spectral lines in the infrared region that he first observed in 1908. He established the now widely used Paschen curve in his article *"Über die zum Funkenübergang in Luft, Wasserstoff und Kohlensäure bei verschiedenen Drücken erforderliche Potentialdifferenz"*.[1]

Contents

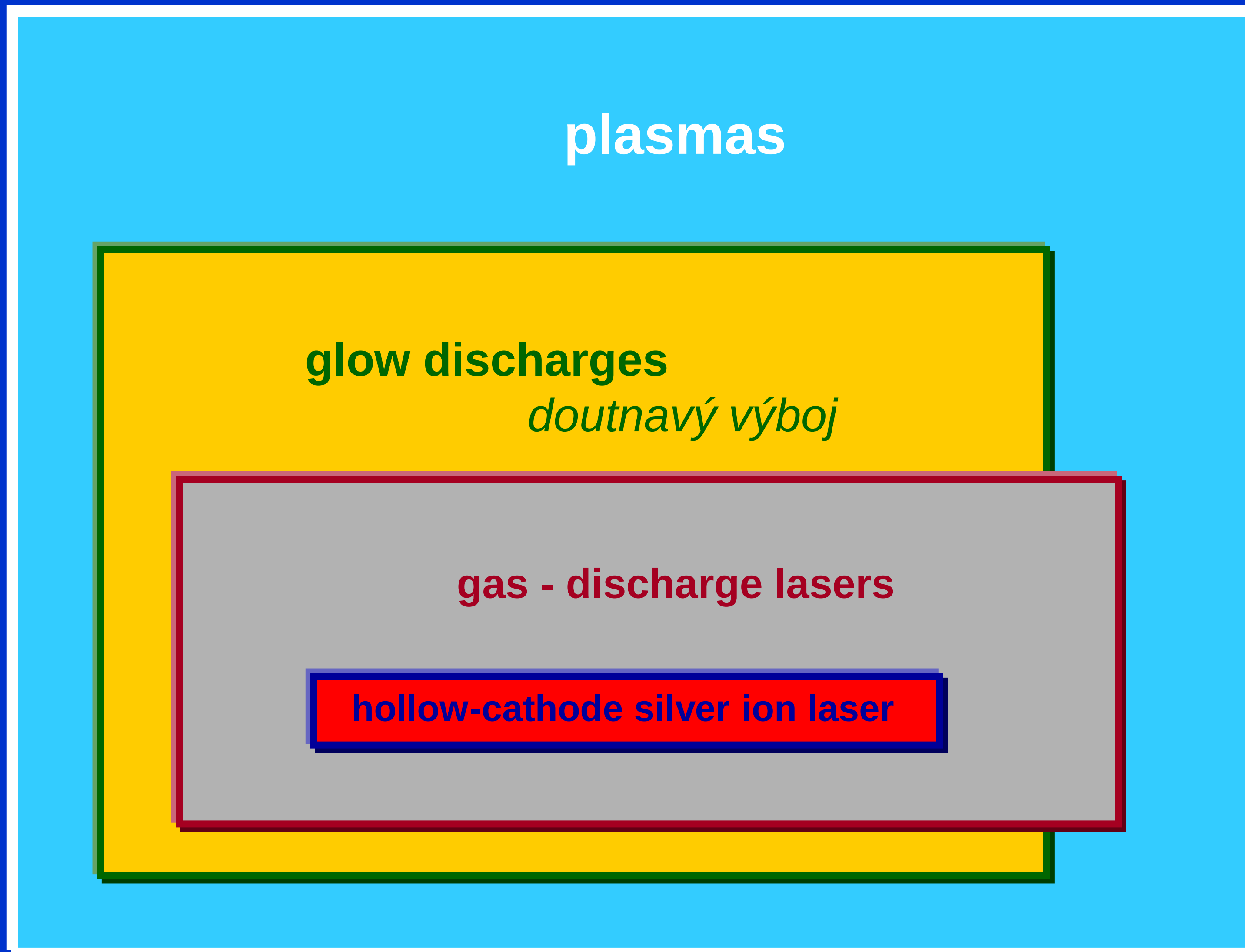
plasmas
glow discharges
doutnavý výboj
gas - discharge lasers
hollow-cathode silver ion laser

Electric discharges V-A characteristic

Direct current (DC) glow discharge

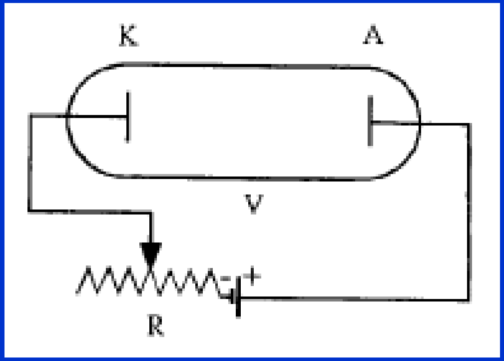

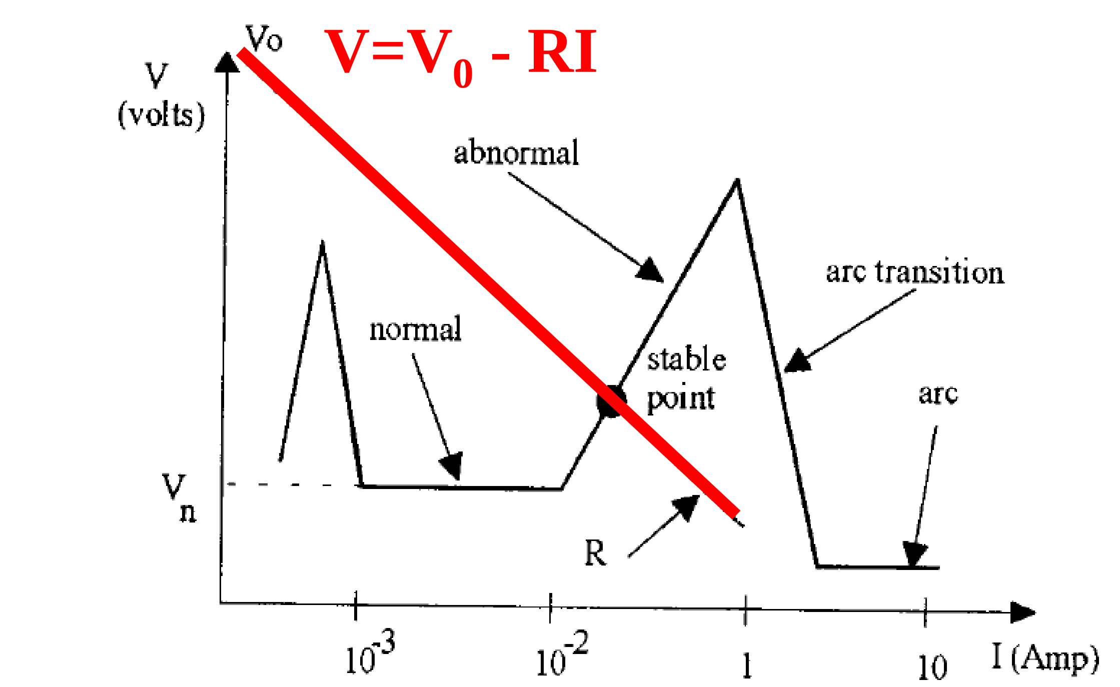

Fig. 1-3

Glow discharge setup (a)

$V = f(I)$ Characteristic in glow discharge. Stable working point (b).

Doporučená literatura:

Reactive plasmas
Andre Ricard

Glow discharges

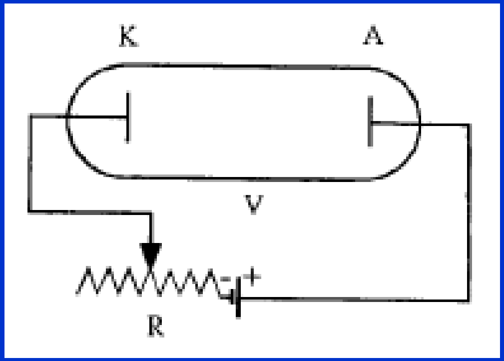

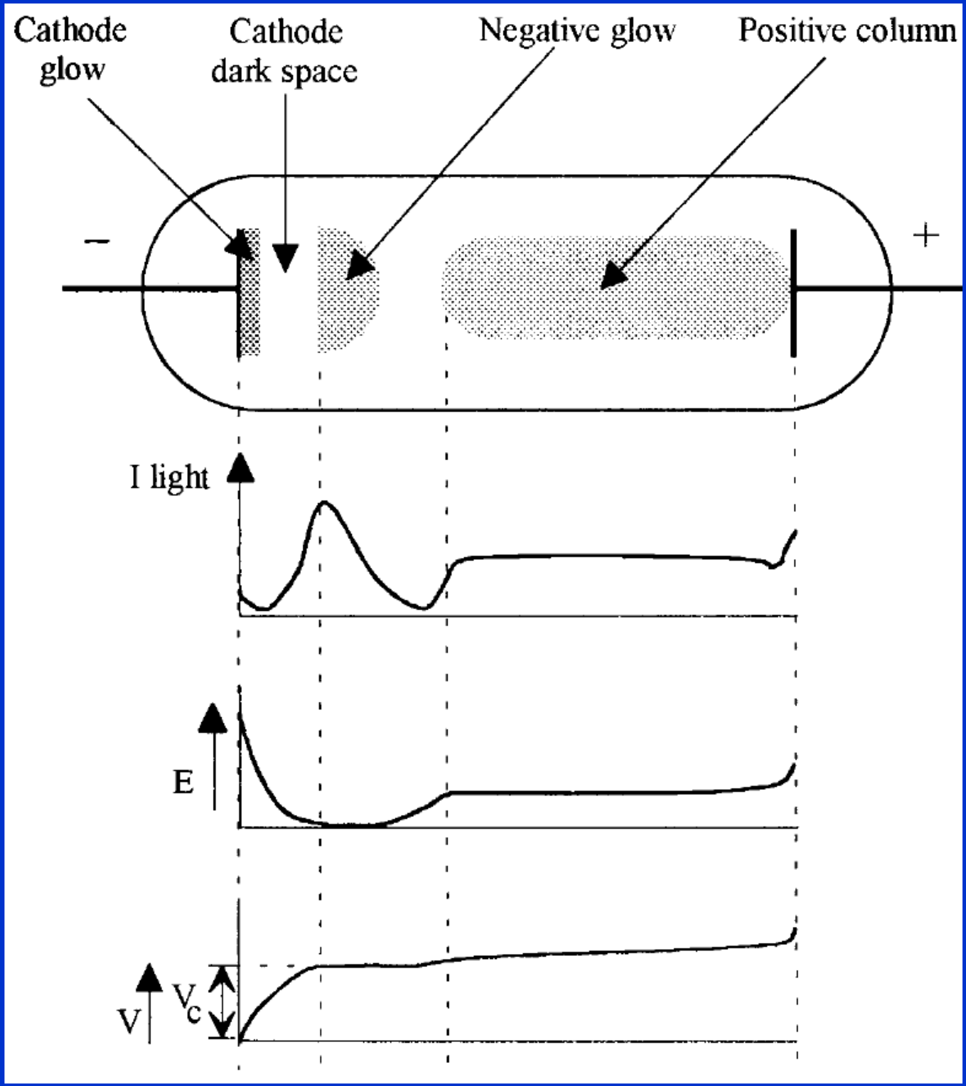

Several parts of a glow discharge.
Luminous intensity (I light), electric field (E) and voltage (V).
V_c cathode potential.

Glow discharges

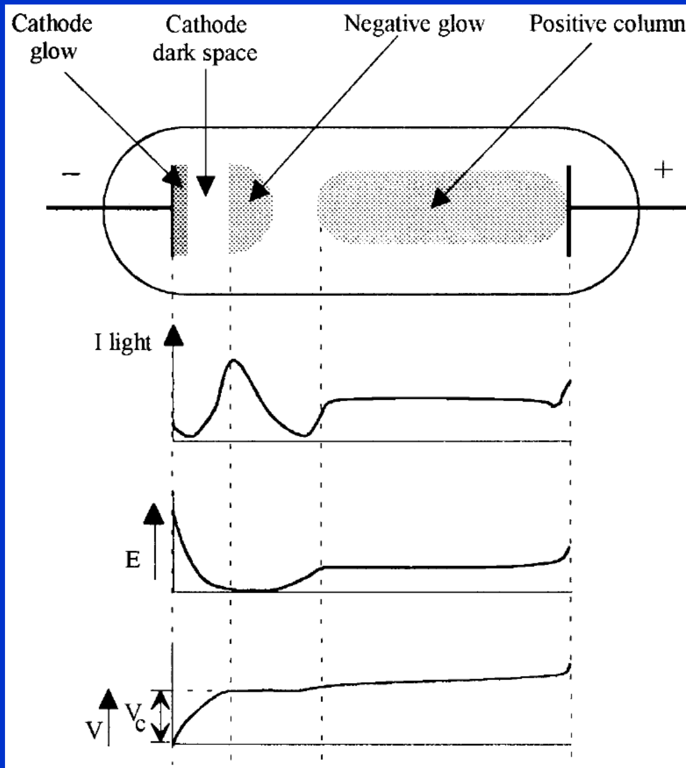

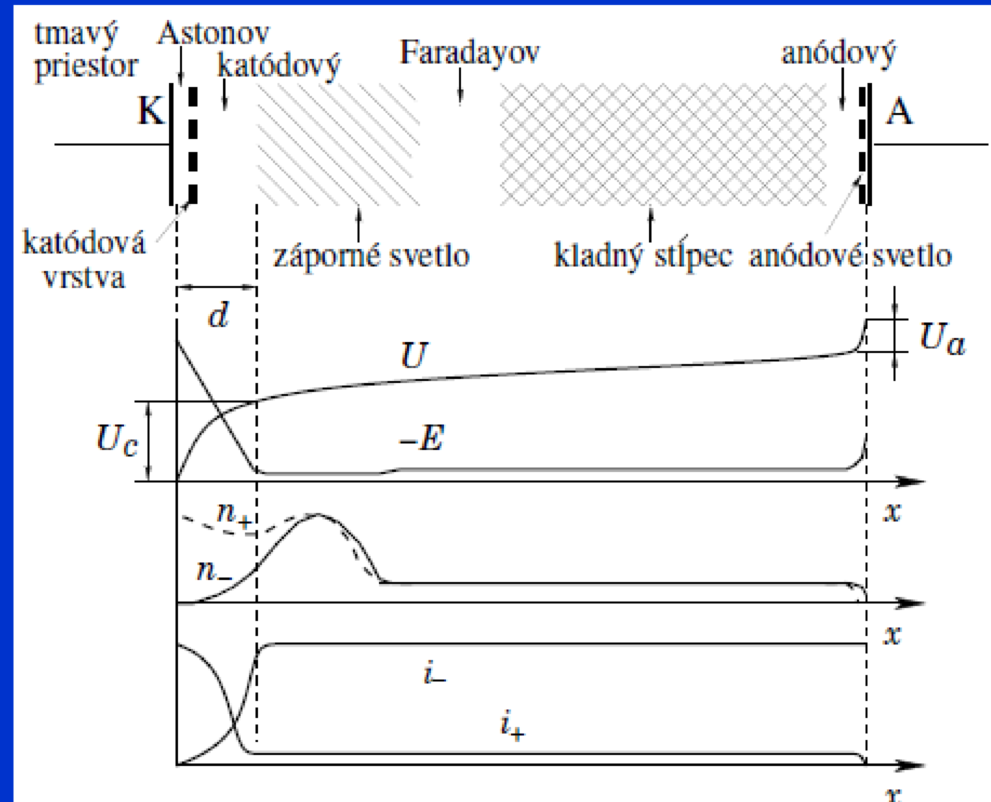

Obr. 5.9: Štruktúra tlecieho výboja a priebehy pozdĺžneho poľa E, potenciálu U, koncentrácie nabitých častíc n_+ a n_- a hustoty prúdu kladných iónov a elekrónov i_+ a i_-

Struktúra tlecieho výboja a priebehy pozdlzneho pola E, potenciálu U, koncentrácie nabitých castic n+ a n- a hustoty prúdu kladných iónov a elekrónov i+ a i-

Several parts of a glow discharge.
Luminous intensity (I light), electric field (E) and voltage (V).
V_c cathode potential.

Glow discharges

p ≅ 0.1 – 10 mbar ; U ≅ 150 – 2000 V

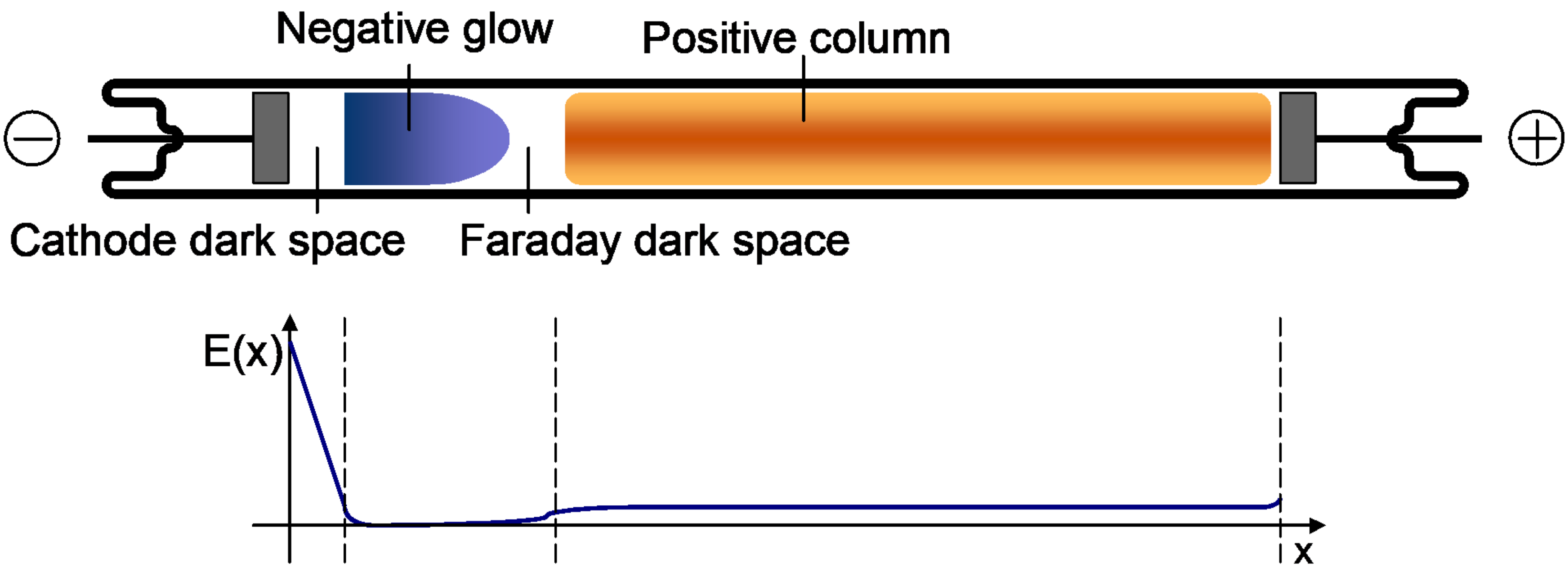

A simple glow discharge theory I. – the positive column

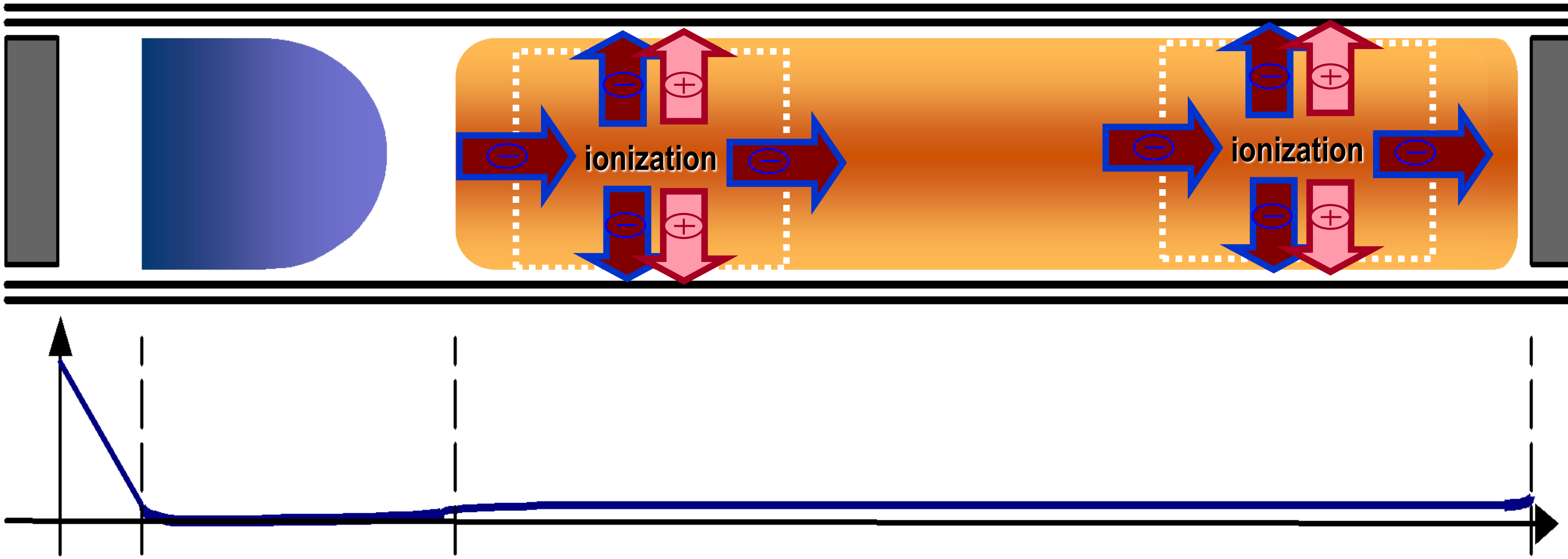

Electron emission from the cathode:

- ~~field (auto) emission~~
- ~~thermal emission~~
- due to bombarding ions

secondary electron emission coef. $\gamma \cong 0.1$

A simple glow discharge theory II. – the negative glow

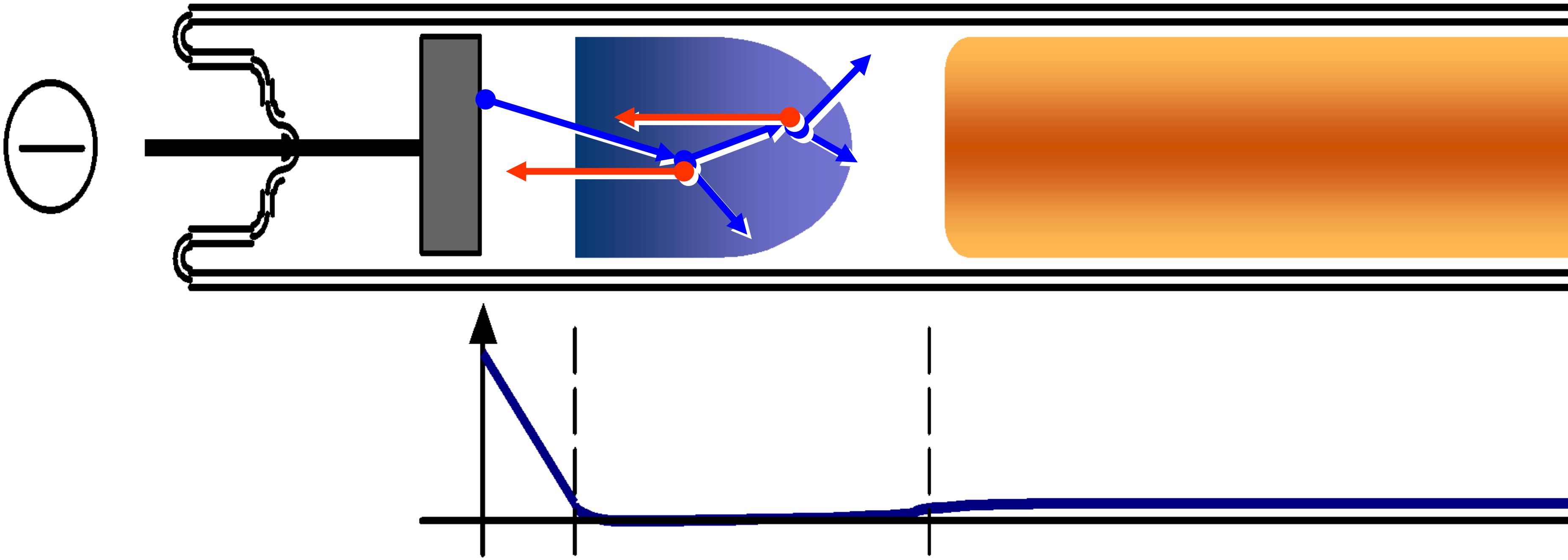

Self sustained discharge: the number of ions created in an avalanche can produce one new electron on the cathode

Gas lasers

1. **Negative glow lasers – hollow cathode lasers**

2. **Positive column lasers**

He-Ne laser

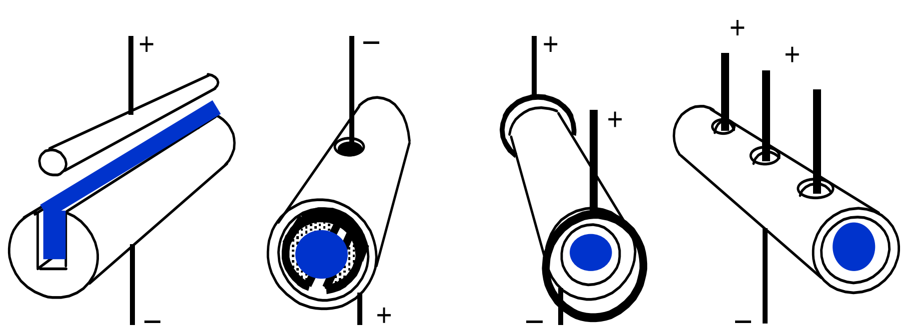

Silver ion laser

The He-Ne laser

how to make population inversion ?

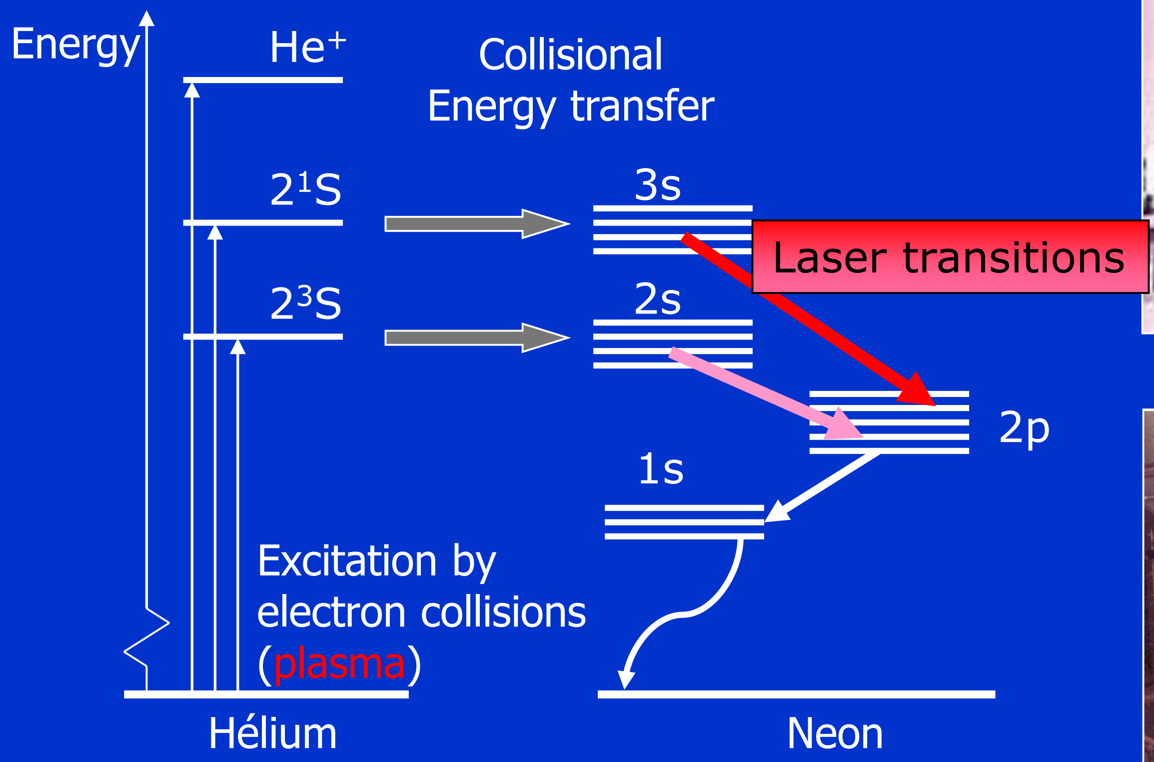

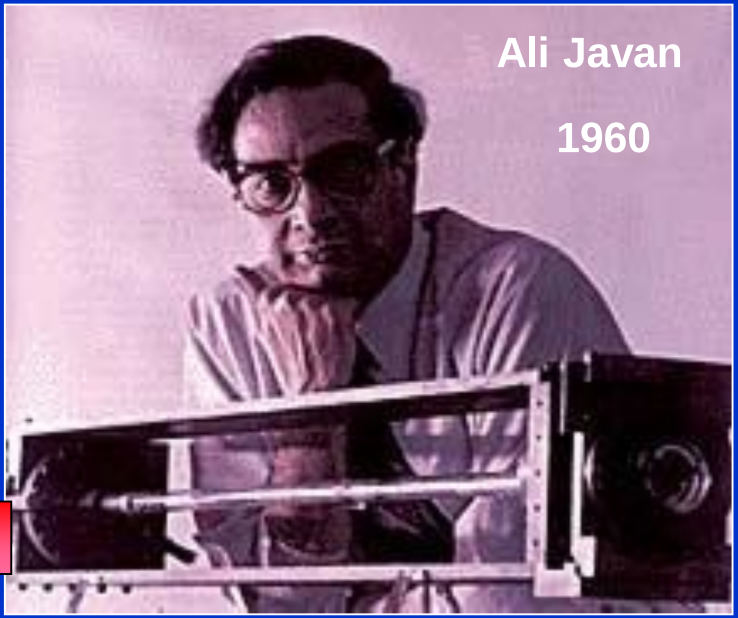

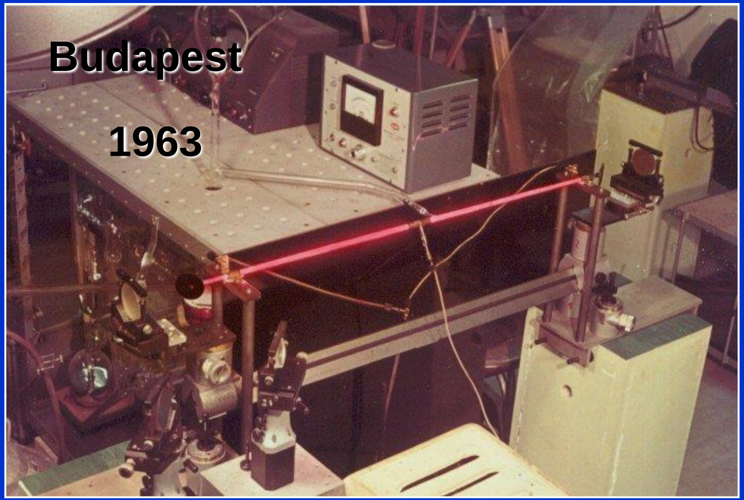

Segmented hollow-cathode silver ion laser

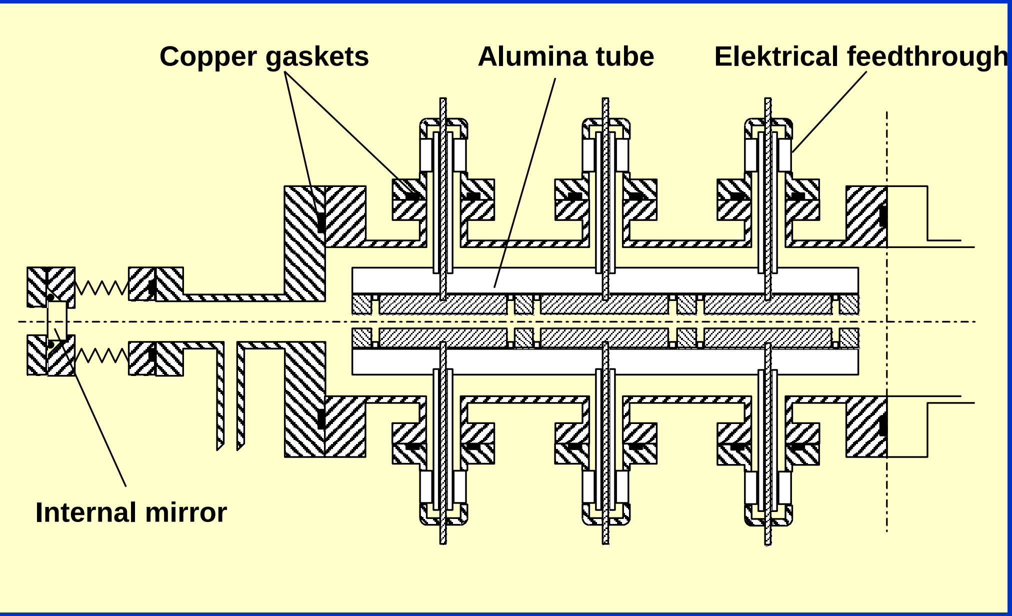

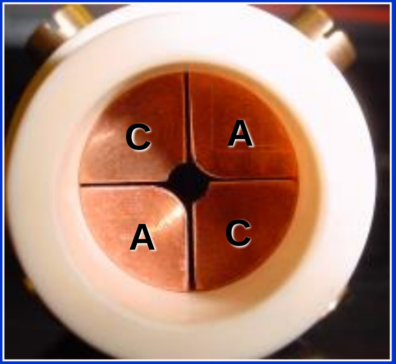

+ 20 μm silver

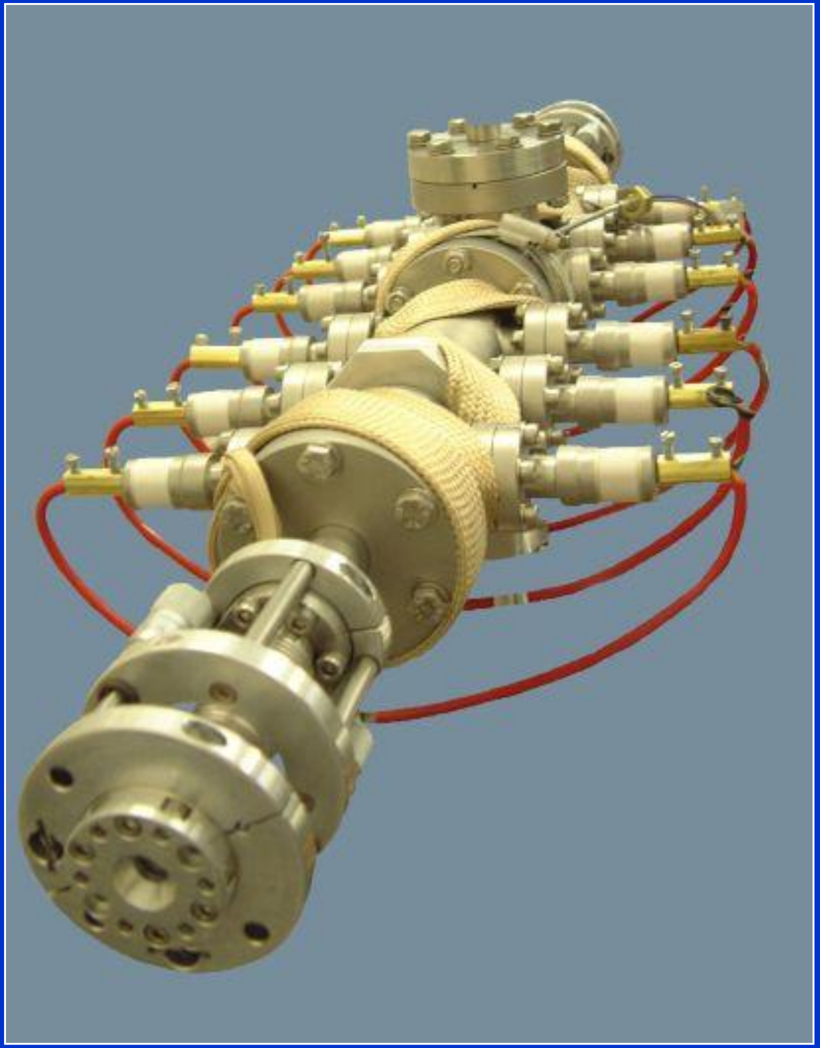

Electric discharges

Introduction to Electric Discharges **FP III/P5 C- 2005**

Electric discharges– Paschen law, time dependencies
Breakdown voltage

Doporučená literatura:

Úvod do fyziky plazmatu
ČSAV, Academia Praha 1984
Francis F. Chen

J. Phys. D: Appl. Phys. **35** (2002) R91–R103
TOPICAL REVIEW
Electrical breakdown in low pressure gases
M M Pejovic, G S Ristic, and J P Karamarkovic

Reactive plasmas
Andre Ricard

RF diode discharge

For technological applications – surface treatments

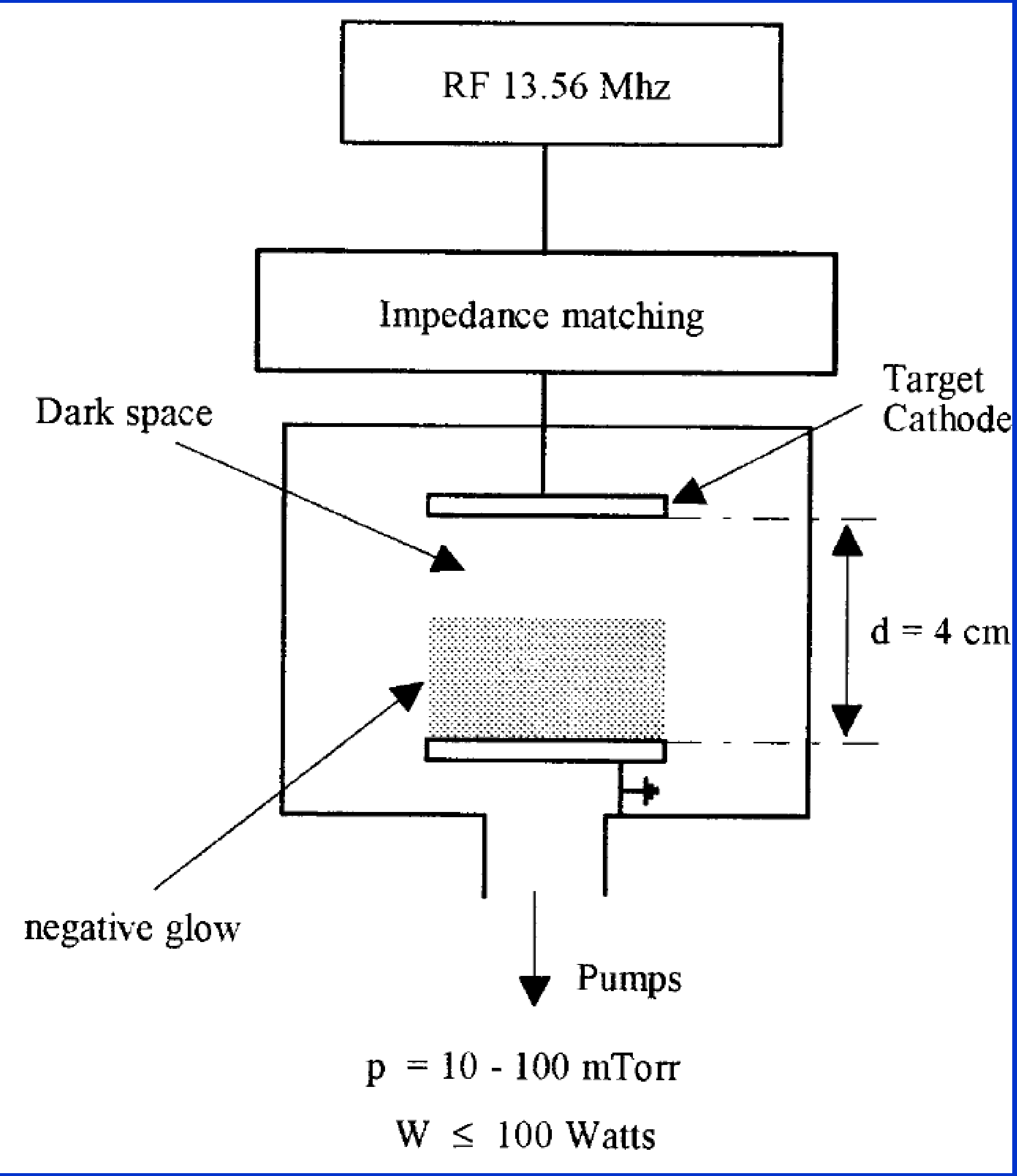

Microwave discharge

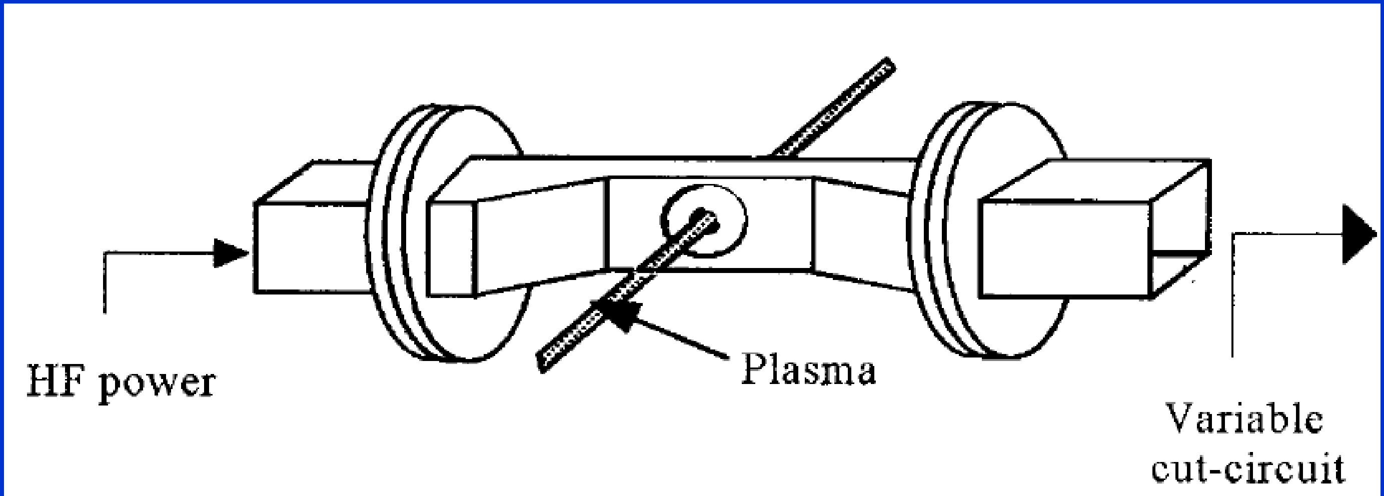

Microwave discharge → surfaguige discharge

Vlnovod ….waveguide

Surfatron discharge

A special characteristic of surface waves is to propagate along the discharge tube wall and to penetrate inside the tube to create the plasma. The radial distribution of electric field is given by the following equation *(note 2 p. 11)* :

$$E(r) = A\, I_o\, (B\, n_e^{1/2}\, r) \qquad (1\text{-}34)$$

where A and B are constant values and I_o is the modified Bessel function.

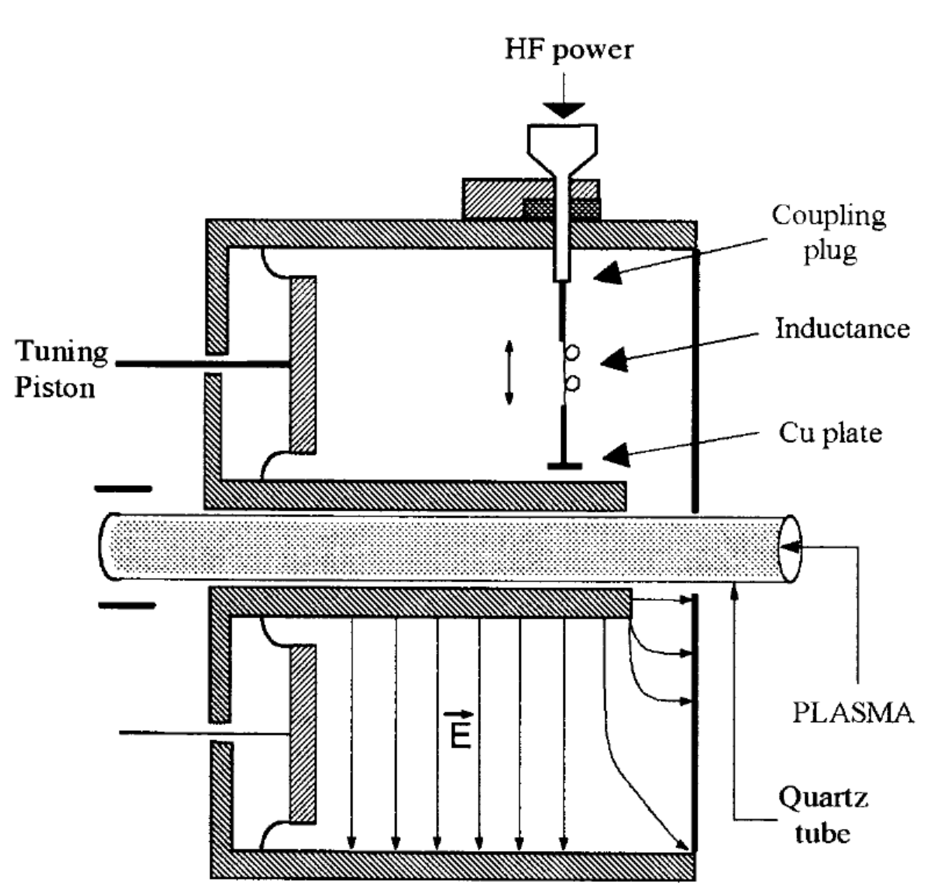

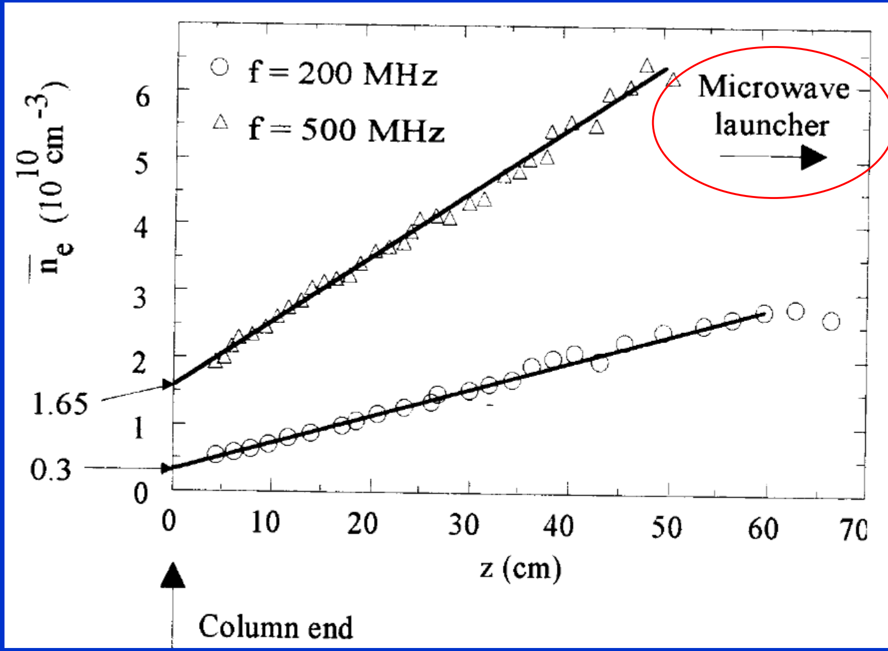

Axial distribution of electron density, measured in microwave plasma columns (Ar, 0.1 Torr, R = 1.3 cm) at 200 and 500 MHz.

Surfatron

Thus, the E(r) value is maximum for r = R and it is minimum for r = 0. The local maximum of electric field at the tube wall is more pronounced as the electron density and the tube radius increase. This effect has been observed by analyzing the plasma light[9]

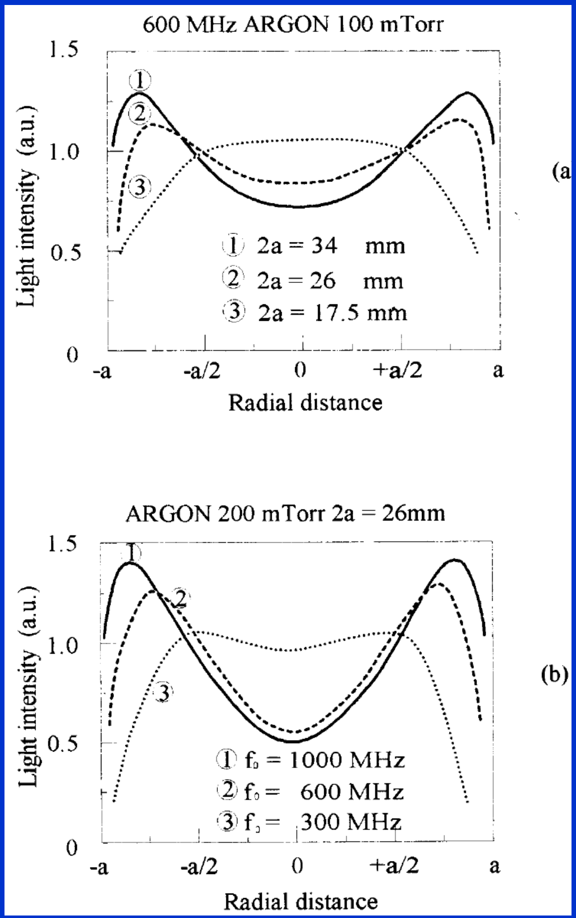

Radial distribution of the Ar I 549.6 nm line intensity in microwave discharge.

(a) 600 MHz, 0.1 Torr and several values of diameter (2a)

(b) diameter 2a = 26 mm and several values of microwave frequencies.

Two Sputtering Systems

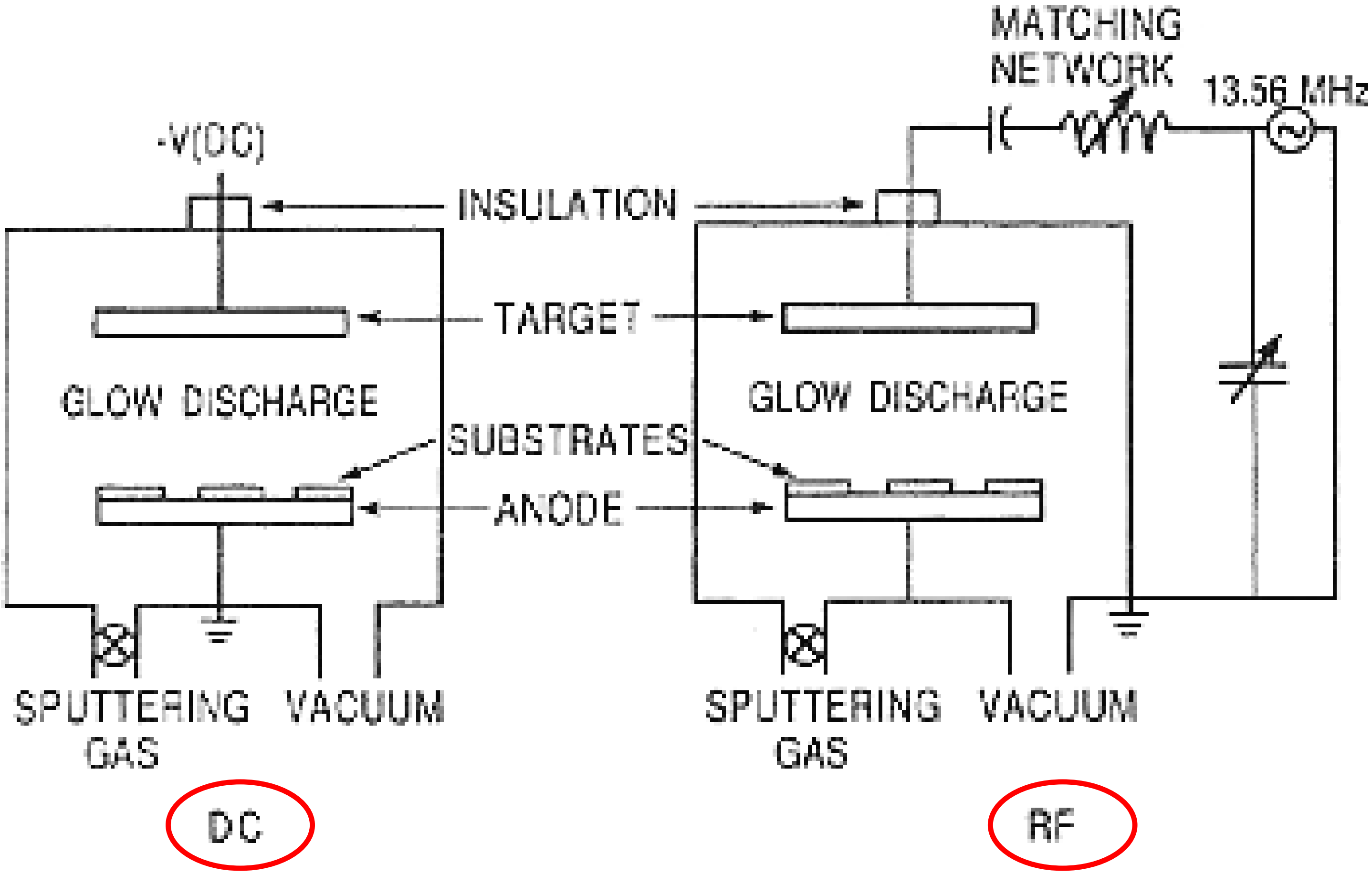

Several kilovolts are applied and gas pressures usually range from a few to a hundreds millitorr.

Types of plasmas (electron density)

- Stars (density $n < 10^7$ cm^{-3})
- Solar winds (density $n < 10^7$ cm^{-3})
- Coronas (density $n < 10^7$ cm^{-3})
- Ionosphere (density $n < 10^7$ cm^{-3})
- Glow discharge (density $n = 10^8 \sim 10^{14}$ cm^{-3})
- Arcs (density $n = 10^8 \sim 10^{14}$ cm^{-3})
- High-pressure arc (density $n \sim 10^{20}$ cm^{-3})
- Shock tubes (density $n \sim 10^{20}$ cm^{-3})
- Fusion reactors (density $n \sim 10^{20}$ cm^{-3})

Principal Glow Discharge Mechanism by Biased Parallelplate

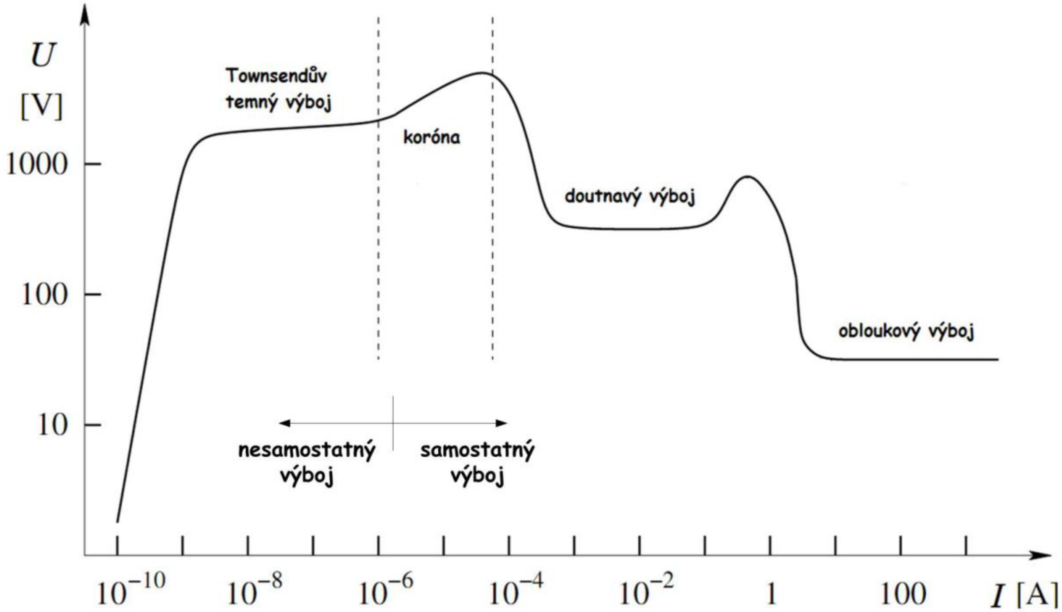

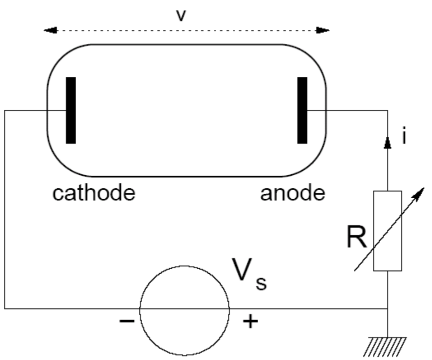

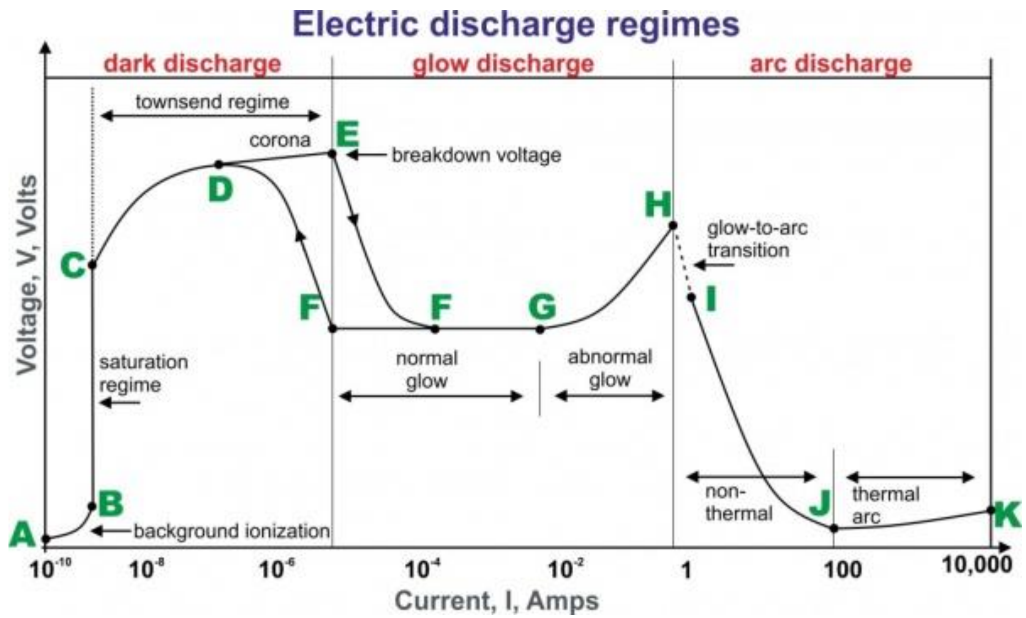

Principal Glow Discharge Mechanism by Biased Parallelplate

1. A stray electron near the cathode carrying an initial current i_o is accelerated toward the anode by the applied electric field (E).
2. After gaining sufficient energy the electron collides with a neutral gas atom (A) converting it into a positively charged ion (A^+), i.e., $e^- + A \rightarrow 2e^- + A^+$.
3. Two electrons are generated and are accelerated and bombard two additional neutral gas atoms, generating more ions and electrons, and so on.
4. Meanwhile, the electric field drives ions in the opposite direction.
5. Ions collide with the cathode, ejecting, among other particles, *secondary electrons*.
6. Secondary electrons also undergo charge multiplication. (step 2)
7. The effect snowballs until a sufficiently large avalanch current ultimately causes the gas to breakdown.

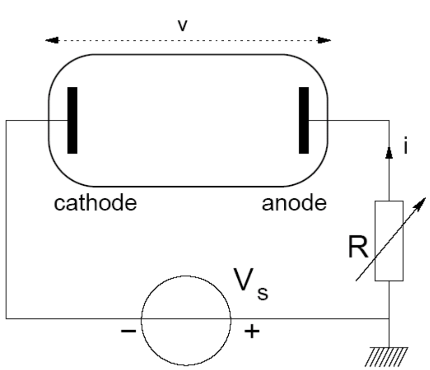

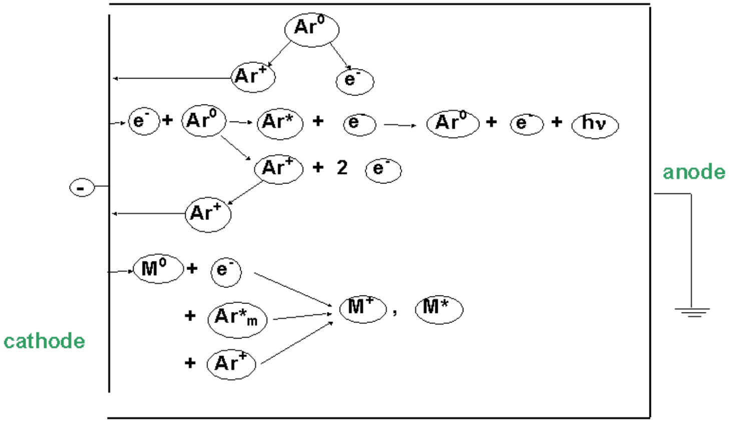

http://webhost.ua.ac.be/plasma/pages/glow-discharge.html

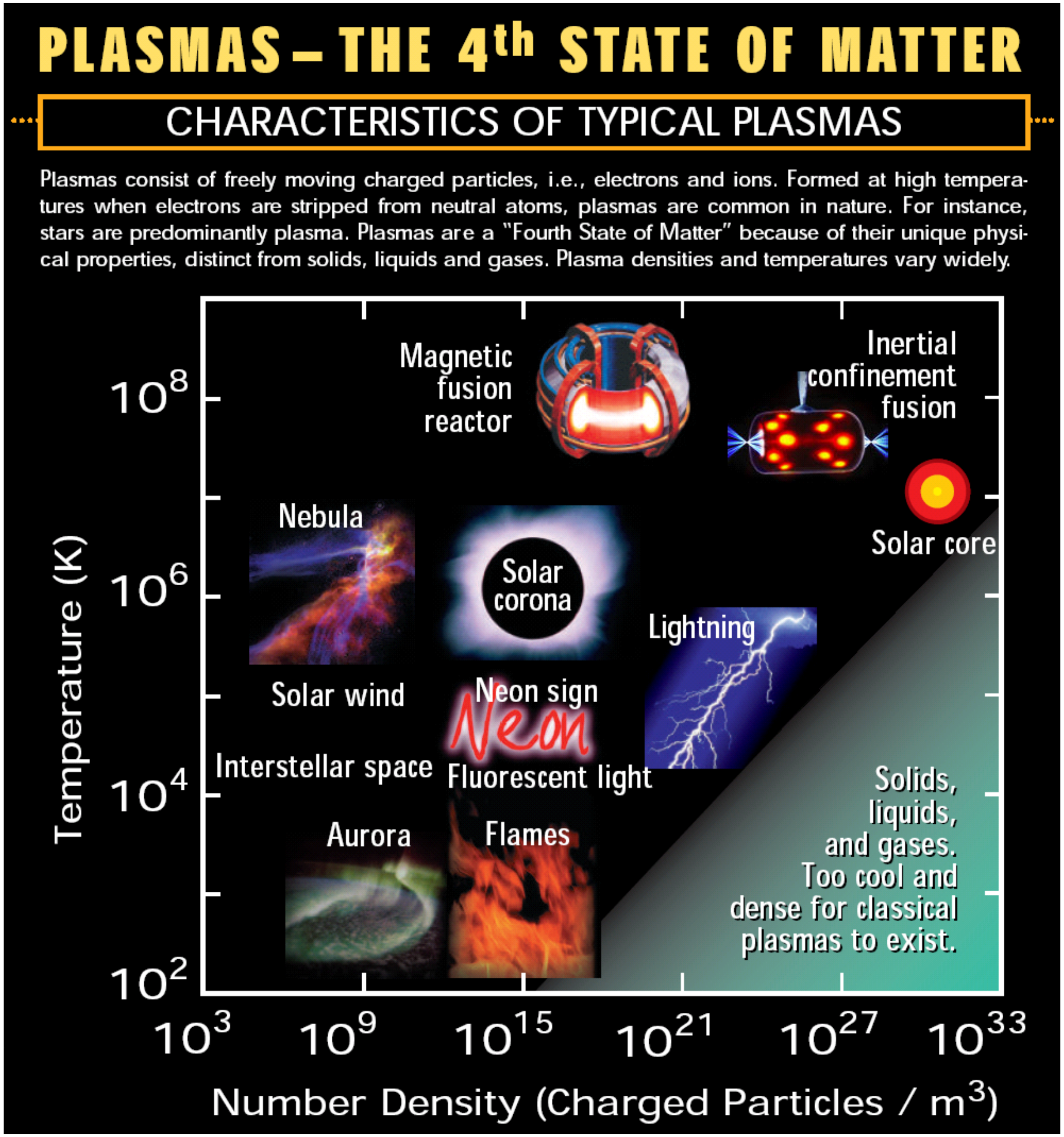

http://fusedweb.pppl.gov/CPEP/Translations.html j~f(d)

E/N

j~f(d,E/N)

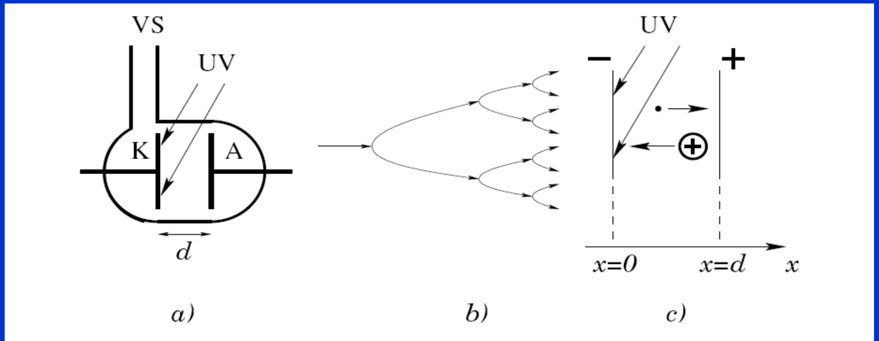

Obr. 5.2: Zapaľovanie výboja: *a)* výbojka na meranie zapaľovacieho napätia: K - katóda, A - anóda, UV - ultrafialové žiarenie zabezpečujúce emisiu primárnych elektrónov, VS - napojenie na vákuový systém; *b)* elektrónová lavína; *c)* označenie polohy elektród

$$\frac{\mathrm{d}j_-}{\mathrm{d}x} = \alpha n_- = \frac{\alpha}{V_-} n_- V_- = \delta j_-$$

$j \sim j_0 \exp(\alpha x)$

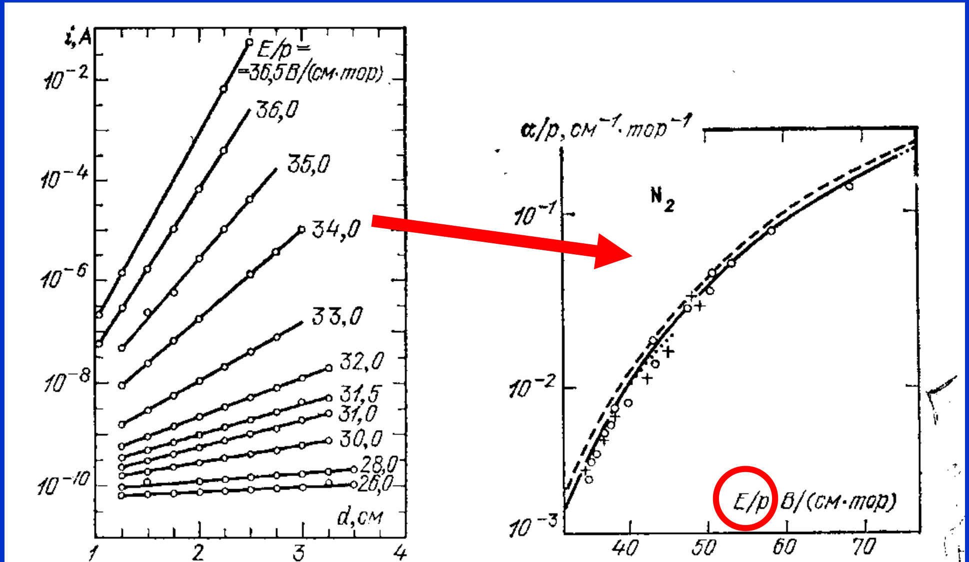

Р и с. 5.3. Экспериментальный график, демонстрирующий постоянство α и экспоненциальный характер нарастания тока в разрядном промежутке; ионизационные коэффициенты определяются наклонами прямых [6]

Р и с. 5.4. Ионизационный коэффициент Таунсенда α в N_2 по разным измерениям

E/N …… 1 Townsend = 1 Td = 10^{-17} Vcm^2 = 10^{-21} Vm^2

E/p at 293 K (cca 20 C)……. 1V/cmTorr=3.034Td, resp. 1 Td = 0,3296V/cmTorr

Electric discharges

Electron Impact Ionization in a Constant Field

Ionization in case of Maxwell distribution

Ionization Frequency

$n(\varepsilon)$ is the electron energy distribution

$$(dn_e/dt)_i = \nu_i n_e = k_i N n_e$$

$$\nu_i = N \int n(\varepsilon) v \sigma_i(\varepsilon) d\varepsilon \Big/ \int n(\varepsilon) d\varepsilon = N \langle v \sigma_i \rangle \equiv N k_i$$

$$n(\varepsilon) \propto \exp(-\varepsilon/kT_e) \qquad \sigma_i(\varepsilon) = C_i(\varepsilon - I)$$

$$\nu_i = N \bar{v} C_i (I + 2kT_e) \exp(-I/kT_e)\,, \quad \bar{v} = (8kT_e/\pi m)^{1/2}$$

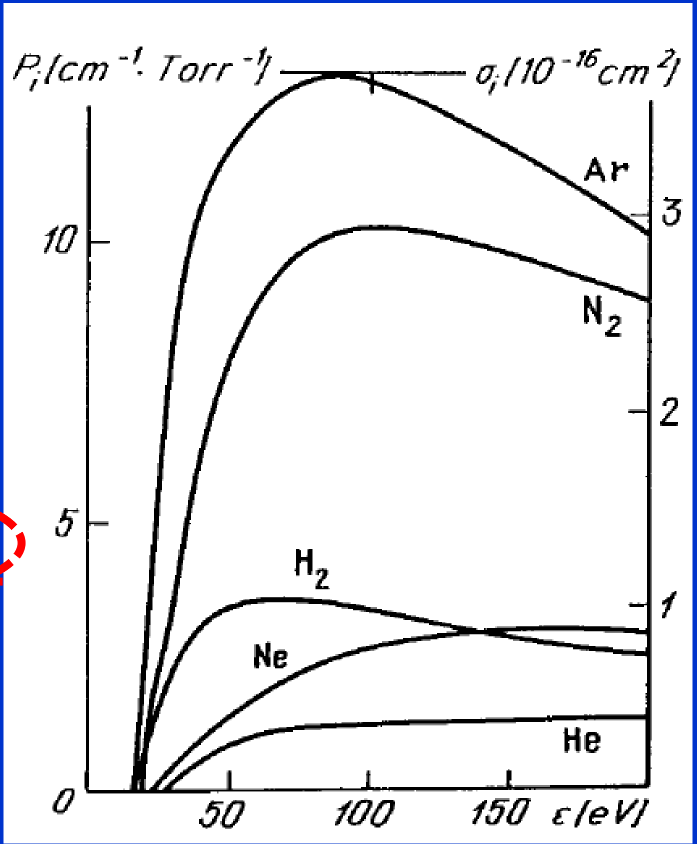

Fig. 4.1. Cross sections and probabilities of electron impact ionization. From [4.1]

For example, in argon, $C_i = 2 \cdot 10^{-17}\,\mathrm{cm^2/eV}$. If $T_e = 1\,\mathrm{eV}$, then $\bar{v} = 6.7 \cdot 10^7\,\mathrm{cm/s}$ and $k_i = \langle v\sigma_i \rangle = 3 \cdot 10^{-16}\,\mathrm{cm^3/s}$. If $p = 50\,\mathrm{Torr}$ and $T = 300\,\mathrm{K}$, then $N = 1.7 \cdot 10^{18}\,\mathrm{cm^{-3}}$. This gives $\nu_i = 510\,\mathrm{s^{-1}}$. At these T_e and N, the equilibrium degree of ionization is $(n_e)_{eq}/N = 0.021$. The values of C_i for several other gases (in $10^{-17}\,\mathrm{cm^2/eV}$) are

He – 0.13 , Ne – 0.16 , Hg – 7.9 , N_2 – 0.85 , O_2 – 0.68 , H_2 – 0.59 .

Breakdown cannot be simply explained by ionization

Ionization frequency and ionization coefficient

For example, in argon, $C_i = 2 \cdot 10^{-17}\,\mathrm{cm^2/eV}$. If $T_e = 1\,\mathrm{eV}$, then $\bar{v} = 6.7 \cdot 10^7\,\mathrm{cm/s}$ and $k_i = \langle v\sigma_i \rangle = 3 \cdot 10^{-16}\,\mathrm{cm^3/s}$. If $p = 50\,\mathrm{Torr}$ and $T = 300\,\mathrm{K}$, then $N = 1.7 \cdot 10^{18}\,\mathrm{cm^{-3}}$. This gives $\nu_i = 510\,\mathrm{s^{-1}}$. At these T_e and N, the equilibrium degree of ionization is $(n_e)_{eq}/N = 0.021$. The values of C_i for several other gases (in $10^{-17}\,\mathrm{cm^2/eV}$) are

$$\mathrm{He} - 0.13\,,\ \mathrm{Ne} - 0.16\,,\ \mathrm{Hg} - 7.9\,,\ \mathrm{N_2} - 0.85\,,\ \mathrm{O_2} - 0.68\,,\ \mathrm{H_2} - 0.59\,.$$

N will be double within 1.4ms → if n_0=1 → at T=1eV equilibrium will be reached within 75ms
Experiments are giving time many times shorter

It is more convenient, therefore, to characterize the rate of ionization not by frequency $\nu_i\,\mathrm{s^{-1}}$, but by the *ionization coefficient* $\alpha\,\mathrm{cm^{-1}}$, that is, the number of ionization events performed by an electron in a 1 cm path along the field.

$$\alpha = \nu_i / v_d\,, \qquad \nu_i = \alpha v_d$$

Note that the primary and complete characteristic of the rate of ionization is the frequency ν_i, not α. The distribution function gives us this frequency, as well as the drift velocity. The ionization coefficient α is a derived quantity, found from (4.3). Actually, α is not very meaningful in fast-oscillating fields. However, dc measurements give us α, not ν_i.

Breakdown cannot be simply explained by ionization

Electric discharges – data semi-empirical approach

$$\frac{\mathrm{d}j_-}{\mathrm{d}x} = \alpha n_- = \frac{\alpha}{V_-} n_- V_- = \delta j_-$$

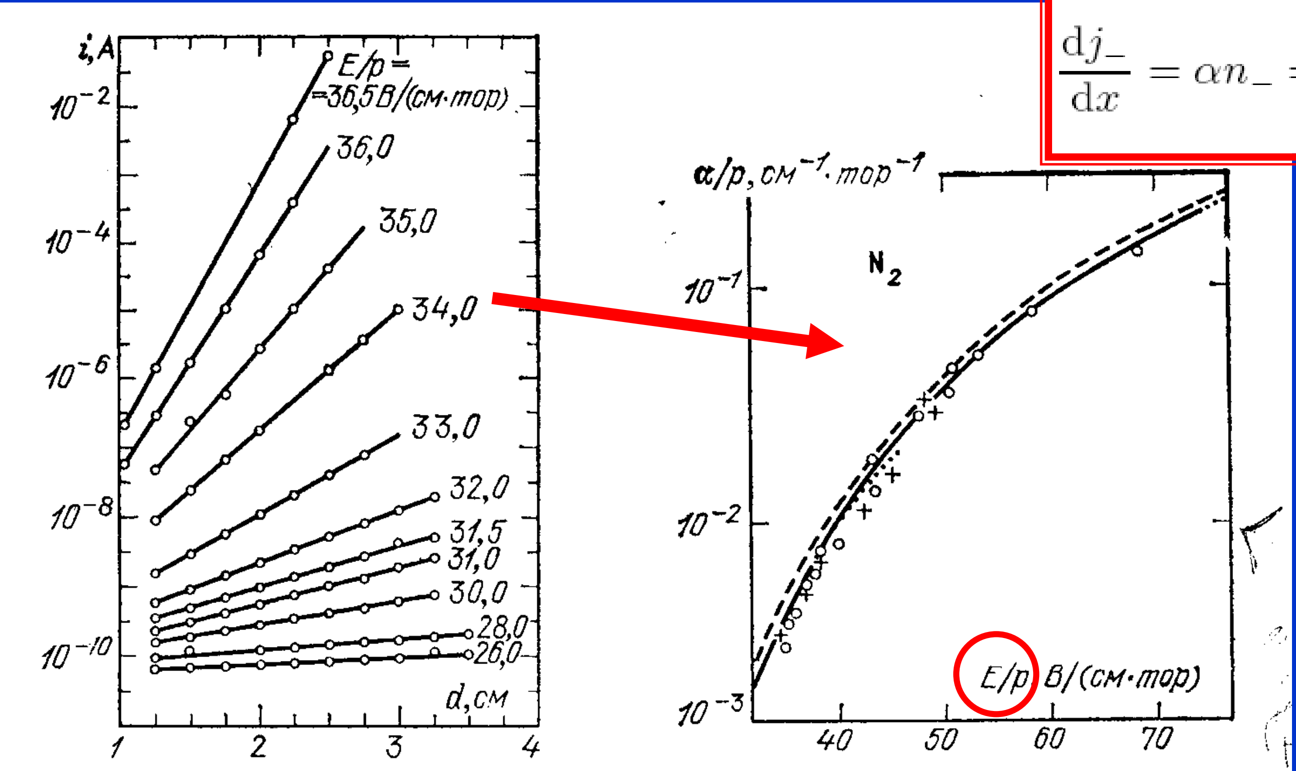

Рис. 5.3. Экспериментальный график, демонстрирующий постоянство α и экспоненциальный характер нарастания тока в разрядном промежутке; ионизационные коэффициенты определяются наклонами прямых [6]

Рис. 5.4. Ионизационный коэффициент Таунсенда α в N_2 по разным измерениям

E/N …… 1 Townsend = 1 Td = 10^{-17} Vcm^2 = 10^{-21} Vm^2

E/p at 293 K (cca 20 C)……. 1V/cmTorr=3.034Td, resp. 1 Td = 0,3296V/cmTorr

Breakdown cannot be simply explained by ionization

POZOR ROZDIEL

$$\frac{\mathrm{d}j_-}{\mathrm{d}x} = \alpha n_- = \frac{\alpha}{V_-} n_- V_- = \delta j_-$$

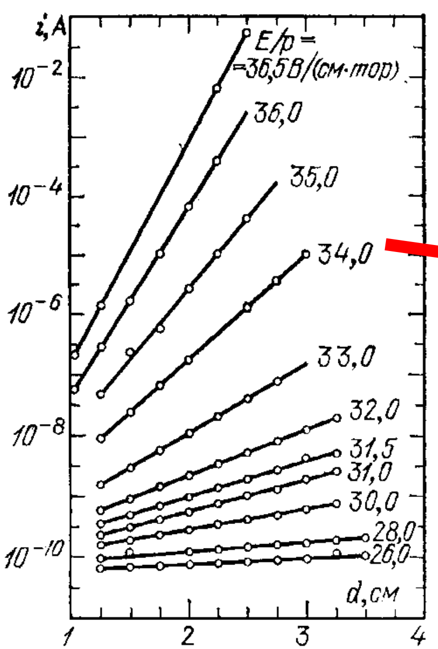

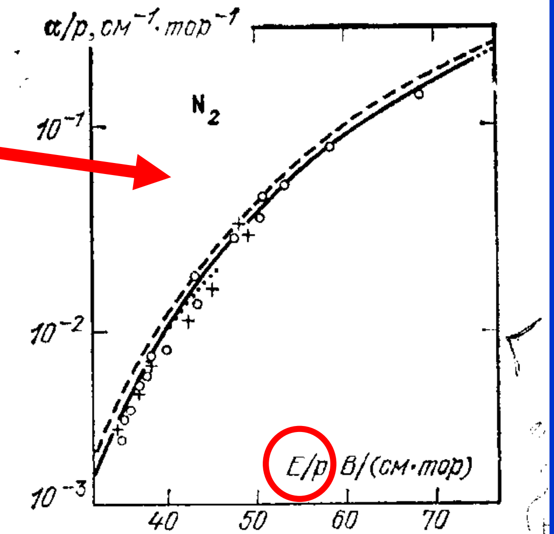

Р и с. 5.3. Экспериментальный график, демонстрирующий постоянство α и экспоненциальный характер нарастания тока в разрядном промежутке; ионизационные коэффициенты определяются наклонами прямых [6]

Р и с. 5.4. Ионизационный коэффициент Таунсенда α в N_2 по разным измерениям

i : *charge current*

α : *Townsend ionization coefficient*

γ_e : *Townsend secondary – electron emission coefficient*

d : *Distance between electrodes*

Breakdown cannot be simply explained by ionization

Measurements of α and similarity laws

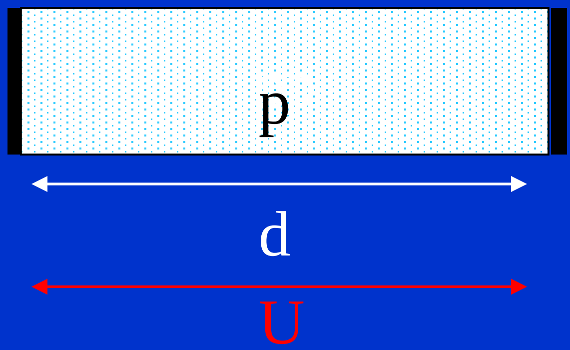

$$dN/dx = \alpha N \,, \quad N(x) = N_0 \exp(\alpha x)$$

The electron current at the anode is $i = eN_0 \exp(\alpha d)$

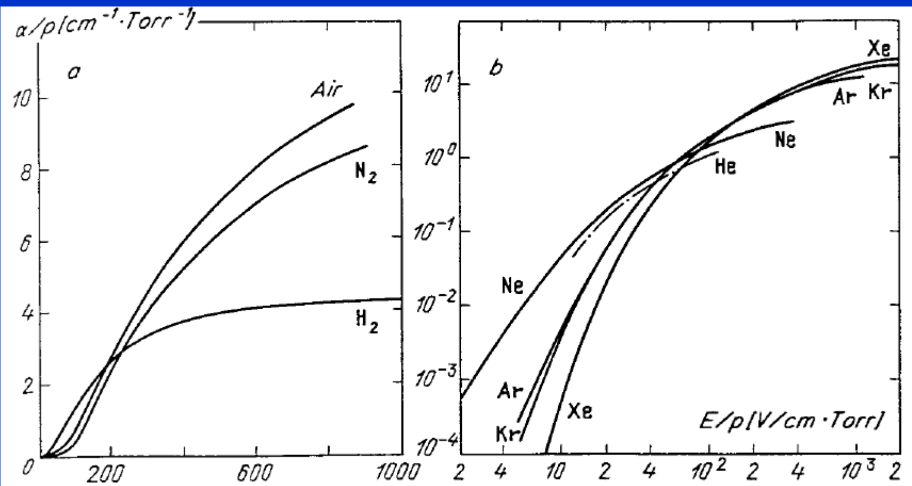

Fig. 4.3. Ionization coefficients for a wide range of E/p values (a) in molecular gases, (b) in inert gases. From [4.3]

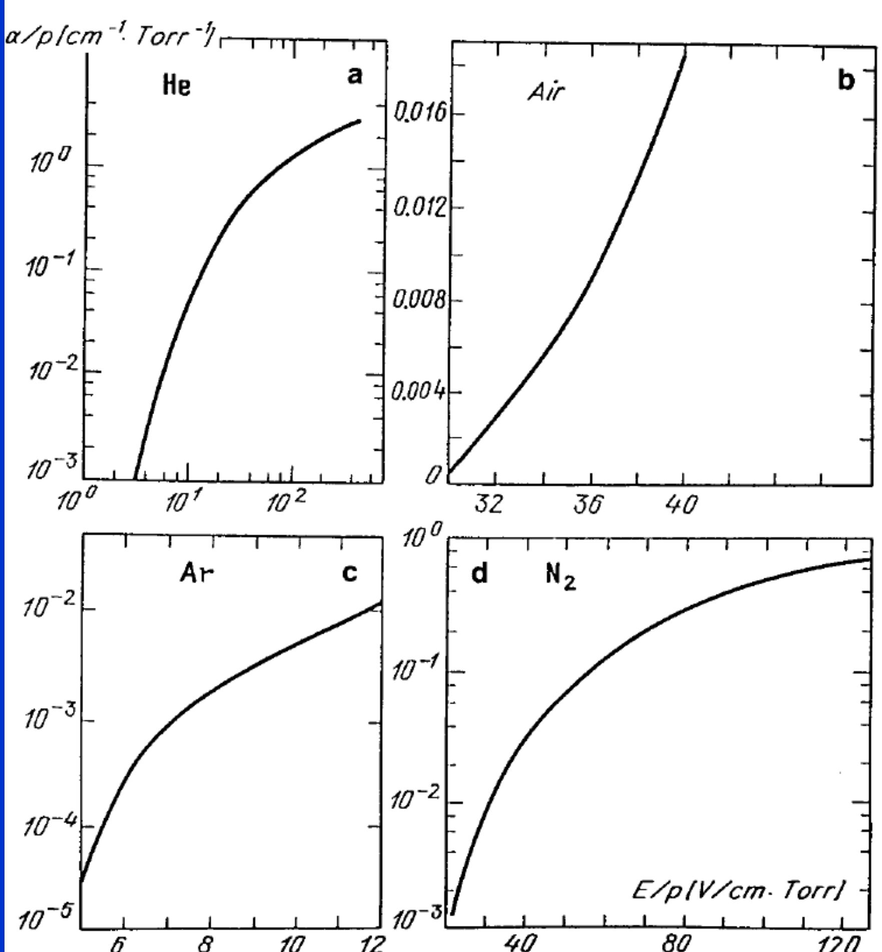

Fig. 4.2. Ionization coefficient in a) He, b) air, c) Ar, d) N_2. From [4.2]

dU/dt is not considered

Data for Paschen law

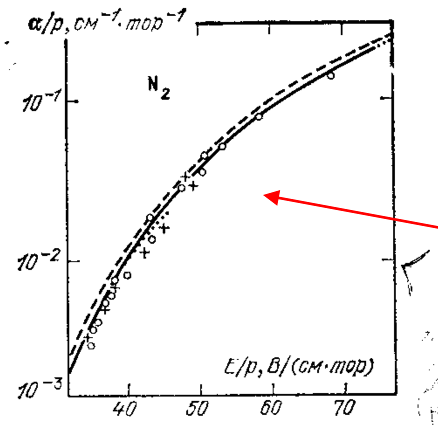

к, демонстрирующий постоянство α и экс-
тока в разрядном промежутке; ионизацион-
еляются наклонами прямых [6]

ент Таунсенда α в N_2 по разным измере-
ниям

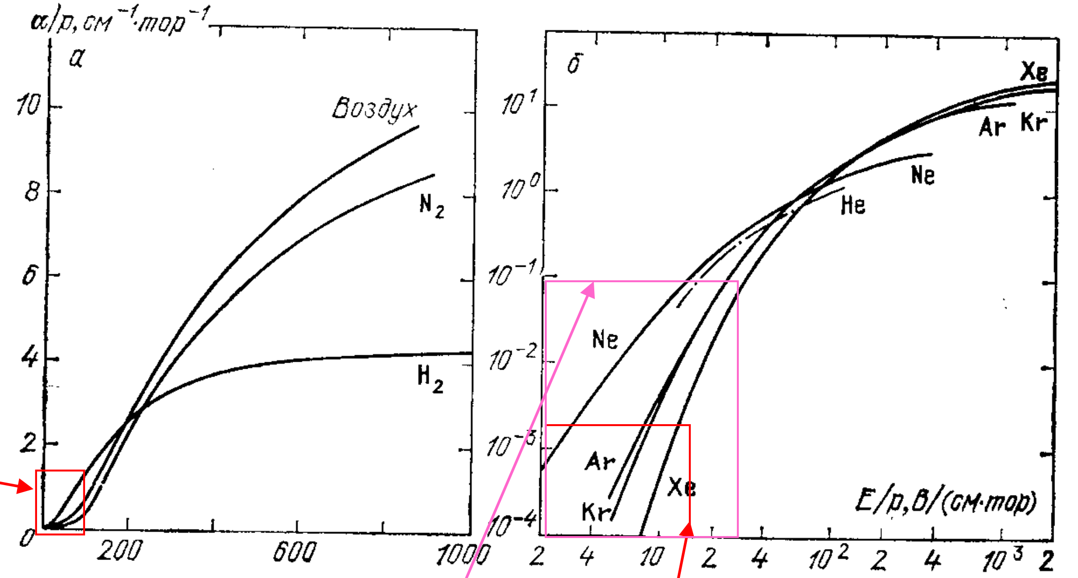

Р и с. 5.6. Ионизационный коэффициент в широком диапазоне E/p: *а* — в H_2, N_2 и в воздухе; *б* — в инертных газах [6]

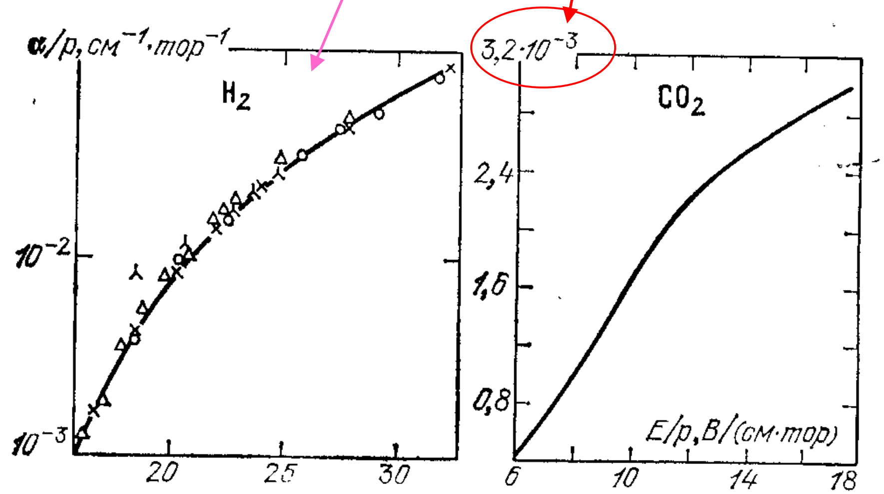

Р и с. 5.7. Ионизационный коэффициент в H_2 [26] и CO_2 [6]

Electric discharges

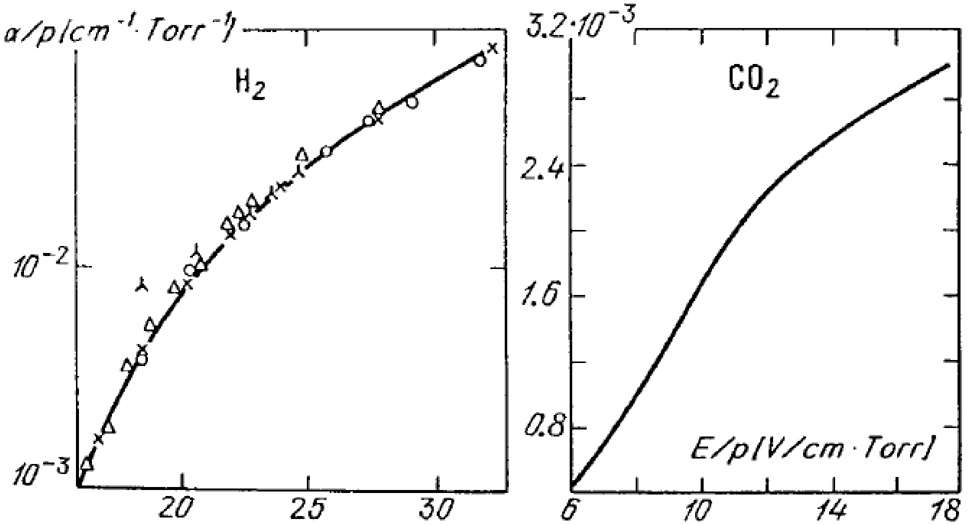

Fig. 4.4. Ionization coefficients in H_2 and CO_2. From [4.2]

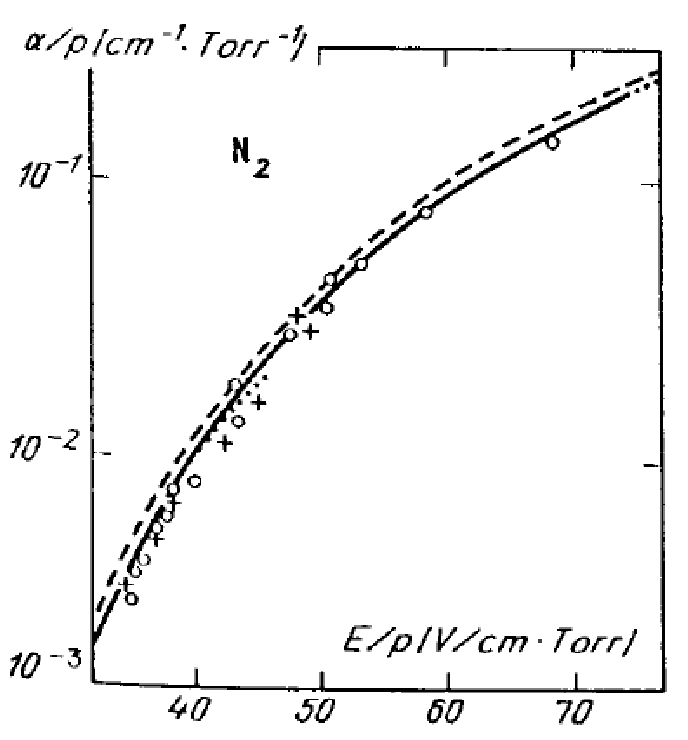

Electric discharges

$$dN/dx = \alpha N \,, \quad N(x) = N_0 \exp(\alpha x)$$

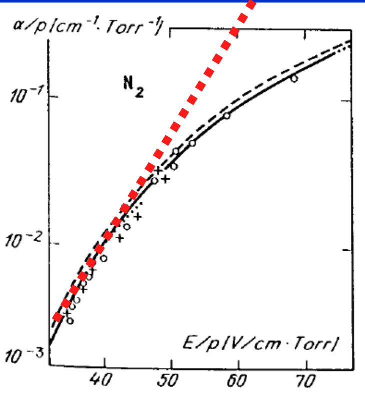

4.1.5 Interpolation Formula for α

The theoretical and numerical analysis of discharges widely uses a conventional empirical formula suggested by Townsend:

$$\alpha = Ap \exp(-Bp/E) \,. \tag{4.5}$$

The constants A and B are determined by approximating the experimental curves (Table 4.1). In a number of cases the relation (4.5) can be attributed a certain physical meaning. Assume, for example, that an electron undergoes only ionizing collisions. (This assumption may be realistic at high E/p and moderate energies.) The energy picked up by an electron along a free path length x is slightly greater than the ionization potential I. The probability that it will move the distance $x = I/eE$ without collisions and then be involved in an ionizing collision in a distance dx is $\alpha\, dx = dx\, l^{-1} \exp(-I/eEl)$, where $l = l_1/p$ is the mean-free-path length. This gives us (4.5) with $A = l_1^{-1}$, $B = I/el_1$. If $\sigma = 5 \cdot 10^{-16}\,\mathrm{cm}^2$, then $l_1 = 0.06\,\mathrm{cm} \cdot \mathrm{Torr}$; if $I = 15\,\mathrm{eV}$, then $A = 17$, $B = 250$, which is quite close to tabulated values.

Table 4.1. Constants in the formulas for the ionization coefficient, and regions of applicability [4.4,5]

Gas	A	B	E/p	C	D	$E/p <$
	cm^{-1}Torr^{-1}	V/(cm · Torr)	V/(cm · Torr)	cm^{-1}Torr^{-1}	V/(cm · Torr)$^{1/2}$	V/(cm · Torr)
He	3	34	20–150	4.4	14	100
Ne	4	100	100–400	8.2	17	250
Ar	12	180	100–600	29.2	26.6	700
Kr	17	240	100–1000	35.7	28.2	900
Xe	26	350	200–800	65.3	36.1	1200
Hg	20	370	150-600			
H_2	5	130	150-600			
N_2	12	342	100–600			
N_2	8.8	275	27–200			
Air	15	365	100–800			
CO_2	20	466	500–1000			
H_2O	13	290	150–1000			

See next slide

The fraction of electrons in a Maxwellian spectrum that are capable of ionizing an atom is proportional to $\exp(-I/kT_e)$. If $T_e \propto E/p$ (see Sect. 2.3.5), we again arrive at a dependence of ν_i and α on E of type (4.5), but now the constant B has a different meaning. It will be shown in Sect. 7.4.7 that an approximate solution of the kinetic equation that takes into account the large role of inelastic losses of electron energy on excitation also leads to a relation of type (4.5), but again with a changed meaning of B. For inert gases, the formula

$$\alpha = Cp \exp\left[-D(p/E)^{1/2}\right] \tag{4.6}$$

Electric discharges semi-empirical approach

The theoretical and numerical analysis of discharges widely uses a conventional empirical formula suggested by Townsend:

$$\alpha = Ap\exp(-Bp/E)$$

$$\alpha = Cp\exp\left[-D(p/E)^{1/2}\right]$$

Table 4.1. Constants in the formulas for the ionization coefficient, and regions of applicability [4.4,5]

Gas	A	B	E/p	C	D	$E/p <$
	$\mathrm{cm^{-1}Torr^{-1}}$	V/(cm · Torr)	V/(cm · Torr)	$\mathrm{cm^{-1}Torr^{-1}}$	$\mathrm{V/(cm \cdot Torr)^{1/2}}$	V/(cm · Torr)
He	3	34	20–150	4.4	14	100
Ne	4	100	100–400	8.2	17	250
Ar	12	180	100–600	29.2	26.6	700
Kr	17	240	100–1000	35.7	28.2	900
Xe	26	350	200–800	65.3	36.1	1200
Hg	20	370	150-600			
H_2	5	130	150-600			
N_2	12	342	100–600			
N_2	8.8	275	27–200			
Air	15	365	100–800			
CO_2	20	466	500–1000			
H_2O	13	290	150–1000			

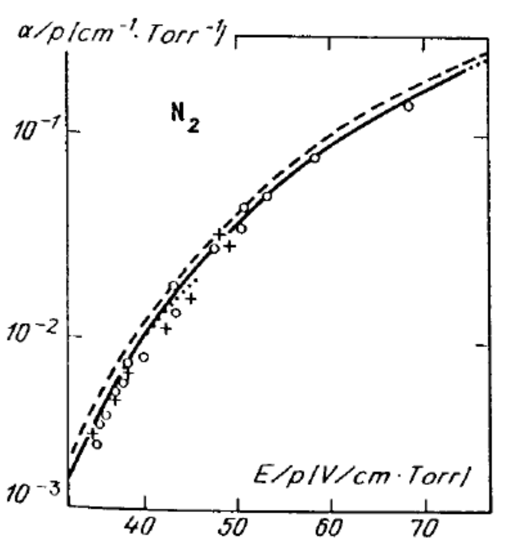

empirical formula for air at relatively high E/p (see also Table 12.1)

$$\alpha/p = 1.17 \cdot 10^{-4}(E/p - 32.2)^2\,\mathrm{cm^{-1}\,Torr^{-1}}\ ,$$

$$E/p \approx 44 - 176\,\mathrm{V/(cm \cdot Torr)}\ .$$

Electric discharges other processes involved in breakdown of a discharge

4.1.7 Stepwise Ionization

The atoms of a weakly ionized gas are mostly ionized from the ground state. Many excited atoms and molecules may be formed if the gas is highly ionized, and stepwise ionization may be predominant. Atoms are first excited by electron impact and then ionized by subsequent collisions. Long-lived metastable excited particles play an important role in this process (Table 4.2); their ionization cross sections are rather high (Fig. 4.6).

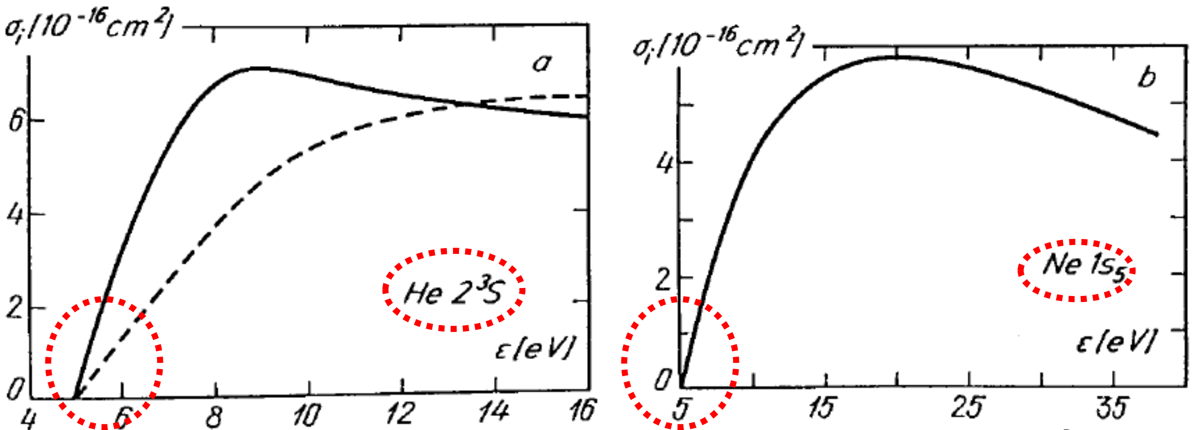

Fig. 4.6. Cross sections of ionization of excited metastables by electron impact: **(a)** He 2^3S; experimental data [4.6] – *solid curve*; theory [4.7] – *dashed curve*; **(b)** Ne $1s_5$ – theory. From [4.7]

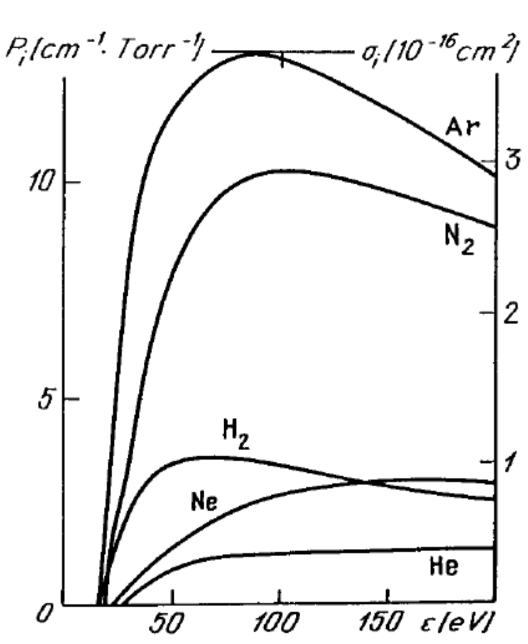

Fig. 4.1. Cross sections and probabilities of electron impact ionization. From [4.1]

Comparable values

lower threshold energies ➔ higher probability at given T_e

Electric discharges

Table 4.3. Cross sections of photoionization of atoms and molecules from the ground state close to the threshold

Gas	$\hbar\omega = I$, eV	λ, Å	σ_ν, 10^{-18} cm^2
H	13.6	912	6.3
He	24.6	504	7.4
Ne	21.6	575	4.0
Ar	15.8	787	35
Na	5.14	2412	0.12
K	4.34	2860	0.012
Cs	3.89	3185	0.22
N	14.6	852	9
O	13.6	910	2.6
O_2	12.2	1020	~ 1
N_2	15.58	798	26
H_2	15.4	805	7

Electric discharges – Hornbeck Molnar ionization

4.2.3 Associative Ionization

This process of type $A + A^* \rightarrow A_2^+ + e$, discovered by Hornbeck and Molnar in 1951, is sometimes important in inert gases. The separation of an electron is facilitated by the release of a small binding energy of order 1 eV in the association of an ion and an atom into a molecular ion. A reaction in helium involves atoms excited to states with the principal quantum number $n = 3$; their electron binding energies are from 1.52 to 1.62 eV. The binding energy of He_2^+ is somewhat higher, 2.23 eV, so that the electron can be ejected. At $T = 400\,K$, the reaction cross sections are $2 \cdot 10^{-16} - 2 \cdot 10^{-15}\,cm^2$. The *associative ionization* in mercury vapor involves two excited atoms,

$$Hg\left(6^3P_1,\ E^* = 4.9\,eV\right) + Hg\left(6^3P_0,\ E^* = 4.7\,eV\right) \rightarrow Hg_2^+ + e\ ,$$

the first atom being in a resonance and the second, in a metastable state. The total energy is 9.6 eV, less than that required to ionize an Hg atom ($I_{Hg} = 10.4\,eV$); together with the binding energy of an Hg_2^+ molecular ion, however (0.15 eV), it is sufficient to ionize the molecule ($I_{Hg_2} = 9.7\,eV$).

Electric discharges - Penning ionization

4.2.2 Ionization by Excited Atoms

Even the high kinetic energy of slow heavy particles is not effective in ionization processes. Ionization requires the velocities of atoms and molecules to be comparable to the electron velocity in atoms, 10^8 cm/s, which corresponds to energies of 10 to 100 keV, not realizable in discharge conditions. On the other hand, the atomic excitation energy E^* is easily spent on liberating an electron from another atom, provided, of course, that it exceeds the ionization potential I. Resonance-excited atoms are especially effective in this respect. Thus the ionization cross sections of Ar, Kr, Xe, N_2, and O_2 in impacts by $He(2^1P)$ atoms with $E^* = 21.2\,eV$ is $\sigma \approx 2 \cdot 10^{-14}\,cm^2$, which is much greater than the gas-kinetic value [4.8]. Cross sections for ionization by metastable atoms, also with $E^* > I$ (*Penning effect*), are smaller but metastable atoms are much more numerous than short-lived resonance-excited atoms. Cross sections for ionization of Ar, Xe, N_2, CO_2 by metastable $He(2^3S)$ atoms with $E^* = 19.8\,eV$ reach $10^{-15}\,cm^2$, and that of Hg is exceptionally large: $1.4 \cdot 10^{-14}\,cm^2$ [4.8].

Electric discharges – processes going again ionization

4.3.1 Decay of Plasma

In the absence of an electric field, the charge densities $n_e = n_+$ in a plasma without electronegative components decay with time according to the law

$$\left(\frac{dn_e}{dt}\right)_r = -\beta n_e n_+ , \quad n_e = \frac{n_e^0}{1+\beta n_e^0 t} \xrightarrow[t\to\infty]{} \frac{1}{\beta t} . \tag{4.8}$$

For example, if the *electron-ion recombination coefficient* $\beta = 10^{-7}\,\mathrm{cm^3/s}$ and the initial plasma density $n_e^0 = 10^{10}\,\mathrm{cm^{-3}}$, then the characteristic decay time $\tau_r = (\beta n_e^0)^{-1} = 10^{-3}\,\mathrm{s}$. The recombination coefficient can be determined experimentally, by measuring $n_e(t)$ and plotting n_e^{-1} as a function of t. The slope of the straight line gives β.

4.3.2 Dissociative Recombination

4.3.3 Radiative Recombination

Cross sections of the process $A^+ + e \rightarrow A + h\nu$ are very small: $\sigma_c \sim 10^{-21}\,\mathrm{cm^2}$. The recombination coefficient is correspondingly small [4.9]

$$\beta_{rr} = \langle v\sigma_c\rangle \approx 2.7\cdot 10^{-13}\{T_e[\mathrm{eV}]\}^{-3/4}\,\mathrm{cm^3/s} \sim 10^{-12}\,\mathrm{cm^3/s} . \tag{4.9}$$

Electric discharges

4.3.4 Radiative Recombination in Three-Body Collisions

This process follows the scheme $A^+ + e + e \rightarrow A + e$; it is the main process in high-density low-temperature equilibrium plasma where $T \approx T_e \sim 10^4$ and the concentration of molecular ions is too low for dissociative recombination to be significant. In three-body collisions, electrons are captured by ions to form very high by excited atoms with a binding energy of order kT. An excited atom is then gradually deactivated by subsequent electron impacts, it "cascades" down the level staircase, and finally falls to the ground state from the lower excited state by radiative transition. This completes the process of recombination; its coefficient is [4.9]

$$\begin{aligned} \beta_{\mathrm{crr}} &= 8.75 \cdot 10^{-27} \{T[\mathrm{eV}]\}^{-9/2} n_e \\ &= 5.2 \cdot 10^{-23} \{T[\mathrm{kK}]\}^{-9/2} n_e \, \mathrm{cm}^3/\mathrm{s} \, . \end{aligned} \tag{4.10}$$

According to (4.9, 10), β_{crr} exceeds the radiative recombination coefficient if

$$n_e > 3.1 \cdot 10^{13} \{T[\mathrm{eV}]\}^{3.75} = 3.2 \cdot 10^9 \{T[\mathrm{kK}]\}^{3.75} \, \mathrm{cm}^{-3} \, . \tag{4.11}$$

The recombination rate constant of triple collisions involving an atom as a third particle, β/N, is less than β_{crr}/n_e of (4.10) by a factor of $10^7 - 10^8$. This process is not typical for discharge conditions and can manifest itself only at very weak ionization and high pressures.

Electric discharges – Electron attachment

4.4 Formation and Decay of Negative Ions

4.4.1 Attachment

$$e + O_2 + 3.6\,\text{eV} \to O + O^- ,$$
$$e + CO_2 + 3.85\,\text{eV} \to CO + O^- ,$$
$$e + H_2O + 4.25\,\text{eV} \to OH + H^- ,$$
$$e + H_2O + 3.6\,\text{eV} \to H_2 + O^- ,$$
$$e + H_2O + 3.2\,\text{eV} \to H + OH^- .$$

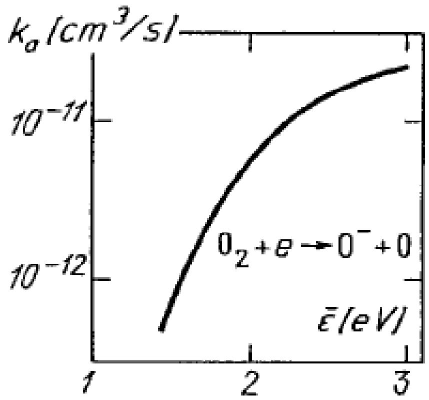

Fig. 4.11. Dissociative attachment rate constant of O_2 as a function of mean electron energy. From [4.12]

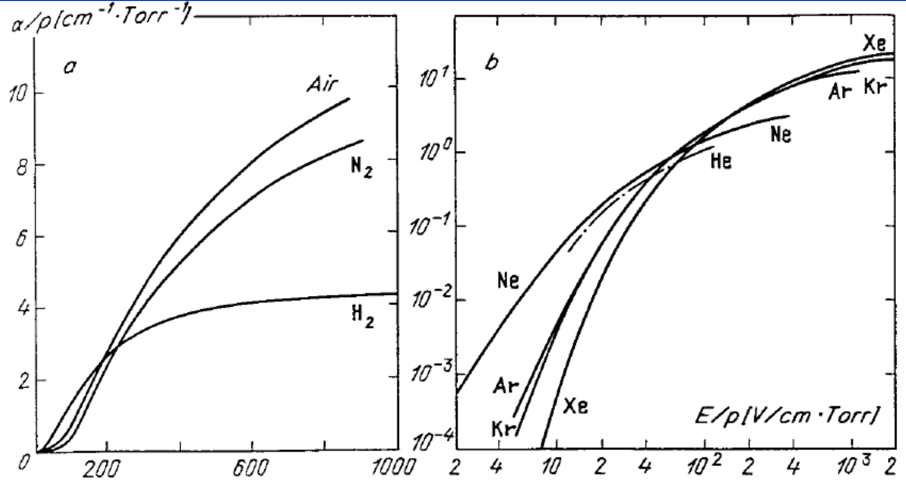

Fig. 4.3. Ionization coefficients for a wide range of E/p values (**a**) in molecular gases, (**b**) in inert gases. From [4.3]

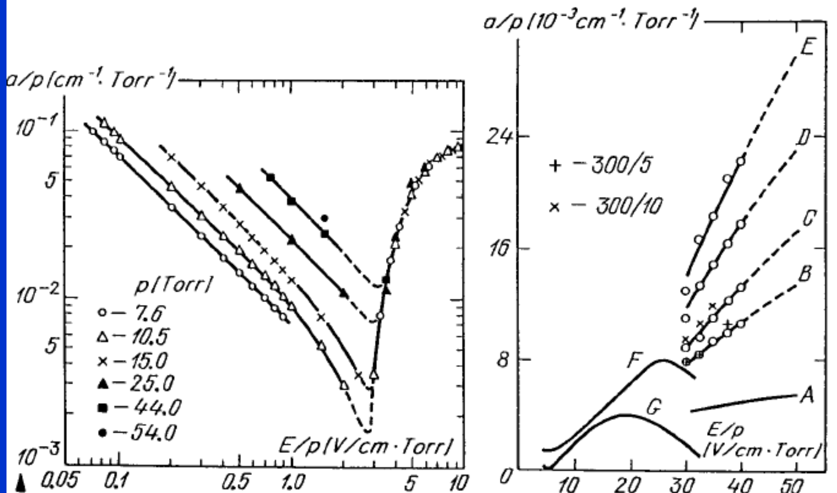

Fig. 4.12. Electron attachment coefficient in pure oxygen at $T = 300\,\text{K}$ and various pressures. From [4.12]

Fig. 4.13. Electron attachment coefficient in moist air, for various air humidity values: *A*: dry air; *B*: total pressure 150 Torr, water vapor pressure 2.5 Torr (150/2.5); *C* (150/5); *D* (150/9); *E* (150/15); *F* and *G* – air with negligible amount of water vapor. From [4.13, 14]

The multiplication of electrons in an avalanche is determined by the effective coefficient $\alpha_{\text{eff}} = \alpha - a$. If $\alpha < a$ (this happens at E/p less than a certain value for a given gas, see Sect. 7.2.5), multiplication becomes impossible.

Ionization contra electron attachment

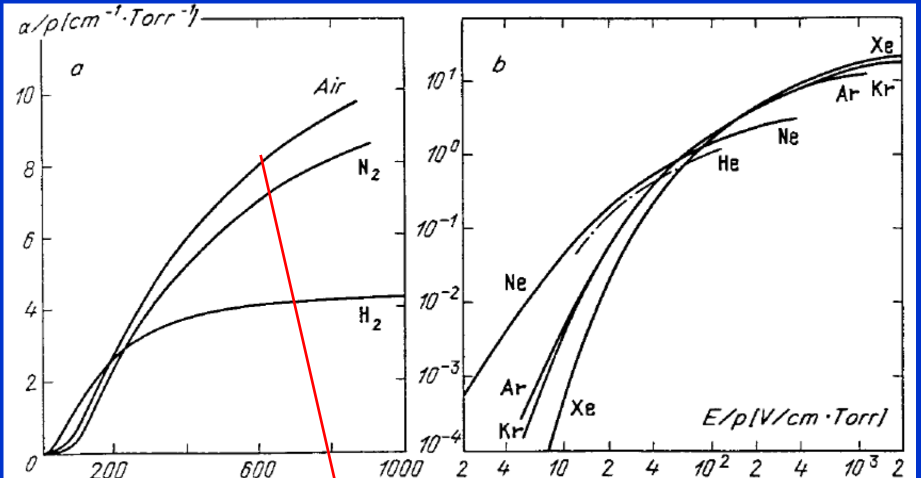

Fig. 4.3. Ionization coefficients for a wide range of E/p values (**a**) in molecular gases, (**b**) in inert gases. From [4.3]

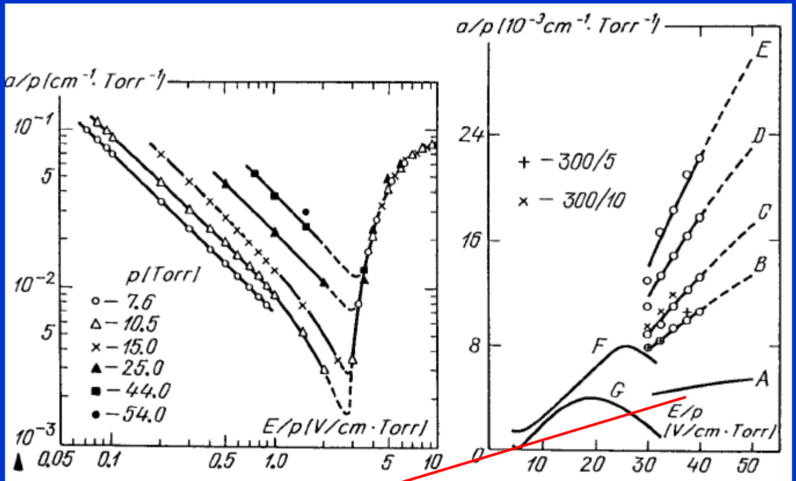

Fig. 4.12. Electron attachment coefficient in pure oxygen at $T = 300$ K and various pressures. From [4.12]

Fig. 4.13. Electron attachment coefficient in moist air, for various air humidity values: A: dry air; B: total pressure 150 Torr, water vapor pressure 2.5 Torr (150/2.5); C (150/5); D (150/9); E (150/15); F and G – air with negligible amount of water vapor. From [4.13, 14]

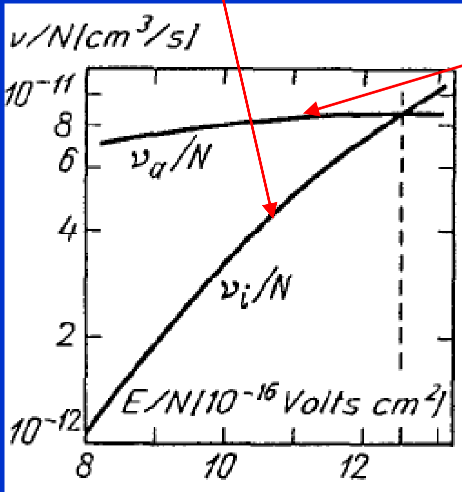

$$dN_e/dx = (\alpha - a)N_e\,, \quad N_e \propto \exp(\alpha - a)x\,;$$

Breakdown condition

Fig. 7.5. Ionization and attachment frequencies in air, calculated using the solution of the kinetic equation. Intersection at $E/p = 41$ V/cm·Torr

Electric discharges - cathode

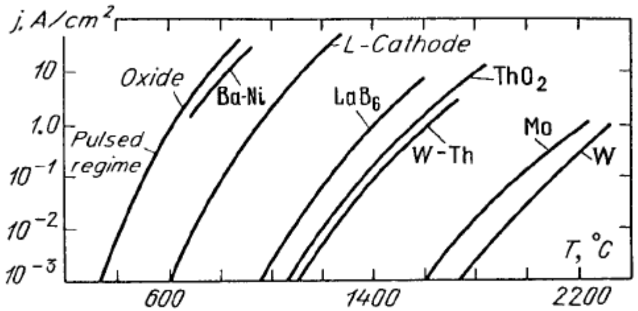

Fig. 4.14. Current density of thermionic emission as a function of cathode temperature for a number of materials. From [4.16]

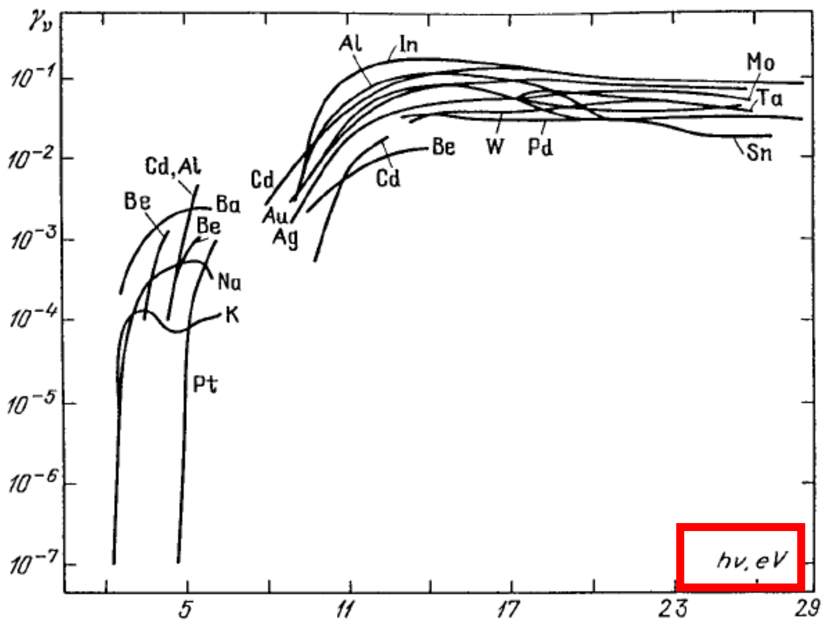

Fig. 4.16. Photoelectron emission coefficients (quantum yield) for various metals as functions of photon energy. From [4.2]

Paschen law – data gama

$$i = \frac{i_0 \exp(\delta d)}{1 - \gamma[\exp(\delta d) - 1]}\,, \qquad (5.5)$$

V důsledku emise opouští povrch katody elektrony s hustotou toku γj_+

$E/p \sim 30$—40 В/(см·тор), характерных для пробоя плотных газов, в

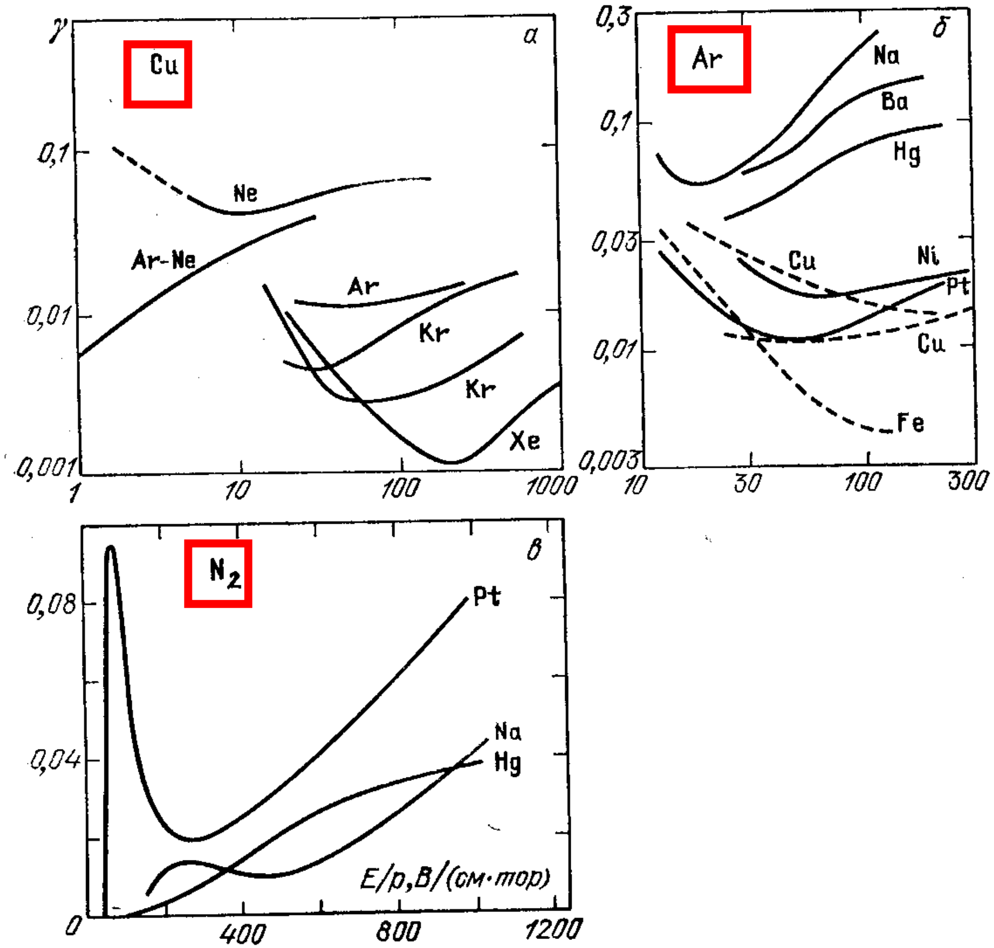

Р и с. 6.13. Коэффициент ионно-электронной эмиссии, определенный из разрядного эксперимента (п. 4.1): *а* — медный катод в инертных газах; *б* — различные металлы в Ar; *в* — различные металлы в N_2 [6]

Electric discharges

7.2 Breakdown and Triggering of Self-Sustained Discharge in a Constant Homogeneous Field at Moderately Large Product of Pressure and Discharge Gap Width

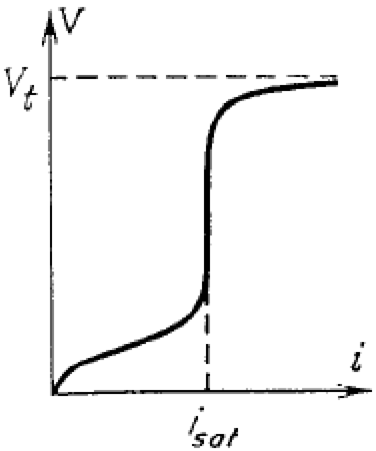

Fig. 7.1. $V - i$ characteristic of non-self-sustaining discharge between plane electrodes

Electric discharges Townsend avalanche theory

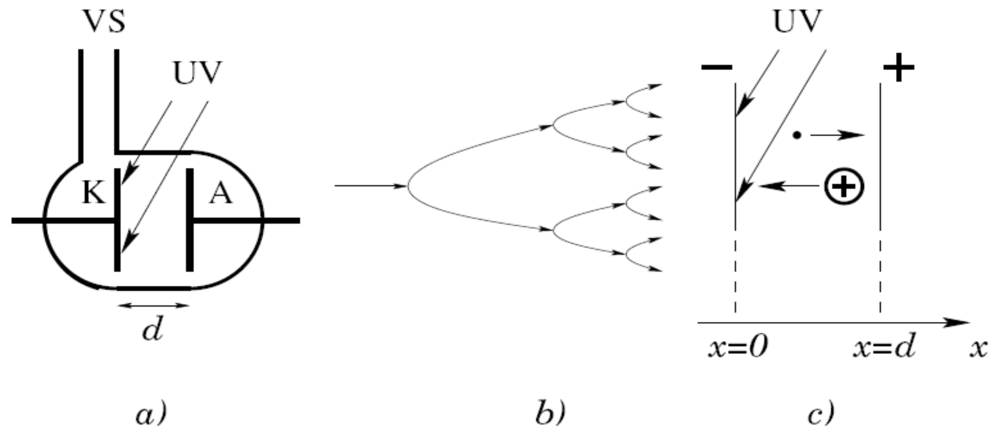

Obr. 5.2: Zapaľovanie výboja: *a*) výbojka na meranie zapaľovacieho napätia: K - katóda, A - anóda, UV - ultrafialové žiarenie zabezpečujúce emisiu primárnych elektrónov, VS - napojenie na vákuový systém; *b*) elektrónová lavína; *c*) označenie polohy elektród

Electric discharges Townsend avalanche theory

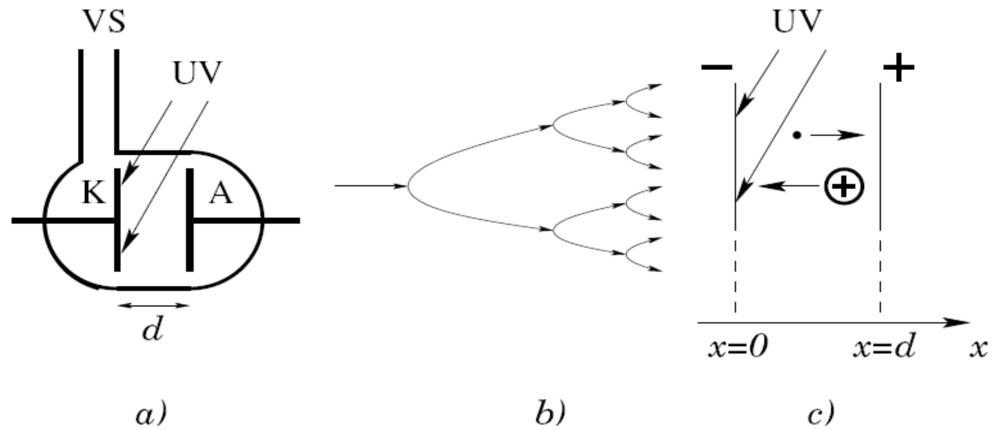

Obr. 5.2: Zapaľovanie výboja: *a*) výbojka na meranie zapaľovacieho napätia: K - katóda, A - anóda, UV - ultrafialové žiarenie zabezpečujúce emisiu primárnych elektrónov, VS - napojenie na vákuový systém; *b*) elektrónová lavína; *c*) označenie polohy elektród

$$\frac{\mathrm{d}j_-}{\mathrm{d}x} = \alpha n_- = \frac{\alpha}{V_-} n_- V_- = \delta j_-$$

medzi elektródami (obr. 5.2 *c*). Povrch katódy K sa nachádza v mieste $x = 0$ a povrch anódy A v mieste $x = d$. Elektróny sa pohybujú smerom k anóde a vytvorené kladné ióny ku katóde, kde zanikajú. Podobne ako v odseku 4.3.1, môžeme napísať rovnicu kontinuity pre elektróny v jednorozmernej geometrii a v ustálenom stave

$$\boxed{\frac{\mathrm{d}j_-}{\mathrm{d}x} = \alpha n_- = \frac{\alpha}{V_-} n_- V_- = \delta j_-}, \tag{5.2}$$

kde V_- je driftová rýchlosť elektrónov v elektrickom poli (v homogénnom poli je konštantná) a $\delta = \alpha / V_-$ je **prvý Townsendov koeficient**. Analogická rovnica platí aj pre kladné ióny

$$\frac{\mathrm{d}j_+}{\mathrm{d}x} = \alpha n_- = \delta j_- \,. \tag{5.3}$$

Townsendov výboj

Prvý Townsendov koeficient δ má rozmer m^{-1} a označuje počet ionizácii, ktoré vykoná jeden elektrón v smere elektrického poľa na jednotkovej dráhe (na rozdiel od ionizačnej frekvencie α udávajúcej počet ionizácií za jednotku času). Ak rovnice odčítame, dostaneme

$$\frac{\mathrm{d}(j_+ - j_-)}{\mathrm{d}x} = 0 \qquad \Rightarrow j_+ - j_- = K = \text{ konšt}\,.$$

Potom hustota elektrického prúdu medzi elektródami $i = e(j_+ - j_-) = eK$ je taktiež konštantná, napriek tomu, že hustoty toku elektrónov a iónov sa menia s polohou x.

V homogénnom poli je Townsendov koeficient δ konštantný a preto môžeme rovnice kontinuity ľahko integrovať

$$j_- = C\exp(\delta x)\,; \qquad j_+ = C\exp(\delta x) + i/e\,,$$

kde C je integračná konštanta. Hodnota tejto integračnej konštanty sa dá určiť z hustoty toku elektrónov na katóde: $C = j_-(0)$. Potom

$$j_- = j_-(0)\exp(\delta x)\,; \qquad j_+ = j_-(0)\exp(\delta x) + i/e\,. \tag{5.4}$$

Problém určenia hustoty toku $j_-(0)$ spočíva v tom, že okrem primárnych elektrónov emitovaných z katódy ultrafialovým žiarením (ich hustotu toku označíme j_0), elektróny emitujú aj dopadajúce kladné ióny. Tento typ emisie sa nazýva **potenciálová emisia**.

Potenciálová emisia

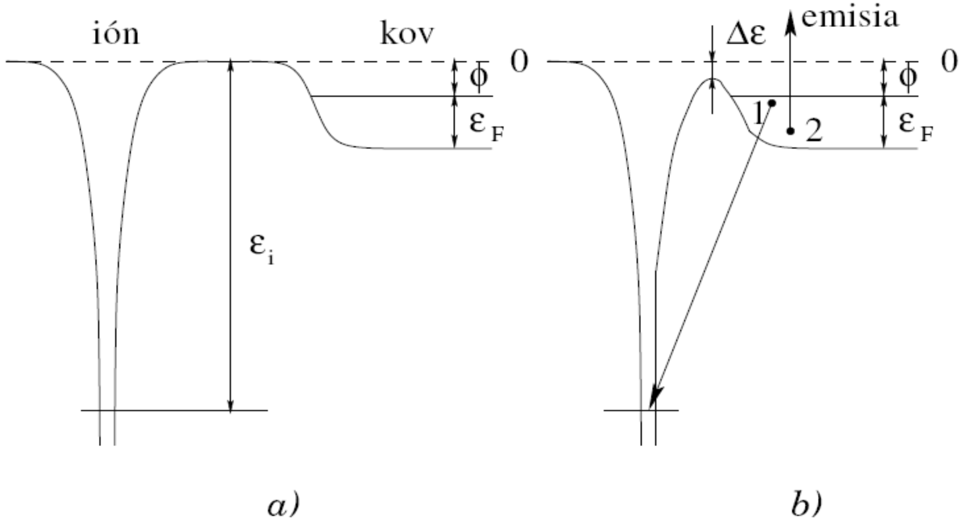

Obr. 5.3: Emisia elektrónu pri dopade kladného iónu na povrch kovu: *a*) ión je ďaleko od povrchu: ε_i - ionizačná energia atómu, Φ - výstupná práca kovu a ε_F - Fermiho energia; *b*) kladný ión pri dopade na povrch kovu: 1 - elektrón prechádza na neobsadenú hladinu v ióne, 2 - emitovaný elektrón preberá prebytočnú energiu

Augerova emisia

plynu. Ak však vypneme ultrafialové žiarenie, hustota primárnych elektrónov i_0 klesne na nulu a potom tiež $i = 0$. Lavínová ionizácia sa teda samostatne neudrží. Preto tento typ výboja nazývame **nesamostatný výboj** alebo tiež **Townsendov výboj**. Townsendov výboj je teda predprierazovým štádiom. Pri dostatočne silných poliach sa začne

lovej emisie opúšťajú povrch elektróny s hustotou toku γj_+. Koeficient γ reprezentuje výťažok elektrónov pri emisii, ktorý sa často (nelogicky) nazýva koeficient sekundárnej emisie. V teórii zapaľovania výboja sa zvykne nazývať **druhý Townsendov koeficient** (v staršej literatúre aj tretí Townsendov koeficient). Obvykle nadobúda hodnoty 0,1 – 10^{-3} (pre ióny veľkých organických molekúl až 10^{-10}).

Breakdown condition: Paschen's law

When the electric field in the in the electrode space ***E* is sufficiently high to create the multiplication** of the electrons and ions, **the avalanche appears**. If this multiplication creates a sufficient number of electrons and ions, it will lead to the electrical breakdown. However, if the processes of free charge species losses are emphasized, the avalanche multiplication can cease. Due to the **statistical nature** of both creation and loss of free species, breakdown may not occur even if applied voltage *U*w is higher than the breakdown voltage *U*b.

The breakdown condition for the gases at low pressures can be obtained using Townsend's theory, including the fact that influence of the space charge can be neglected in the early stage of the breakdown. Space charge is needed for the determination of the regime that will be established after the breakdown.

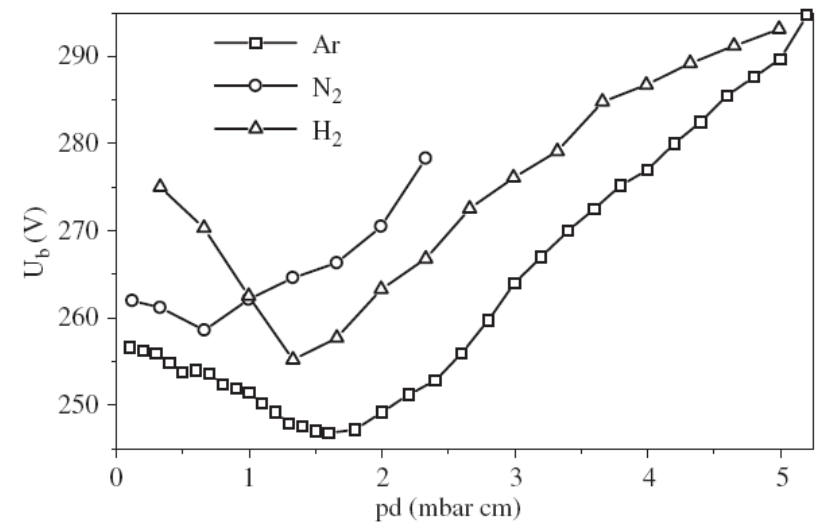

Figure 1. Breakdown voltage U_b in three gases as a function of pd values (Paschen curves).

$$N_a = N_0 \frac{\exp(\alpha d)}{1 - \gamma[\exp(\alpha d) - 1]},$$

The breakdown condition

$$\gamma[\exp(\alpha d) - 1] = 1$$

$$\alpha d = \ln\left(1 + \frac{1}{\gamma}\right)$$

$$\alpha = Ap \exp\left(-\frac{Bp}{E}\right)$$

It also means that the current can be sustained if the external source of radiation is absent ($N_0 = 0$), i.e. it is self-sustaining discharge. In other words, equation (5) represents a condition for breakdown initiation.

$$Apd \exp -\frac{Bp}{E} = \ln\left(1 + \frac{1}{\gamma}\right)$$

$$U_b = \frac{Bpd}{\ln(Apd) - \ln[\ln(1 + 1/\gamma)]}$$

Electric discharges

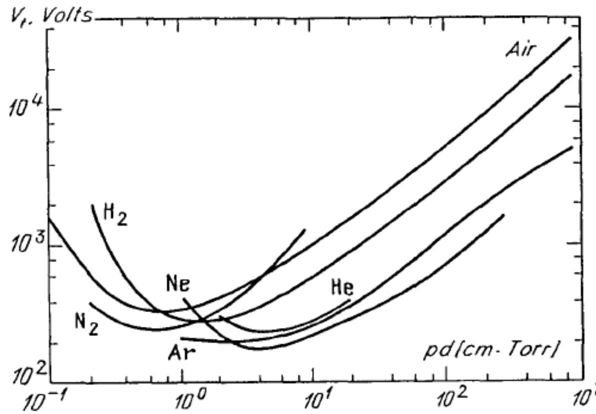

Fig. 7.2. Breakdown potentials in various gases over a wide range of *pd* values (Paschen curves) on the basis of data given in [7.1, 2]

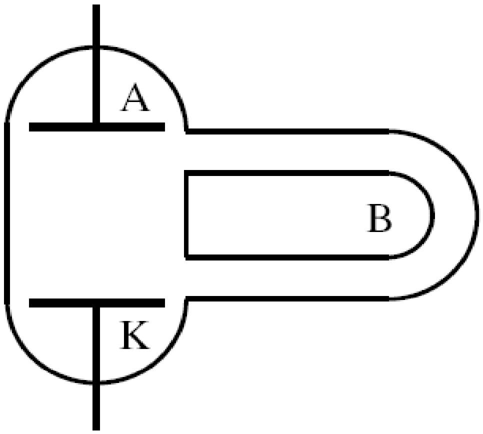

Obr. 5.6: Výbojka s bočnou dráhou B na demonštráciu nestability nízkotlakovej vetvy Paschenovej krivky

Electric discharges

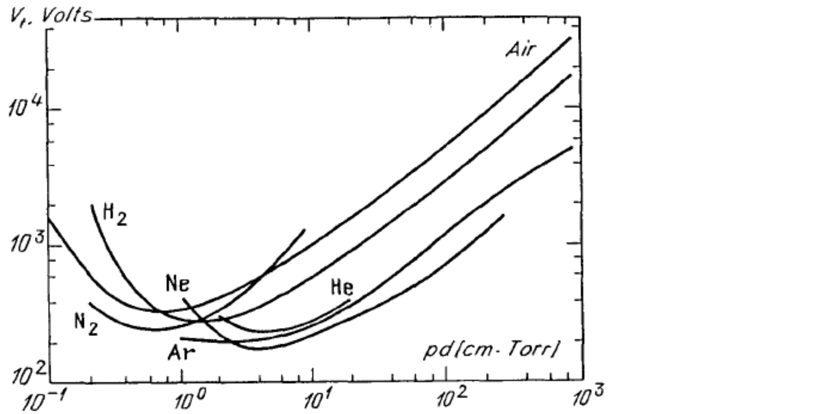

Fig. 7.2. Breakdown potentials in various gases over a wide range of *pd* values (Paschen curves) on the basis of data given in [7.1, 2]

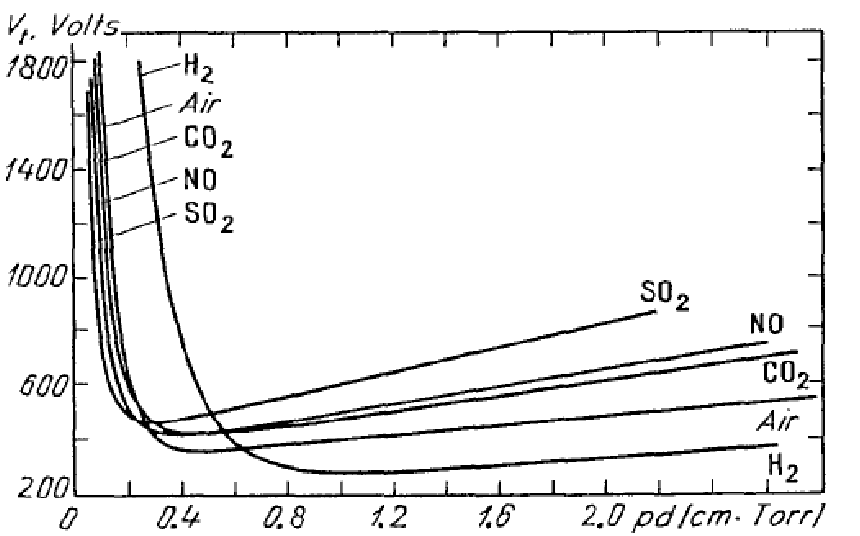

Fig. 7.3. Paschen curves on an enlarged scale [7.3]

$$U_b = \frac{Bpd}{\ln(Apd) - \ln[\ln(1 + 1/\gamma)]}$$

$$(pd)_{\min} = \frac{\bar{e}}{A} \ln\left(\frac{1}{\gamma} + 1\right), \quad \left(\frac{E}{p}\right)_{\min} = B, \quad V_{\min} = \frac{\bar{e}B}{A} \ln\left(\frac{1}{\gamma} + 1\right)$$

Paschen law curves

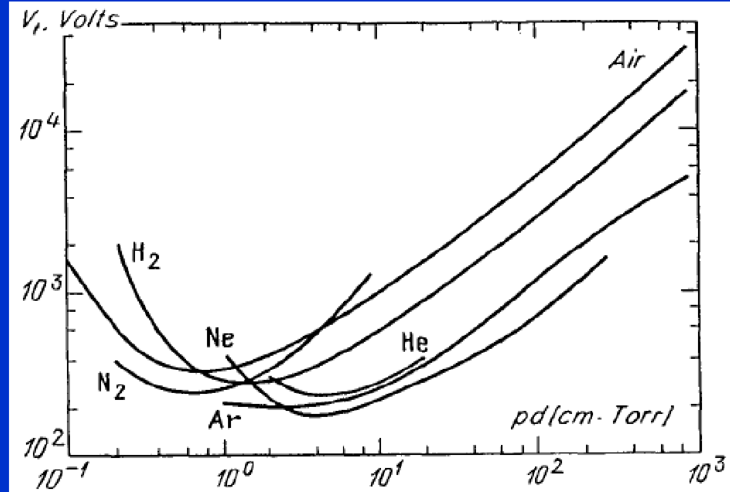

Fig. 7.2. Breakdown potentials in various gases over a wide range of *pd* values (Paschen curves) on the basis of data given in [7.1, 2]

Ar

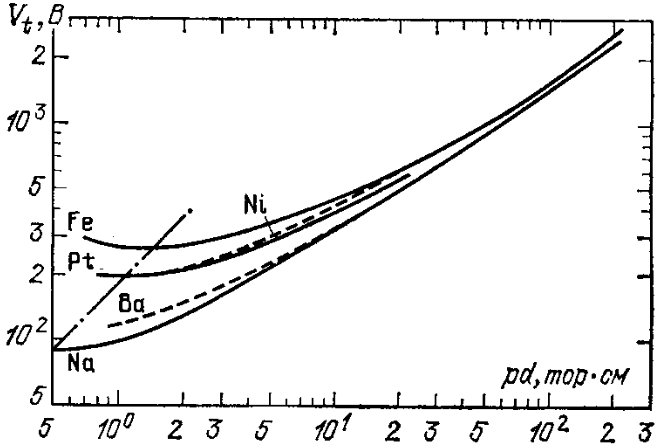

Рис. 13.3. Влияние материала катода на напряжение пробоя аргона. Штрихпунктирная прямая соединяет точки минимума. Ее наклон 45° соответствует независимости $(E/p)_{\min}$ от материала катода [6]

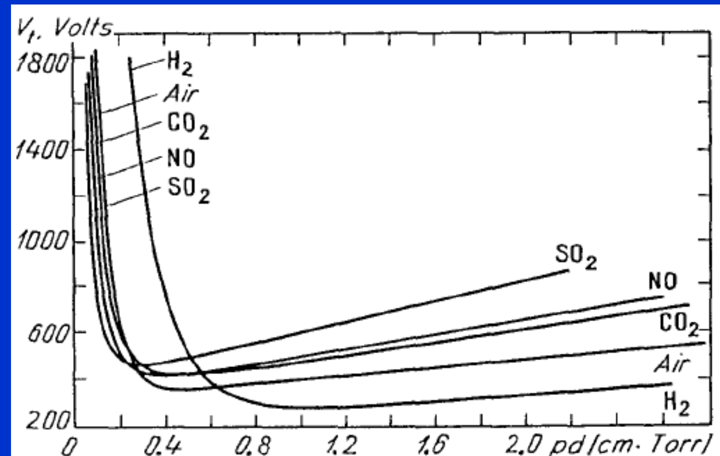

Fig. 7.3. Paschen curves on an enlarged scale [7.3]

Electric discharges

Breakdown Fields in Moderately Large Gaps in Air and Other Electronegative Gases at Atmospheric Pressure. Limiting Values of pd for the Townsend Breakdown Mechanism

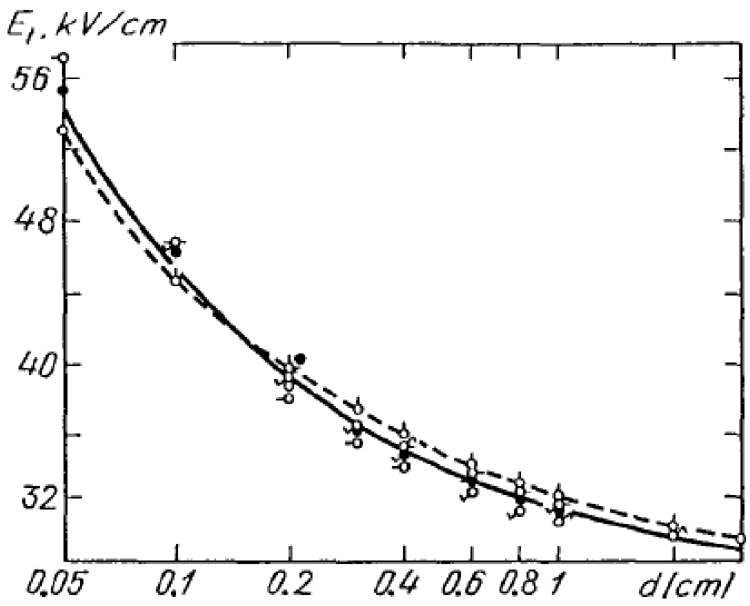

Fig. 7.4. Breakdown fields in a plane gap of length d in air at $p = 1$ atm. From [7.1]

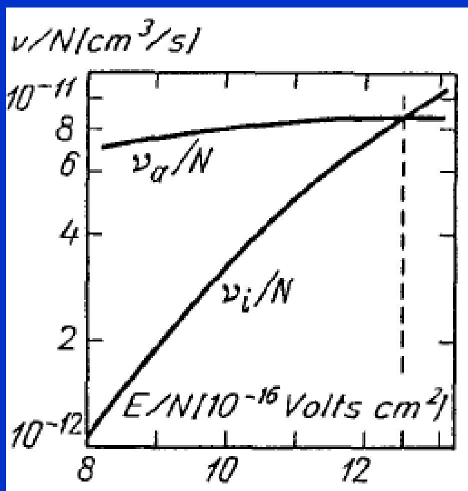

$$dN_e/dx = (\alpha - a)N_e\ , \quad N_e \propto \exp(\alpha - a)x\ ;$$

Fig. 7.5. Ionization and attachment frequencies in air, calculated using the solution of the kinetic equation. Intersection at $E/p = 41$ V/cm·Torr

Electric discharges

Table 7.1. Approximate values of breakdown threshold at high pressure

Gas	Constant field, gap width less than several cm, $p \sim 1$ atm		Microwaves, $p \sim 100$–300 Torr
	E/p kV/(cm·atm)	E/p V/(cm·Torr)	E/p V/(cm·Torr)
He	10	13	3
Ne	1.4	1.9	3–5
Ar	2.7	3.6	5–10
H_2	20	26	10–15
N_2	35	46	$\sim$ 25
O_2	30	40	35
Air	32	42	$\sim$ 30
Cl_2	76	100	
$CCl_2F_2^*$	76	100	
CSF_8	150	200	
CCl_4	180	230	
SF_6	89	117	

* Freon

Breakdown

Таблица 13.1. Ориентировочные пороги пробоя газов при высоких давлениях

Газ	Постоянное поле, недлинные промежутки, $p \sim 1$ атм		СВЧ, $p \sim 100$—300 тор
	E_t/p, кВ/(см·атм)	E_t/p, В/(см·тор)	E_t/p, В/(см·тор)
He	10	13	3
Ne	1,4	1,9	3—5
Ar	2,7	3,6	5—10
H_2	20	26	10—15
N_2	35	46	~25
O_2	30	40	35
Воздух	32	42	~30
Cl_2	76	100	
CCl_2F_2 *)	76	100	
CSF_8	150	200	
CCl_4	180	230	
SF_6 **)	89	117	

*) Фреон
**) Элегаз

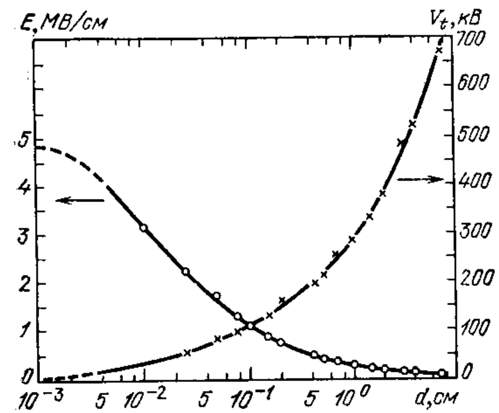

Р и с. 13.7. Напряжение и поле пробоя вакуумного промежутка между шаром диаметром 2,5 см и диском диаметром 5 см из стали в зависимости от длины промежутка [3]

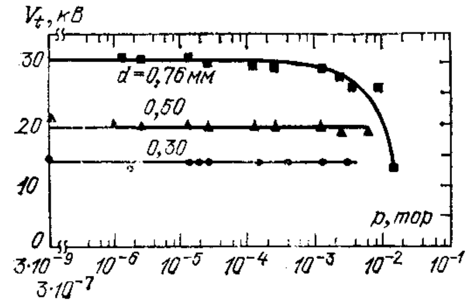

Р и с. 13.8. Напряжения пробоя коротких промежутков d между стальными электродами в зависимости от давления заполняющего их водорода. Независимость от p свидетельствует о вакуумном характере пробоя. Загиб вниз верхней кривой соответствует переходу к левой ветви кривой Пашена [15.3]

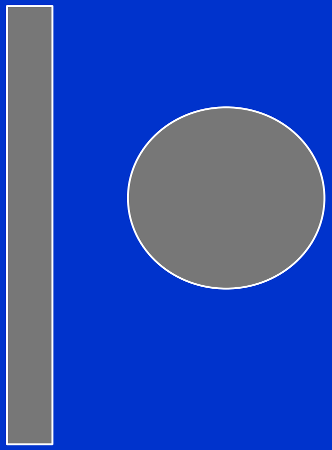

Electric discharges

Breakdown in Microwave Fields and Interpretation of Experimental Data Using the Elementary Theory

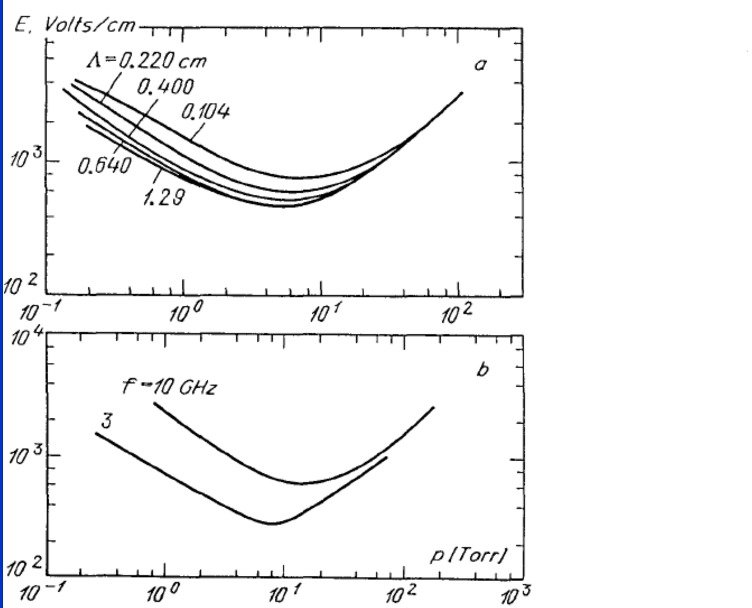

Fig. 7.8. Measured thresholds of microwave breakdown [7.6] (a) air, f = 9.4 GHz, diffusion length Λ is indicated for each curve; (b) Heg gas (He with an admixture of Hg vapor), Λ = 0.6 cm

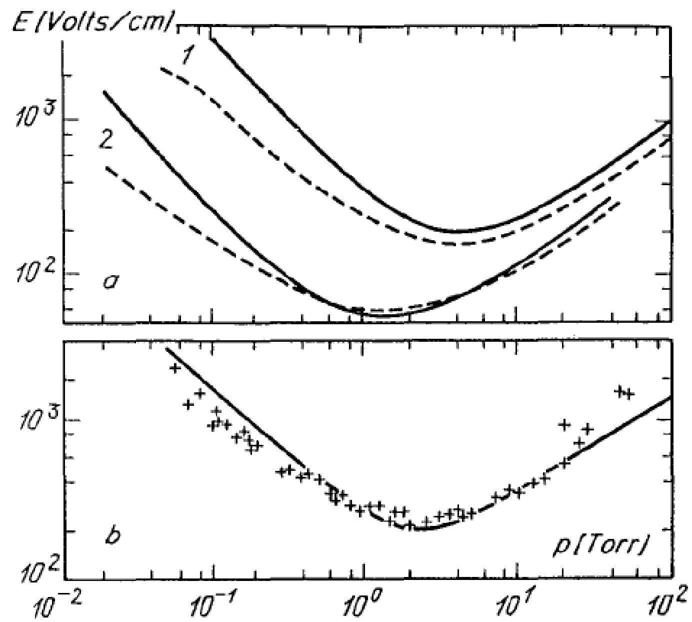

Fig. 7.10. Thresholds of microwave breakdown: (a) Ar, *(1)* f = 2.8 GHz, Λ = 0.15 cm; *(2)* f = 0.99 GHz, Λ = 0.63 cm; (b) Xe, f = 2.8 GHz, Λ = 0.10 cm. *Solid curves*, results of calculations [7.7]; *dashed curves* and *crosses* give experimental data [7.5]

for the total number of electrons, N_e, in the discharge volume:

$$dN_e/dt = (\nu_i - \nu_a - \nu_d)N_e \ , \quad \nu_d = D/\Lambda^2 \ , \tag{7.7}$$

where ν_d is the frequency of diffusion losses of electrons. This equation describes the ionization kinetics of the gas.

Influence of diffusion length

RF discharges

Influence of diffusion length

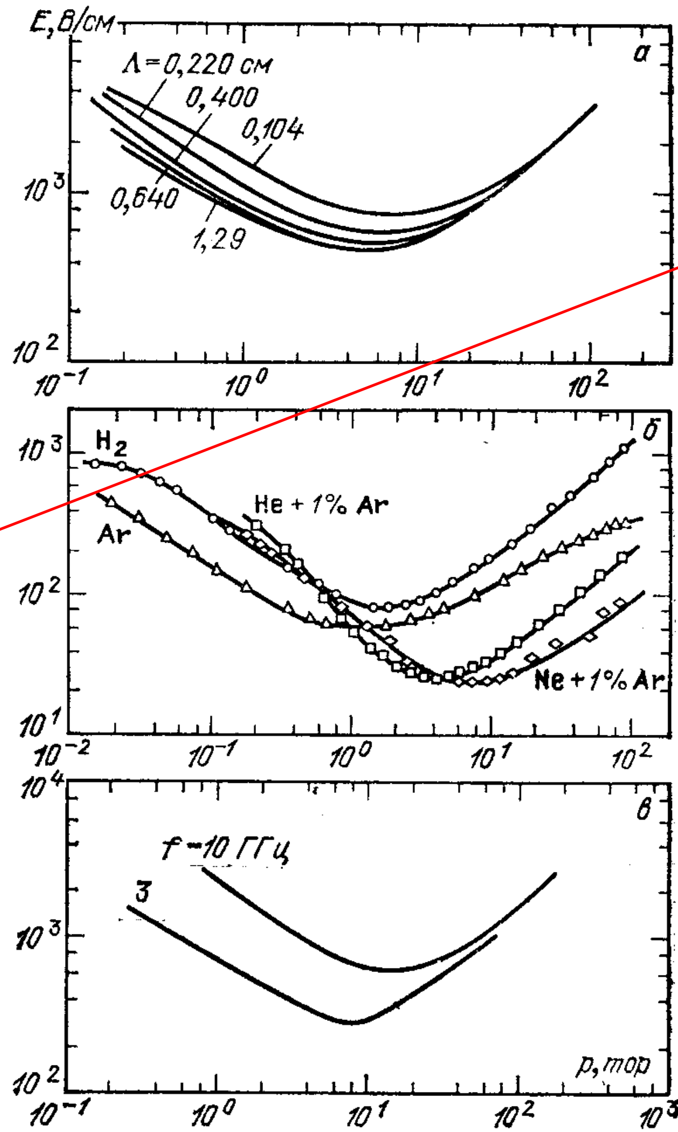

Р и с. 13.10. Измеренные пороги СВЧ пробоя: *а* — воздух, частота f=9,4 ГГц, около кривых указаны диффузионные длины Λ; *б* — несколько газов, f==0,99 ГГц, Λ=0,63 см; *в* — Heg-газ (гелий с добавкой паров ртути), Λ=0,6 см [24]

Electric discharges

Influence of diffusion length

7.3.2 Ionization Kinetics Equation

When oscillation displacements are small, electron densities obey an equation of type (2.44):

$$\partial n_e/\partial t = D\nabla^2 n_e + (\nu_i - \nu_a)n_e\ , \quad D \equiv D_e \tag{7.6}$$

(electrons diffuse freely in breakdown). If the condition $\omega \gg \nu_m \delta$ (Sect. 5.5.2) holds (it is satisfied for microwave frequencies), the electron energy distribution is quasisteady and the ionization and attachment frequencies, ν_i and ν_a, are determined by the root-mean-square field E. The dependencies $\nu_i(E)$, $\nu_a(E)$ are much stronger than $D_e(E)$, so that $D_e(E) \approx$ const. For simplification, assume that the field is spatially homogeneous, and hence, ν_i and ν_a are independent of coordinates. Averaging (7.6) over the volume, we obtain, in accord with the results of Sect. 4.5, an equation for the mean density, or (which is equivalent) for the total number of electrons, N_e, in the discharge volume:

$$dN_e/dt = \underline{(\nu_i - \nu_a - \nu_d)N_e}\ , \quad \nu_d = D/\Lambda^2\ , \tag{7.7}$$

where ν_d is the frequency of diffusion losses of electrons. This equation describes the ionization kinetics of the gas.

Electric discharges

7.3.3 Steady-State Background Criterion

Assume that the external field is switched on in a time small in comparison with the characteristic time of multiplication and remains constant during the avalanche buildup. This constraint covers not only stationary, but also pulsed fields with not too short pulses and sufficiently small rise time. Under this assumption, $\nu_i(t)$, $\nu_a(t)$ = const after the moment $t = 0$ at which the field is switched on, and (7.7) has an exponential solution typical of an avalanche process:

$$N_e = N_{e0} \exp[(\nu_i - \nu_a - \nu_d)] = N_{e0} \exp(t/\Theta) \,, \tag{7.8}$$

where Θ is the *avalanche time constant,* and N_{e0} is the number of seed electrons that start the avalanche.[1] Breakdown is impeded in experiments with short pulses, since the probability of an electron appearing in the region of the field at the necessary moment is quite low and the avalanche has to be initiated by injecting a small number of electrons. For this purpose, a weak radioactive source is used.

According to (7.8), an avalanche develops if $\nu_i - \nu_a - \nu_d > 0$; this condition is met if the field exceeds a threshold E_t determined by the *steady-state breakdown criterion*:

$$\nu_i(E_t) = \nu_d + \nu_a(E_t) \,. \tag{7.9}$$

As an example, consider breakdown in helium, for $p = 1$ Torr, $\lambda = 3$ cm, diffusion length $\Lambda = 1$ cm, $D = 2 \cdot 10^6\,\mathrm{cm^2/s}$, time of diffusion to the walls $\nu_d^{-1} \approx 5 \cdot 10^{-7}$ s, diffusion frequency $\nu_d \approx 2 \cdot 10^6\,\mathrm{s^{-1}}$, and no attachment. The avalanche develops if $\nu_i > \nu_d \approx 2 \cdot 10^6\,\mathrm{s^{-1}}$. We will show a little later that the ionization frequency $\nu_i \propto E^2$ under the most favorable conditions for multiplication (zero electron energy losses). If losses, especially inelastic, are nonzero, the ν_i vs. E curve is much steeper. Hence, if the field increases by 10 % in comparison with E_t, then $\Theta^{-1} = \nu_i - \nu_d \geq 0.2\nu_d \approx 4 \cdot 10^5\,\mathrm{s^{-1}}$. The number of electrons is doubled every $\Theta/\ln 2 \leq 1.7\,\mu$s, which is a very high rate. In many cases, it is sufficient for a reliable realization of breakdown. As a result, stationary criterion (7.9) determines with good accuracy [like criterion (7.1)] the breakdown threshold of gases for "not too short" pulses.

Electric discharges

7.5 Optical Breakdown

The discovery of the *optical breakdown* effect, in 1963 [7.8], became possible only after the development of Q-switched lasers that produce light pulses of tremendous power, called "giant pulses". When the light of such a (ruby) laser was passed through a focusing lens, a spark flashed in the air, in the focal region, as in the electrical breakdown of a discharge gap. The discovery was a complete surprise for physicists and produced a sensation at the time, though the element of surprise has worn off by now. Gas breakdown at optical frequencies requires a tremendous field strength, 10^6–10^7 V/cm, in the light wave; this was unthinkable before the advent of the laser. Furthermore, the necessary light intensity, about 10^5 MW/cm^2, could only be reached by focusing the light of not just an ordinary laser, but one operating in th giant pulse regime. The new effect caused unparalleled interest among physicists. In a short time, it was experimentally and theoretically investigated to such a degree [7.7], that by now we know at least as much about it as about its closest analogue, the microwave field breakdown.

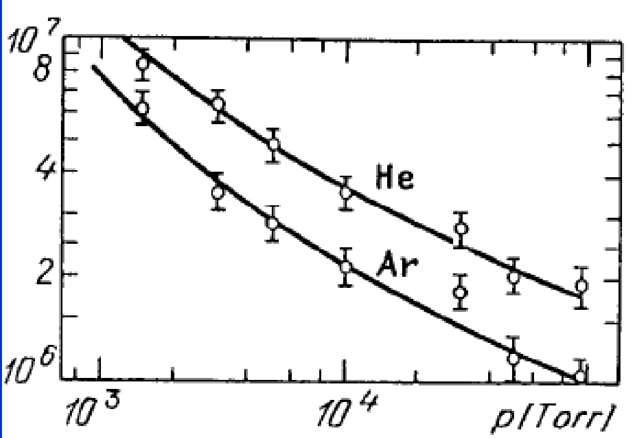

Fig. 7.11. Measured threshold fields for the breakdown of Ar and He by ruby laser radiation; pulse length 30 ns, diameter of focal spot $2 \cdot 10^{-2}$ cm [7.9]

Electric discharges

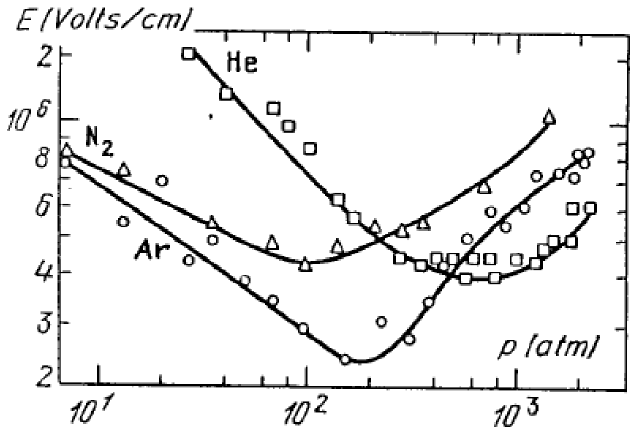

Fig. 7.12. Breakdown thresholds in Ar, He, N_2 for ruby laser radiation over a wide pressure range [7.10]. Pulse length 50 ns, focal spot diameter 10^{-2} cm

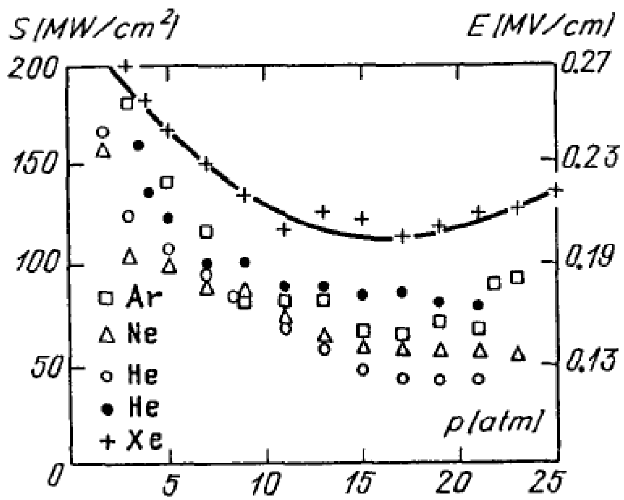

Fig. 7.13. Breakdown thresholds of inert gases in the radiation of a CO_2 laser [7.7]. The *black dots* represent data for helium of a higher purity

7.5.3 Breakdown Thresholds of Atmospheric Air

These data are very important. Quite a few physical experiments employ high-intensity laser beams. Electrical breakdown of air on the beam path to the target is an obstacle for light propagation because of absorption in the plasma. For example, in such experiments with high-power beams as target irradiation for fusion experiments one has to send the beam to the target through vacuum. The threshold intensity for the giant pulse of a ruby laser and an ordinary focal spot diameter of 10^{-2} cm is $S_t \approx 10^{11}$ W/cm^2, and the field is $E_t \approx 6 \cdot 10^6$ V/cm.

The breakdown threshold of nonfiltered air by focused CO_2 laser radiation is roughtly $2 \cdot 10^9$ W/cm^2, and that of dust-free air is not lower than 10^{10} W/cm^2. The tiniest dust particles floating in the air greatly facilitate the breakdown by CO_2 laser radiation, while their effect is negligible for the neodymium and, in particular, ruby lasers. This difference appears because the short-wave radiation of solidstate lasers "supplies itself" with the seed electrons required for starting an avalanche. The long-wave radiation of CO_2 lasers cannot do this in a pure gas.

Electric discharges

7.7 Breakdown in RF and Low-Frequency Ranges

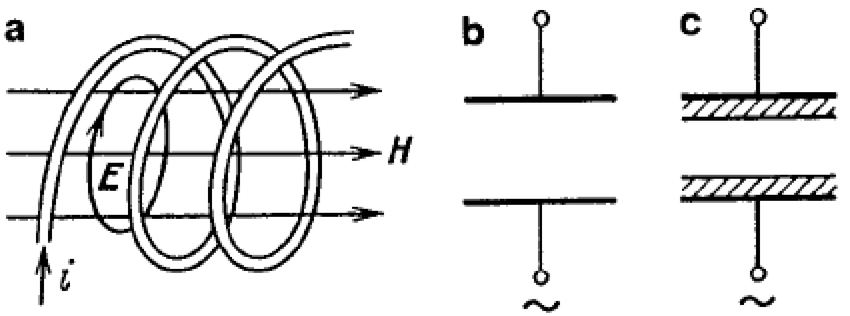

Fig. 7.18. Excitation of rf discharges: (a) inductively coupled through a solenoid coil; (b) voltage applied to electrodes in contact with plasma; (c) electrodes insulated from plasma (electrodeless, capacitively coupled rf discharge)

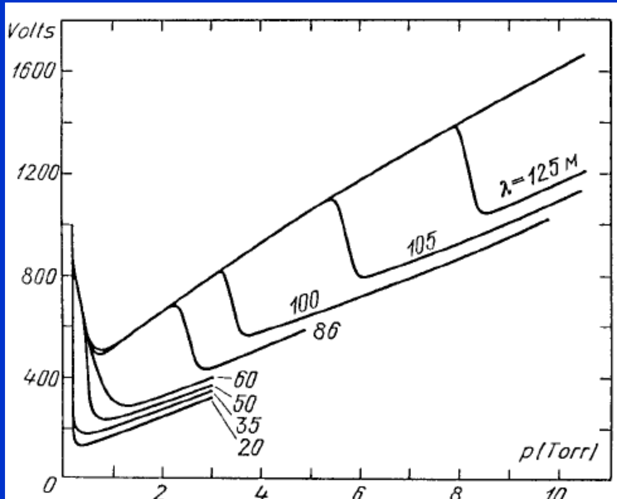

Fig. 7.20. Ignition potentials of ccrf discharge for various oscillation wavelengths [7.15]

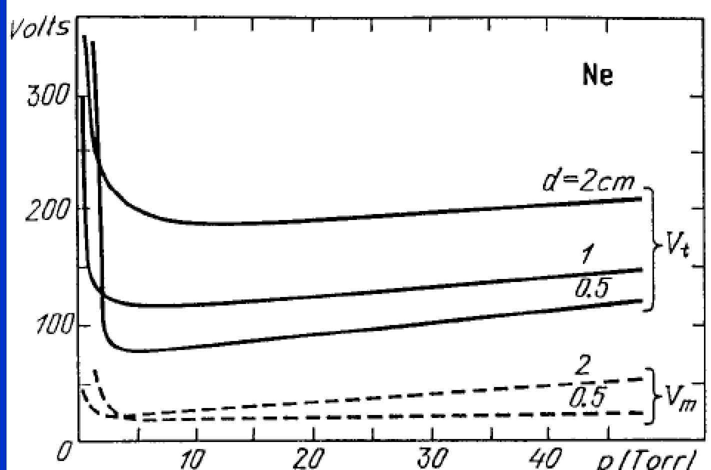

Fig. 7.19. Ignition potential of capacitively coupled rf discharge in neon (V_t), f = 158 MHz; d is the distance between the planar electrodes (which are covered by glass). *Dashed curves* show the burning voltage of a steady discharge, V_m [7.15]

Calculation of avalanche…

Definition of breakdown voltage and time delay

Electrical breakdown in gases does not take place instantly upon applying a voltage U_b to the electrodes of gas-filled tube, but **after a corresponding delay** known as electrical breakdown time delay $\boldsymbol{t_d}$ that is mutually dependent on U_b. Due to the statistical nature of processes which initiate breakdown, U_b and t_d are mutually dependent stochastic variables with certain distributions. The distribution function of t_d defines the probability of electrical breakdown in any time interval.

U_b is the voltage when the gas transits from non-selfsustaining to self-sustaining discharge

Due to the fluctuation of the parameters α and γ with time, the electrical breakdown usually does not occur for the same voltage in a series of experiments. Also, the breakdown voltage depends on the time dependence of the applied voltage.

t_d is the time elapsed from the instant of time when applied voltage reaches the breakdown voltage to the moment when it starts to decrease due to the breakdown in gas-filled tube

The other definition states that t_d is the time interval between the moment of U_w ($U_w > U_s$) application on the tube and the moment when the tube current exhibits a detectable discharge.

The t_d consists of the statistical time delay (t_s) and formative time (t_f), i.e. $t_d = t_s + t_f$

Breakdown voltage as a function of rate

U_b is the measured breakdown voltage and k is the rate of the increase of the applied voltage

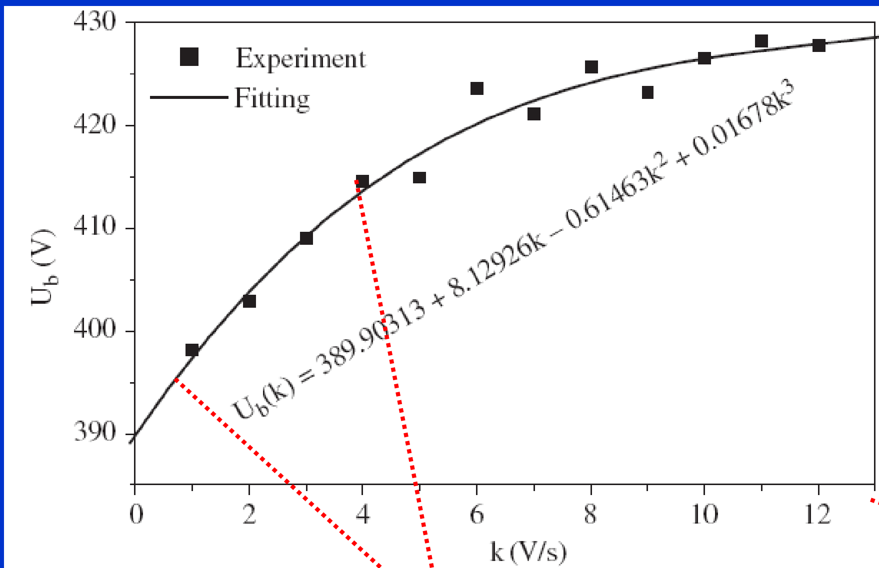

Figure 3. Breakdown voltage U_b as a function of the rate $k = 1$–$12\ \mathrm{V\,s^{-1}}$ of increase of the applied voltage.

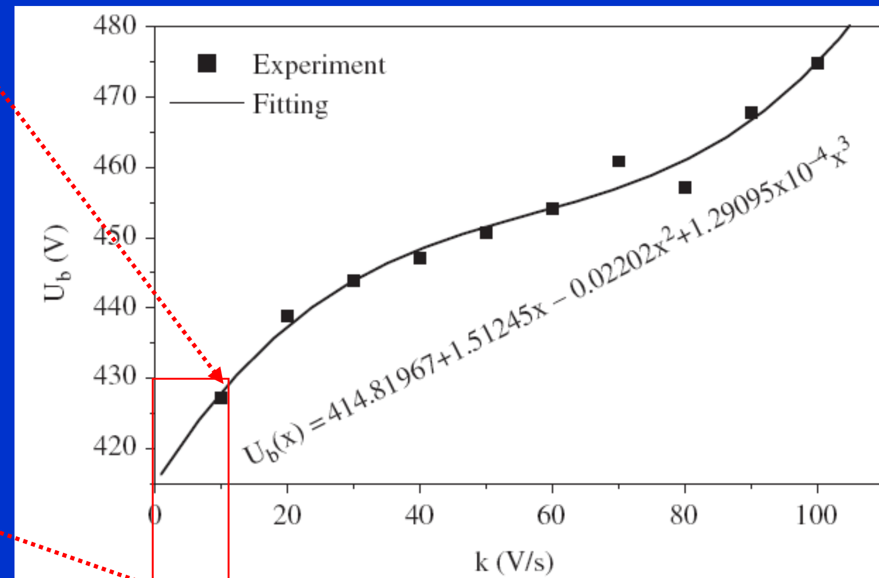

Figure 4. Breakdown voltage U_b as a function of the rate $k = 10$–$100\ \mathrm{V\,s^{-1}}$ of increase of the applied voltage.

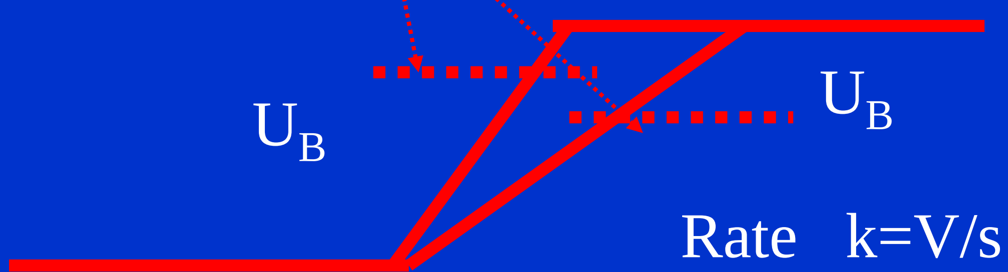

Breakdown voltage as a function of rate

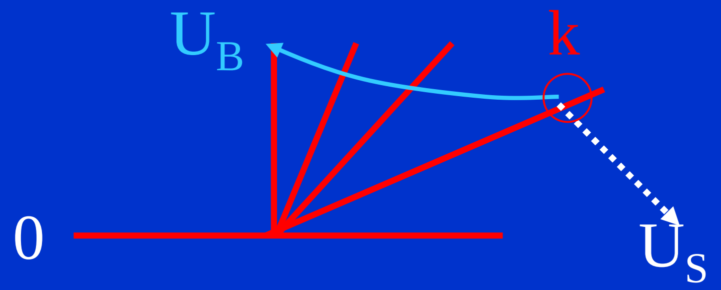

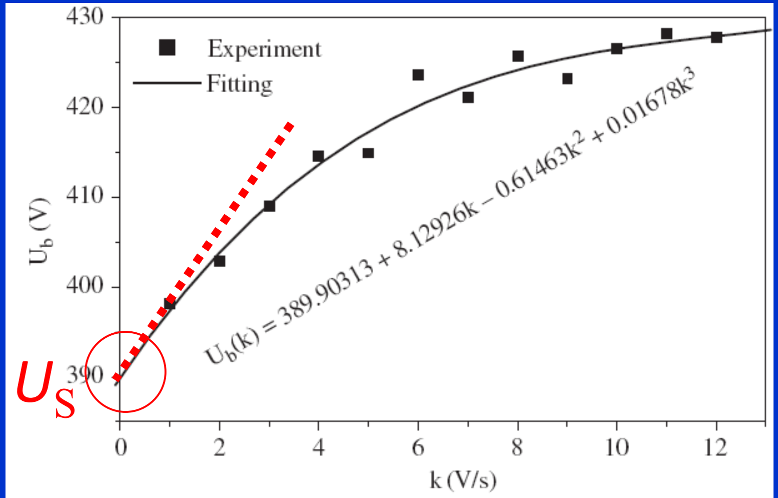

Figure 3. Breakdown voltage U_b as a function of the rate $k = 1\text{–}12\ \mathrm{V\ s^{-1}}$ of increase of the applied voltage.

estimated U_S value was ≈390V

Extrapolation of the $U_b = f(k)$ dependence to the intersect with U_b-axis (for $k = 0$) gives the estimation of U_s.

The t_d consists of the statistical time delay (t_s) and formative time (t_f), i.e. $t_d = t_s + t_f$

Breakdown voltage as a function of rate

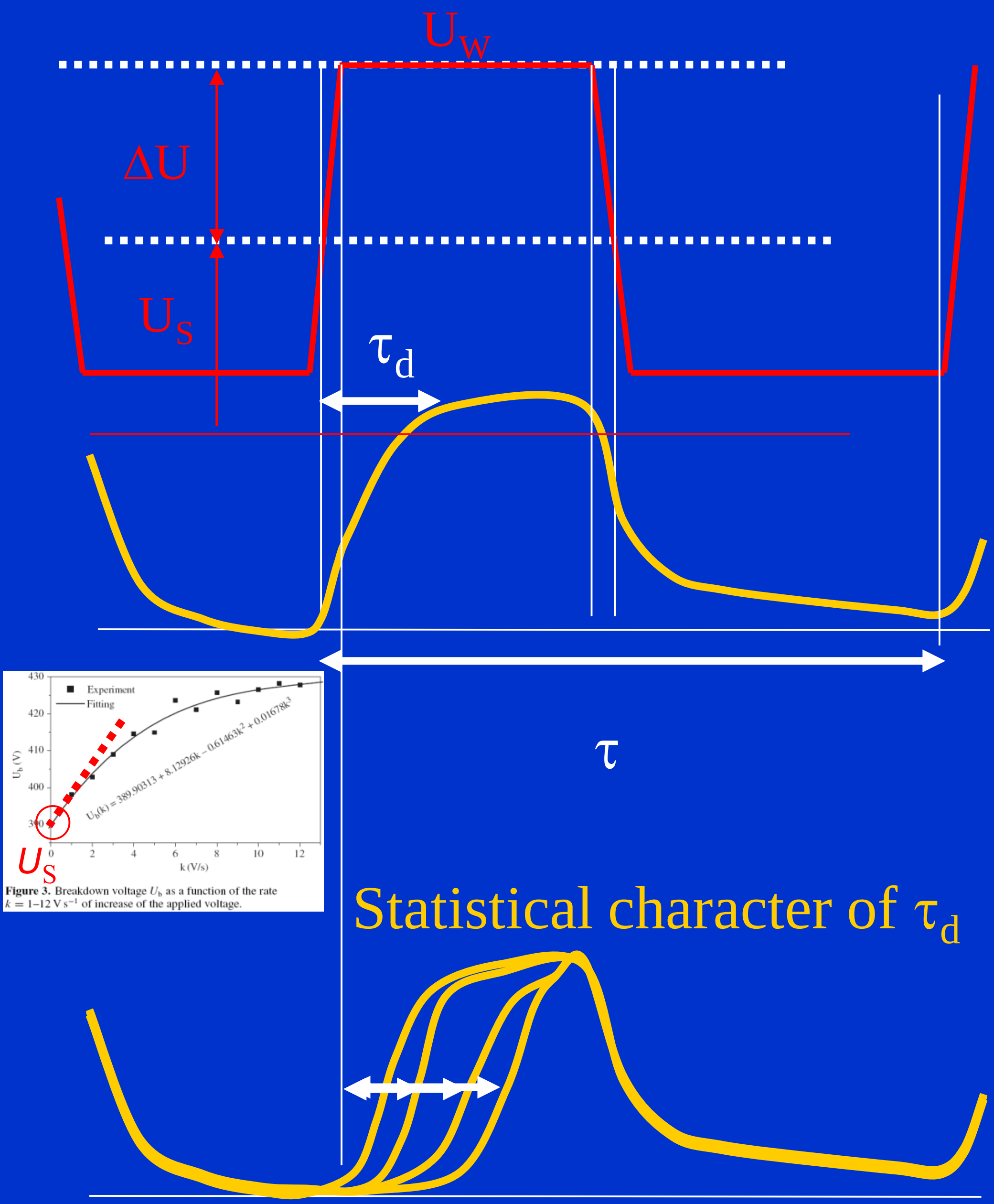

Figure 3. Breakdown voltage U_b as a function of the rate $k = 1$–$12\ \mathrm{V\,s^{-1}}$ of increase of the applied voltage.

Statistical character of τ_d

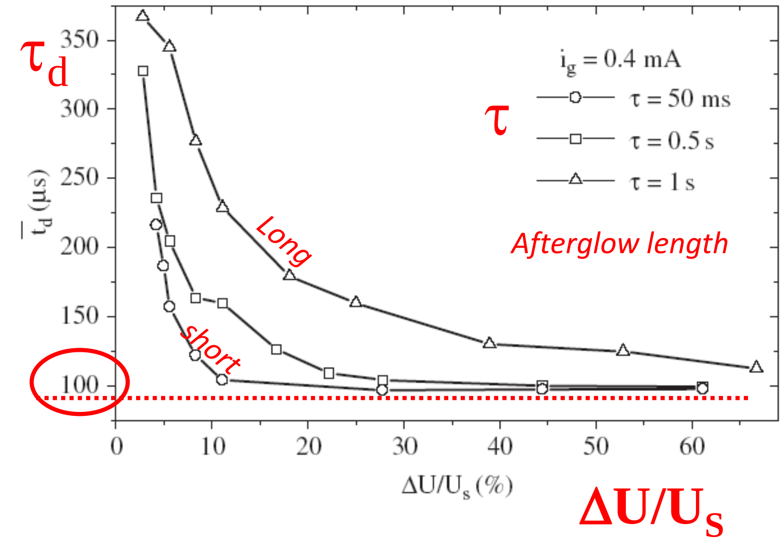

Figure 9. Mean value of time delay $\bar{t}_d$ as a function of overvoltage $\Delta U/U_s$ for three different values of afterglow period for nitrogen-filled tube at pressure 1.3 mbar [27] (©1998 IEEE).

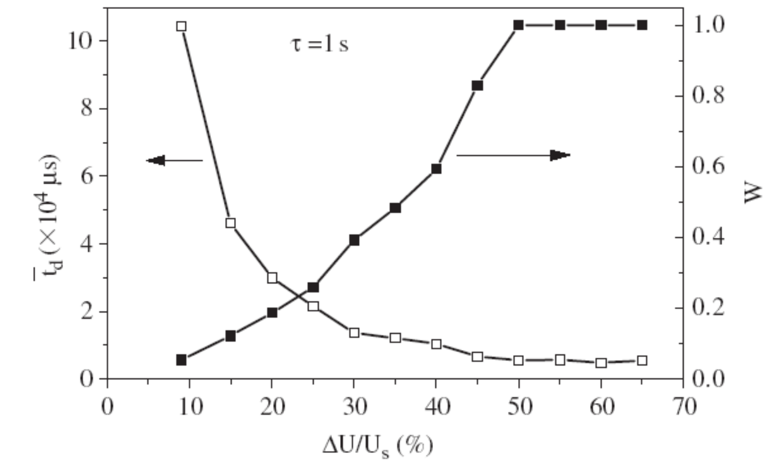

Figure 8. Mean value of time delay $\bar{t}_d$ and breakdown probability W as a function of overvoltage for kripton-filled tube at presssure 2.7 mbar [31].

Breakdown voltage as a function of rate

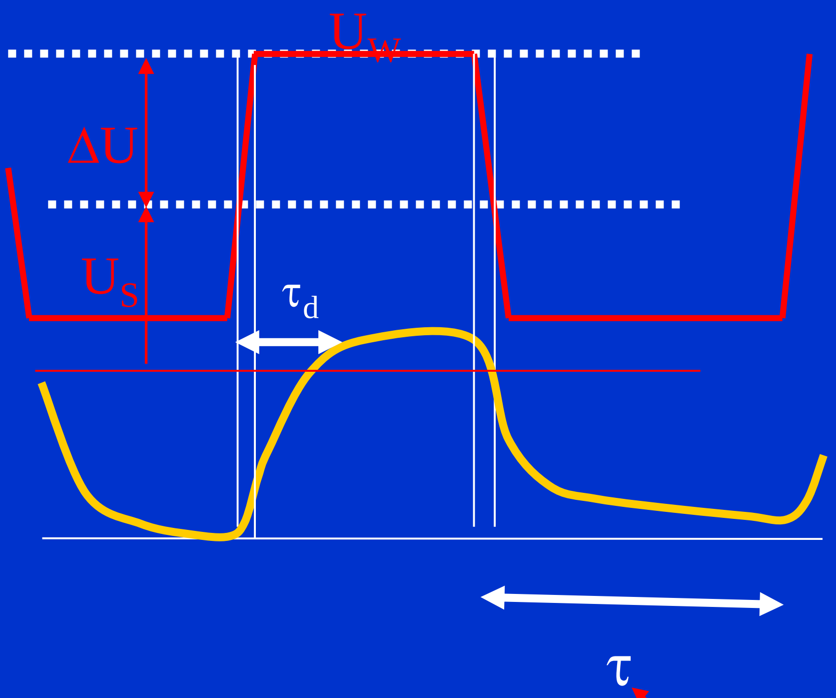

Statistical character of τ_d

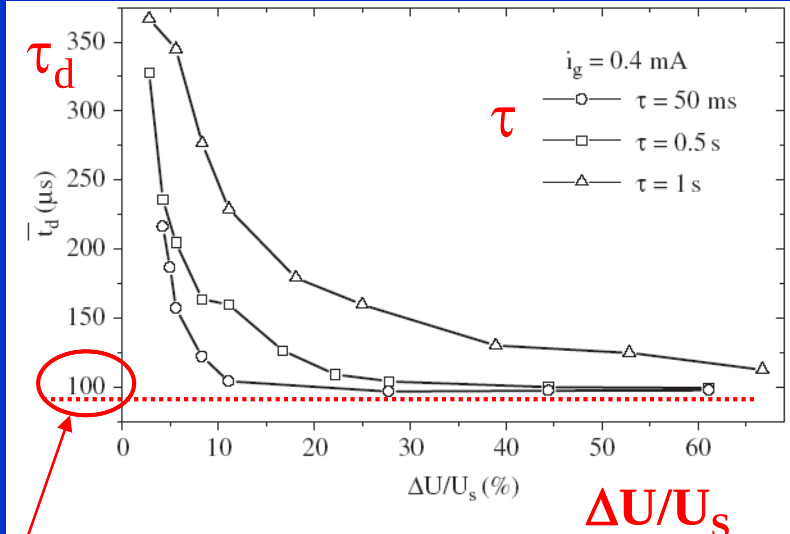

Figure 9. Mean value of time delay $\bar{t}_d$ as a function of overvoltage $\Delta U/U_s$ for three different values of afterglow period for nitrogen-filled tube at pressure 1.3 mbar [27] (©1998 IEEE).

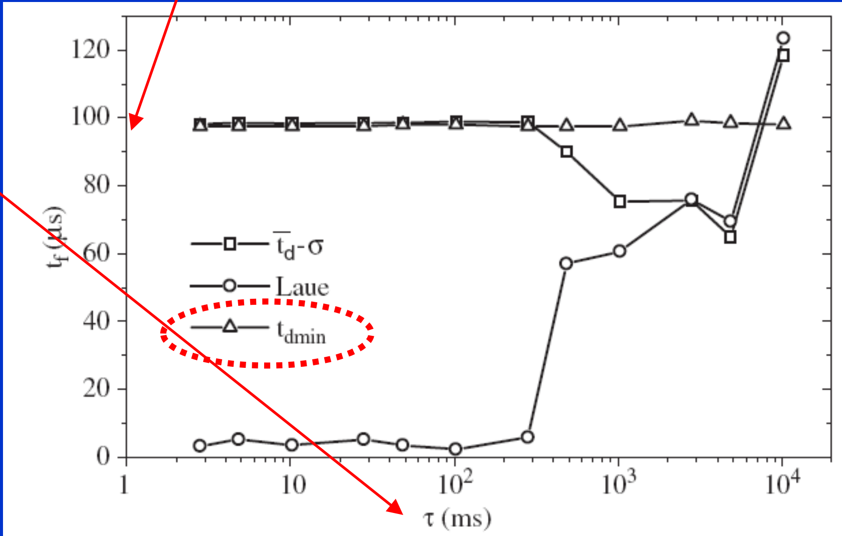

Figure 7. Formative time t_f as a function of afterglow period τ for nitrogen-filled tube at pressure 1.3 mbar [28].

Influence of different experimental parameters on time delay

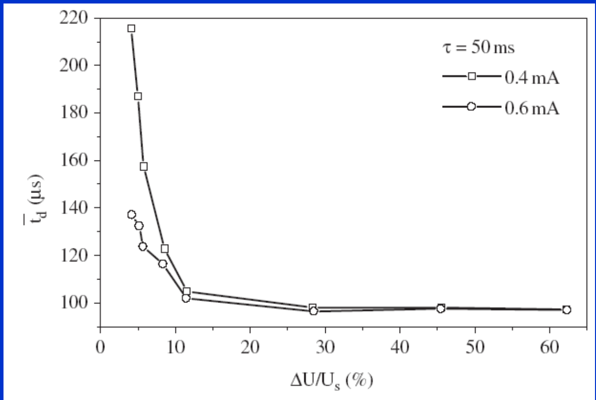

Figure 10. Mean value of time delay $\bar{t}_d$ as a function of overvoltage $\Delta U/U_s$ for two different values of glow current for nitrogen-filled tube at pressure 1.3 mbar [27] (©1998 IEEE).

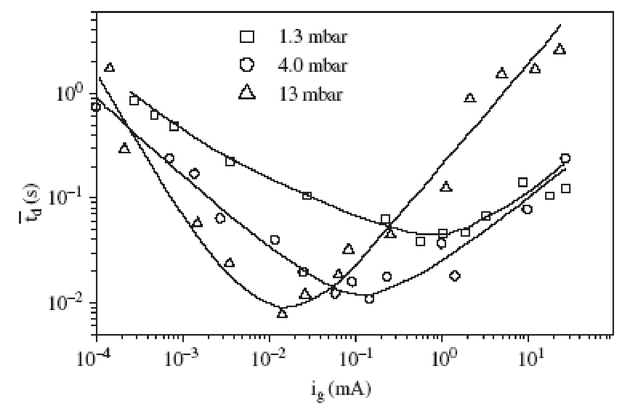

Figure 14. Mean value of time delay $\bar{t}_d$ as a function of glow current i_g for three nitrogen-filled tubes with different pressures [40].

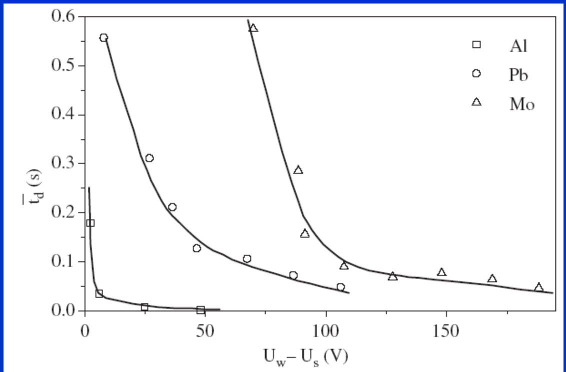

Figure 12. Mean value of time delay $\bar{t}_d$ as a function of difference between the applied voltage and the static breakdown voltage $U_w - U_s$ for nitrogen-filled tube at pressure 7.0 mbar with three pairs of electrodes made of Al, Pb and Mo [35].

Discharge current

Pressure (diffusion…)

Electrode material

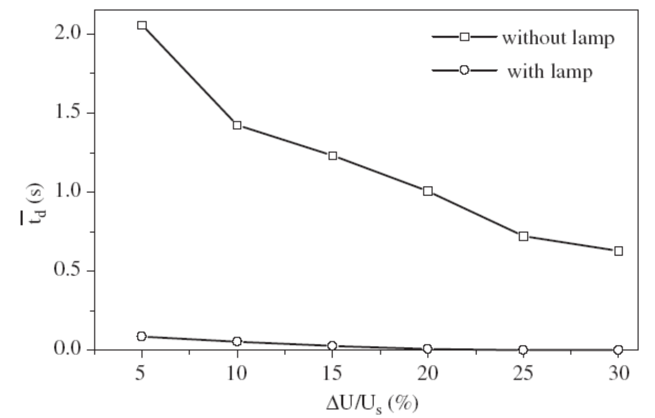

Figure 11. Mean value of time delay $\bar{t}_d$ as a function of overvoltage $\Delta U/U_s$ for nitrogen-filled tube at pressure 1.3 mbar in the cases with/without illumination lamps [32].

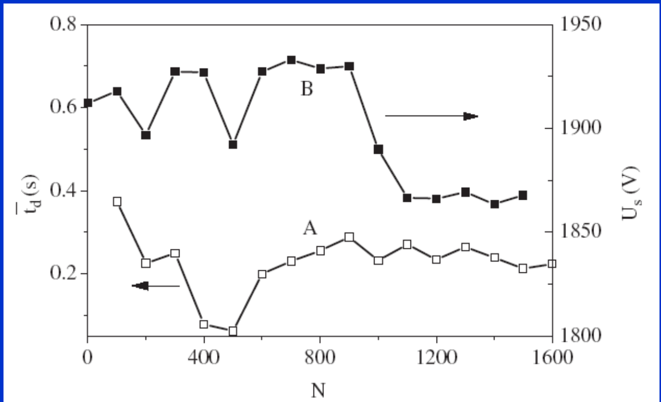

Figure 13. Mean value of time delay $\bar{t}_d$ and static breakdown voltage U_s as a function of a number of breakdowns N for nitrogen-filled tube at pressure 97.5 mbar. (A) $\bar{t}_d = f(N)$, $\tau = 10$ s; (B) $U_s = \varphi(N)$ [39].

Illumination

Number of breakdowns

Breakdown dependence on history

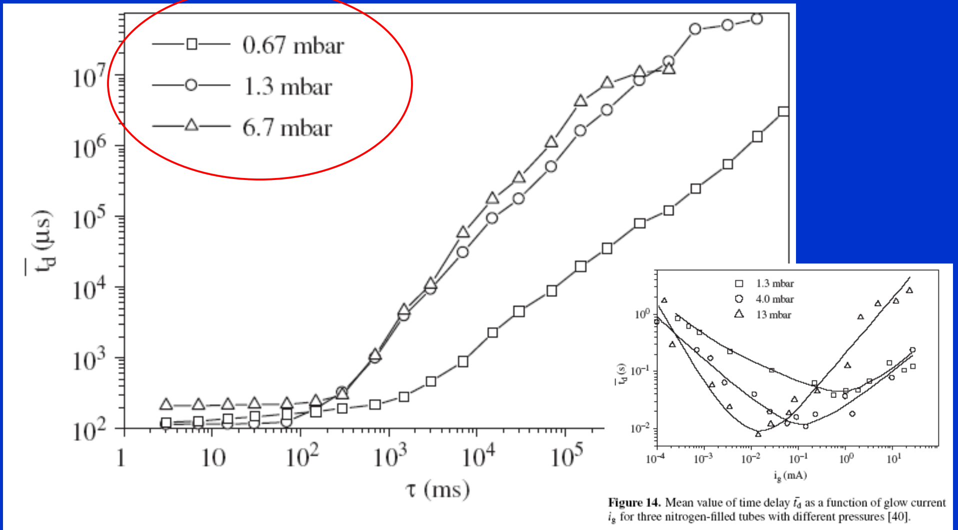

Figure 14. Mean value of time delay $\bar{t}_d$ as a function of glow current i_g for three nitrogen-filled tubes with different pressures [40].

Figure 15. Memory curves for three nitrogen-filled tubes with different pressures.

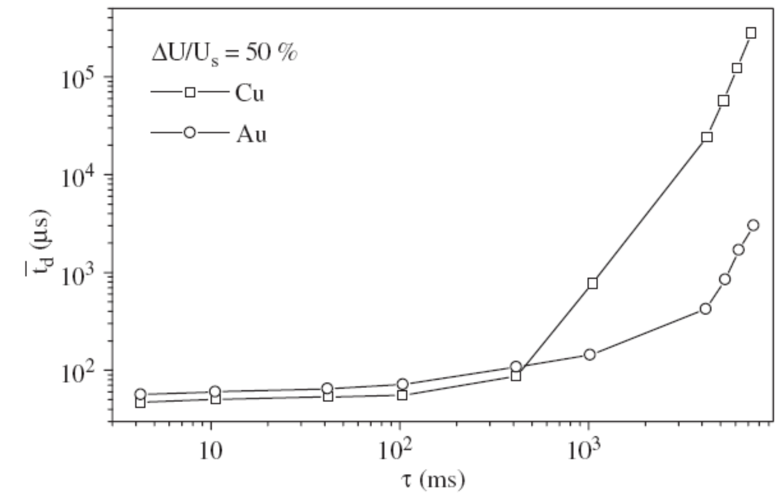

Figure 16. Memory curves for Cu and Au cathode for nitrogen-filled tube at pressure 6.7 mbar [57].

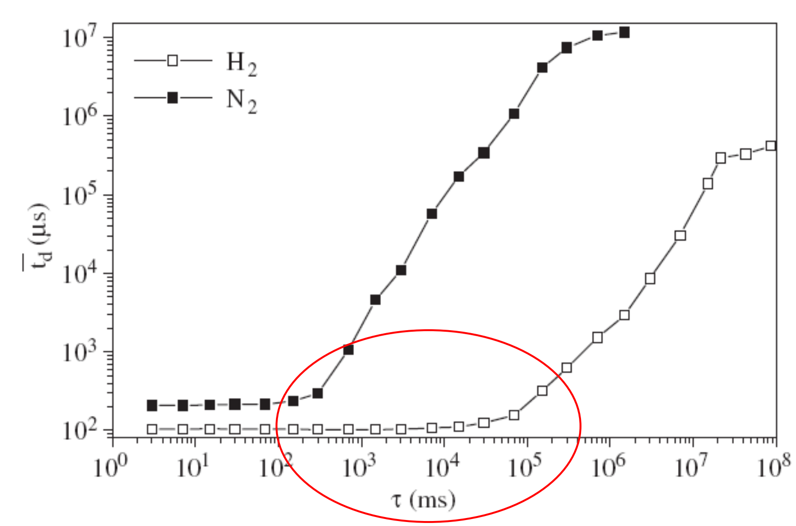

Figure 17. Memory curves for hydrogen-filled tube and nitrogen-filled tube at pressure 6.7 mbar [66].

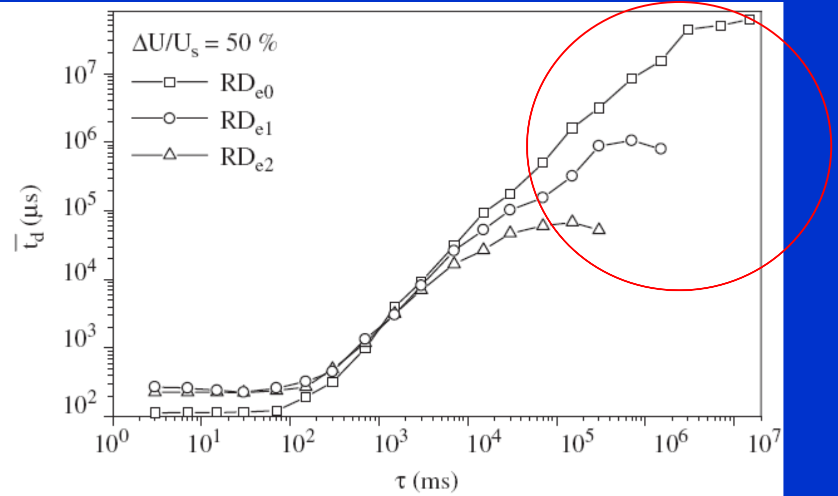

Figure 20. Memory curves for krypton-filled tube at pressure 1.3 mbar without irradiation and two values of irradiation dose rate [71].

DC glow discharges

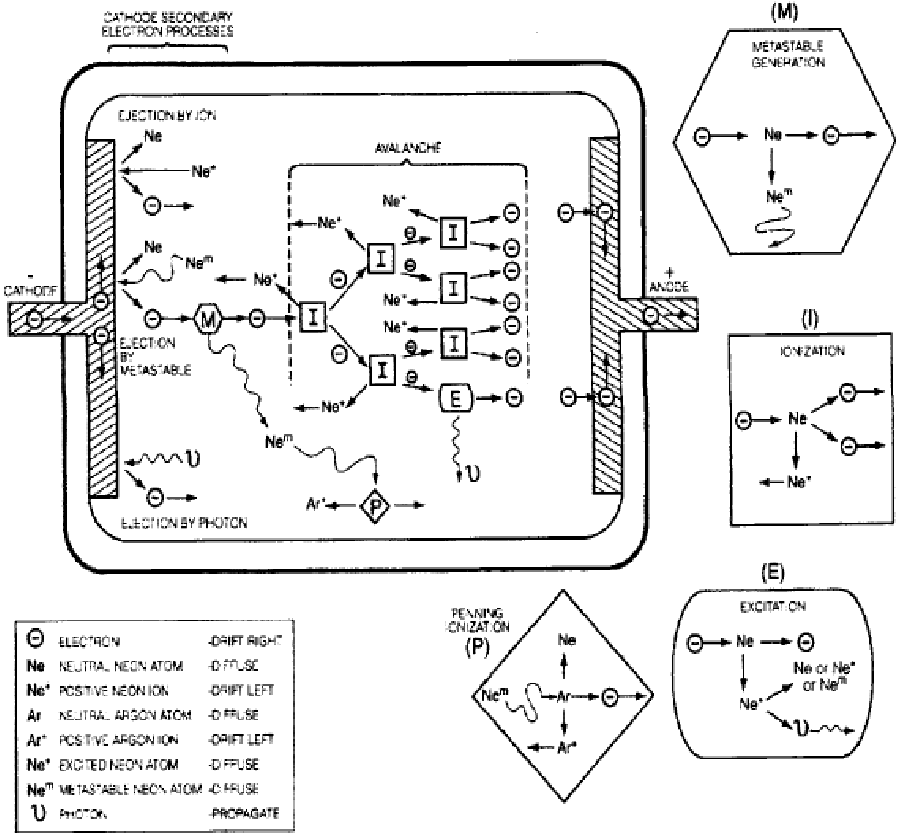

DC 글로우 방전의 모식도

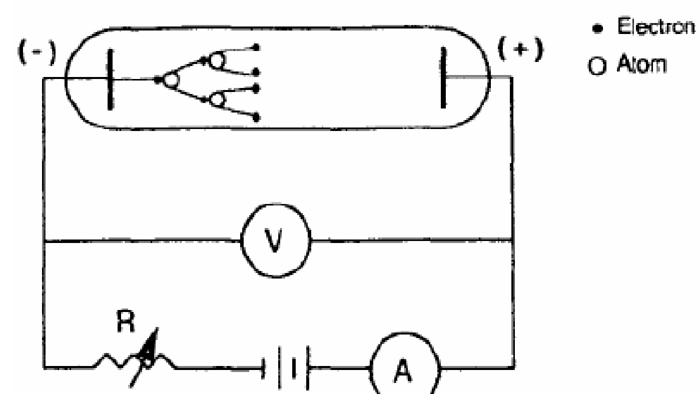

Fig. 2-1 DC glow-discharge setup.

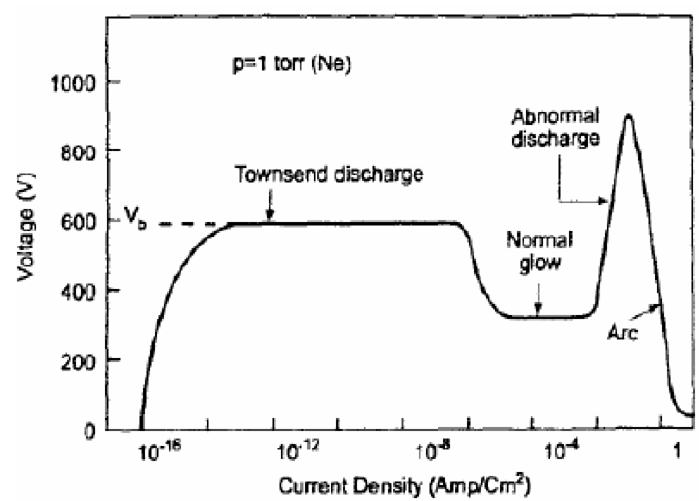

Fig. 2-2 The I-V characteristic of a DC glow discharge.

- Electron multiplication
- Emission of secondary electron from a cathode

Paschen's law 1

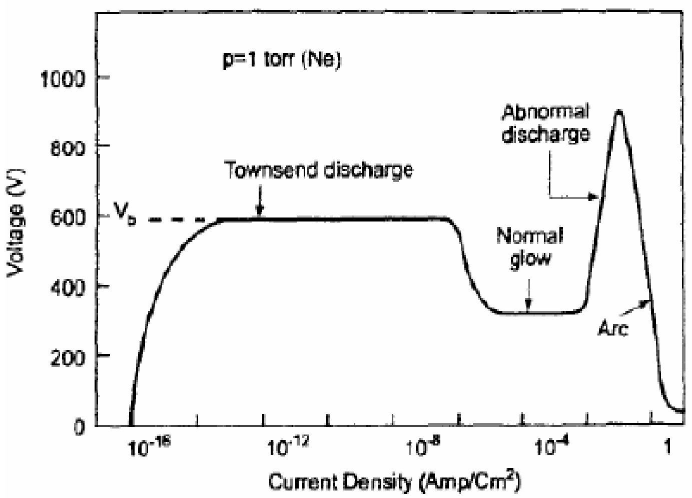

Fig. 2-2 The I-V characteristic of a DC glow discharge.

$$I = \frac{I_0\, e^{\alpha d}}{1 - \gamma(e^{\alpha d} - 1)}$$

When $1 - \gamma(e^{\alpha d} - 1) = 0$, the breakdown occurs.

$$\alpha = A \cdot p \exp\left(-\frac{B \cdot p}{E}\right)$$

and $V_b = Ed$,

$$V_b = \frac{C_1 (pd)}{C_2 + \ln(pd)}$$

where d = distance between electrodes

C_1 and C_2 = constants that change with the nature of the gas

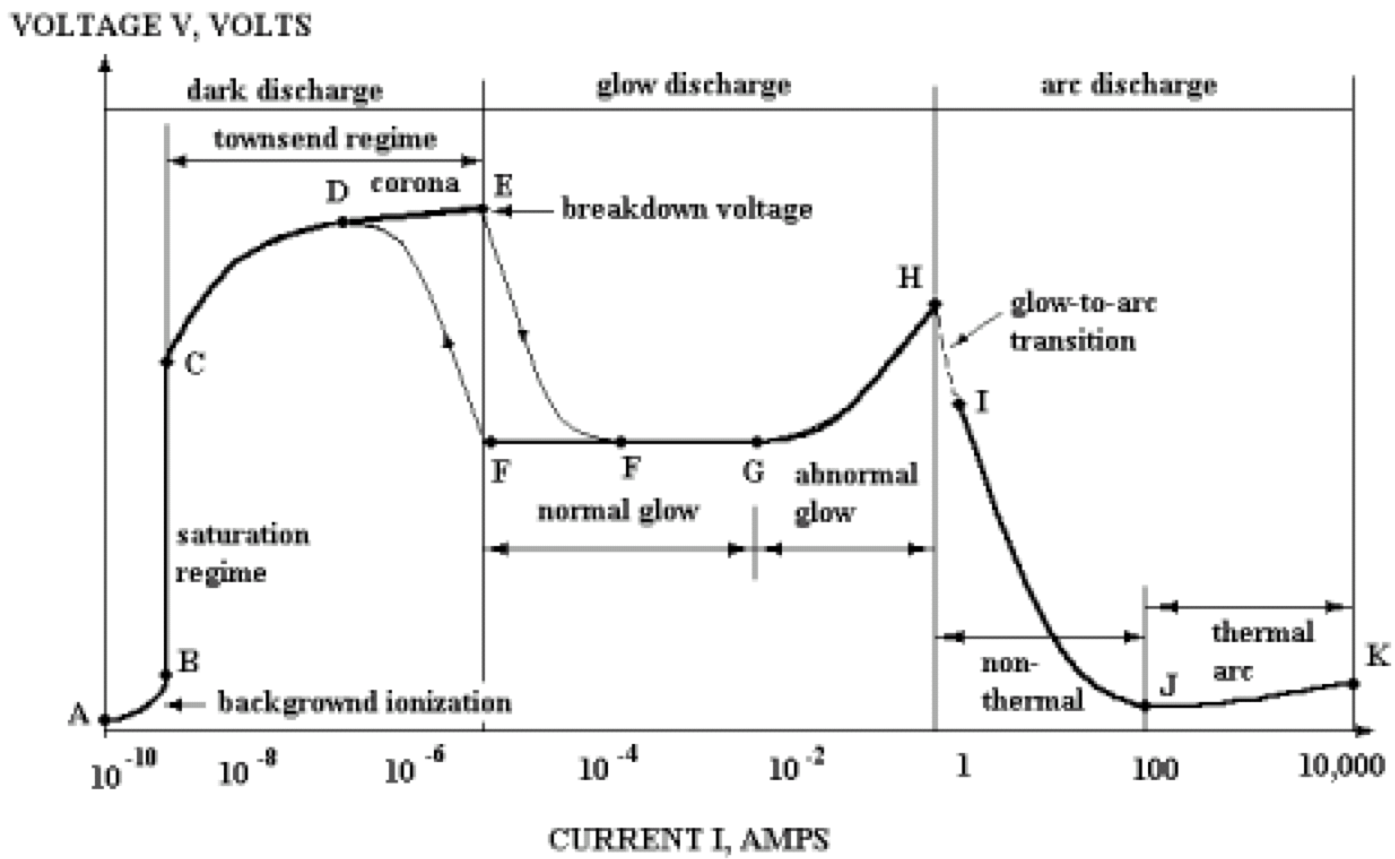

http://science-education.pppl.gov/SummerInst/SGershman/Structure_of_Glow_Discharge.pdf

Current–voltage (i–V) characteristics of direct current (dc) electrical discharge

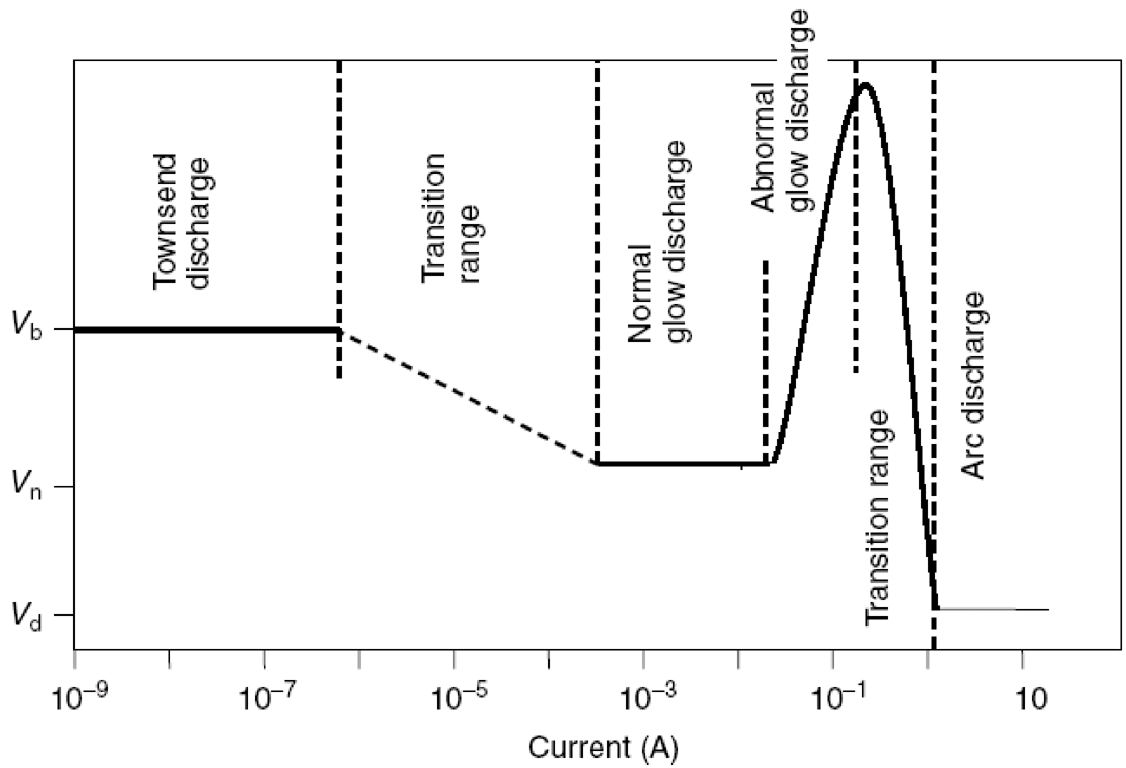

V_b is the breakdown voltage,

V_n is the normal operating voltage, and

V_d is the operating voltage of arc discharge.

http://www.spectroscopynow.com/Spy/pdfs/jwfeed/sample_0471606995.pdf

Characteristics of DC glow discharge 1

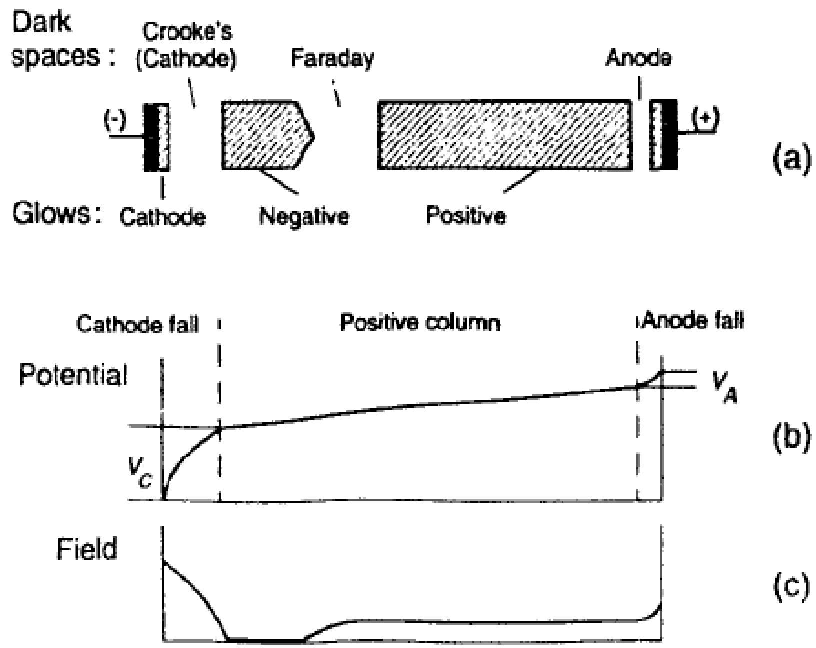

Fig. 2-4 Regions and characteristics of a DC glow discharge: (a) discharge regions; (b) potential distribution in discharge tube; (c) distribution of electric field in discharge tube.

- The dark regions are called the cathode or Crooke's dark space, the Faraday dark space, and the anode dark space.
- The luminous regions are called the cathode glow, the negative glow, and the positive column.

Low pressure normal glow discharge

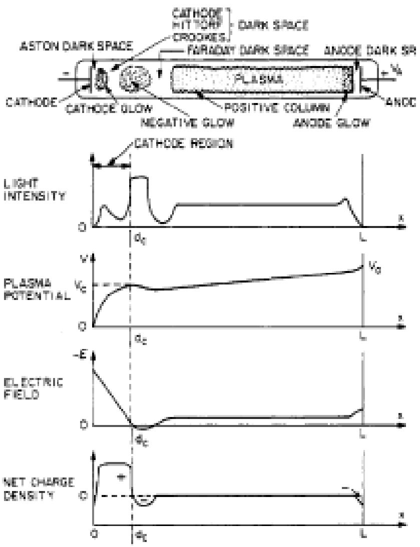

- <u>Cathode</u>: made of an electrically conducting metal, γ, of which has a significant effect on the operation of the discharge tube.
- <u>Aston dark space</u>: a thin region with a strong electric field and a negative space charge. The electrons are of too low a density and/or energy to excite the gas, so it appears dark.
- <u>Cathode glow</u>: has a relatively high ion number density. The length depends on the type of gas and the gas pressure.
- <u>Cathode (Crookes, Hittorf) dark space</u>: has a moderate electric field, a positive space charge, and a relatively high ion density.

Penning discharge plasma sources produce a dense plasma at pressures far below than most other glow discharges

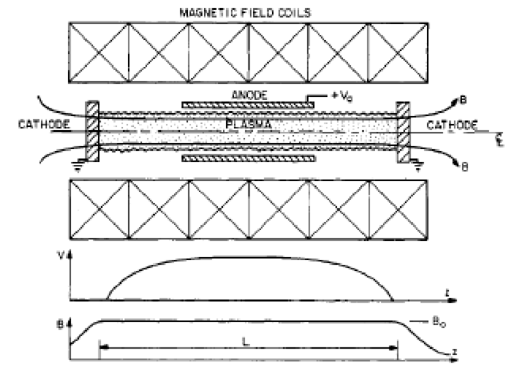

- Strong axial magnetic fields: to prevent electrons from intercepting the anode.
- Axial electric fields: electrons are reflected by opposing cathodes.
- Multiple reflection of the electrons along axis.

http://www.exo.net/~pauld/origins/glowdisharge.html

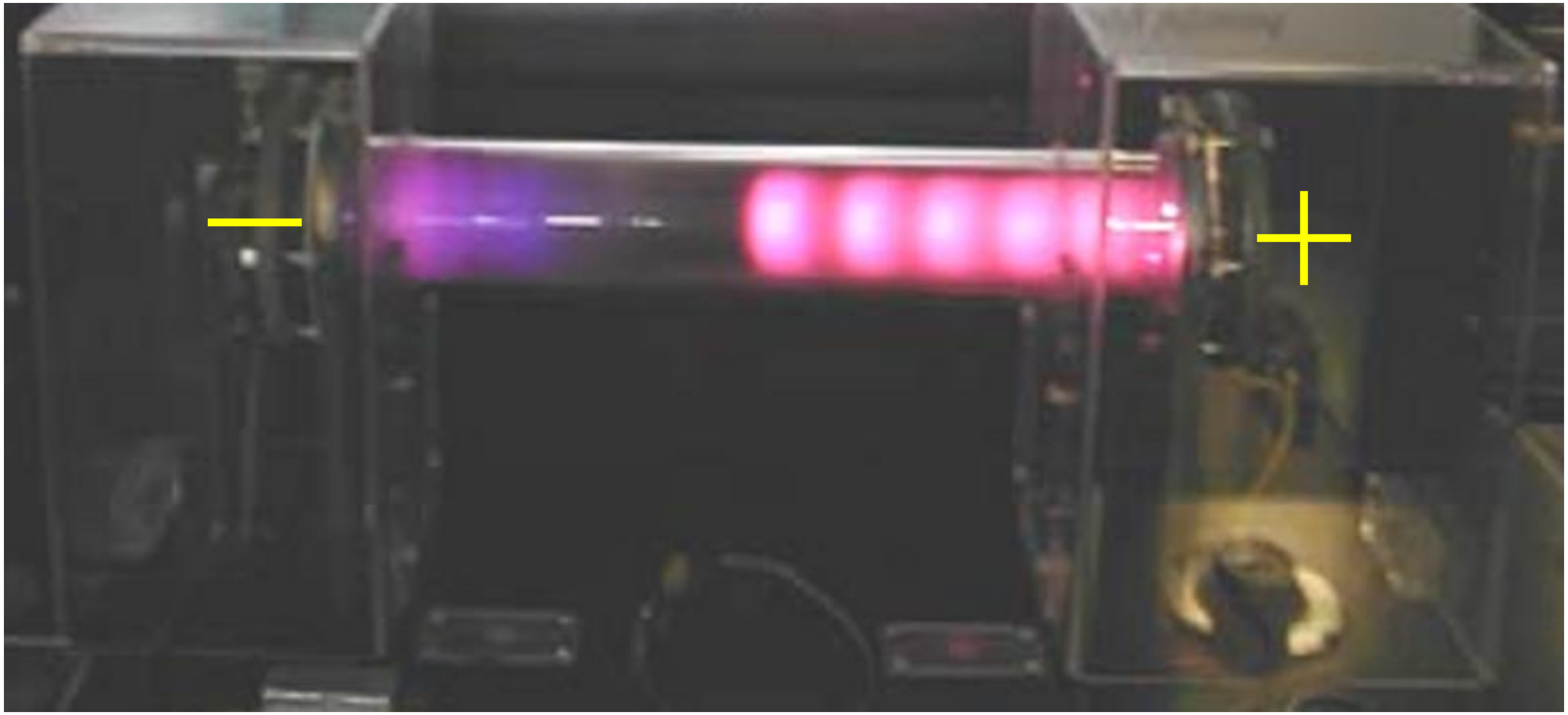

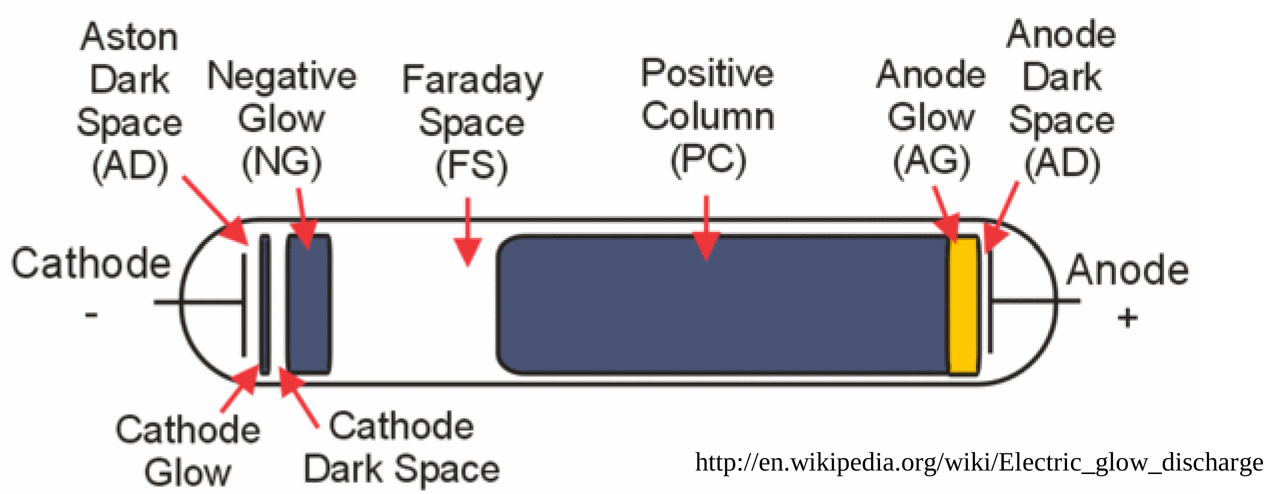

http://www.exo.net/~pauld/origins/glowdisharge.html

Sprite and Glow Discharge Tube

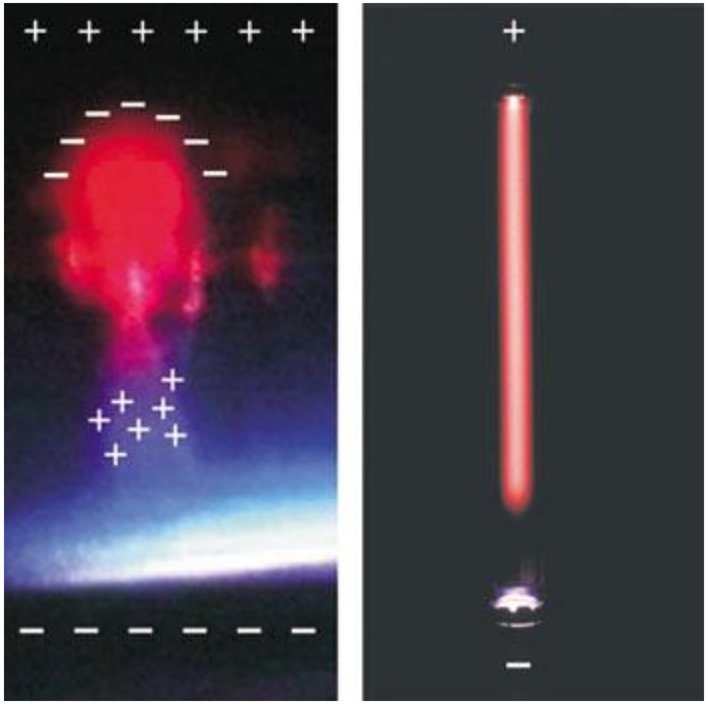

Sprite light in the atmosphere (**left**) and in a laboratory glow discharge tube (**right**). In both cases, the light near the positive (anode) end is red and arises from the collisional excitation of neutral nitrogen molecules by free electrons. Also in both cases, the light near the negative (cathode) end is blue and arises from the collisional excitation of N_2^+ ions by free electrons.

http://www.physicstoday.org/pt/vol-54/iss-11/captions/p41cap3.html http://www.emitech.co.uk/sputter-coating-brief3.htm

Regions in the DC Glow Discharge Tube

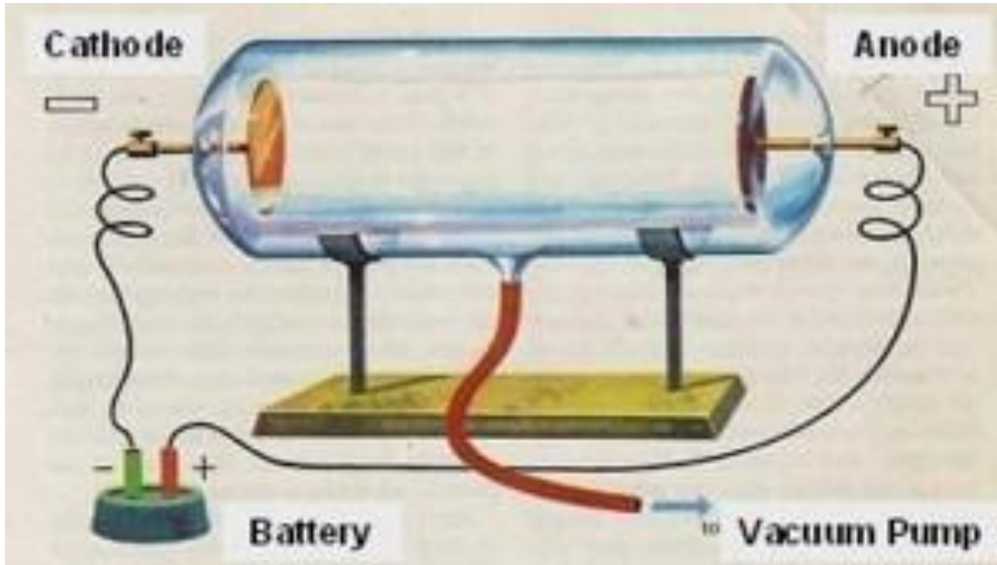

A glass tube, about ***16 inches long*** and ***1 1/2 inches in diameter***, is hermetically sealed at both ends. Two metal probes are fused into the tube at each end. The physicist applies a potential of a few thousand volts across both probes. With the aid of a vacuum pump he sucks the ***air*** out of the tube, thus lowering the pressure inside the glass tube.

http://www.newjerusalemnetwork.net/emmanuel/great_wall3.html

Regions in the Glow Discharge Tube II

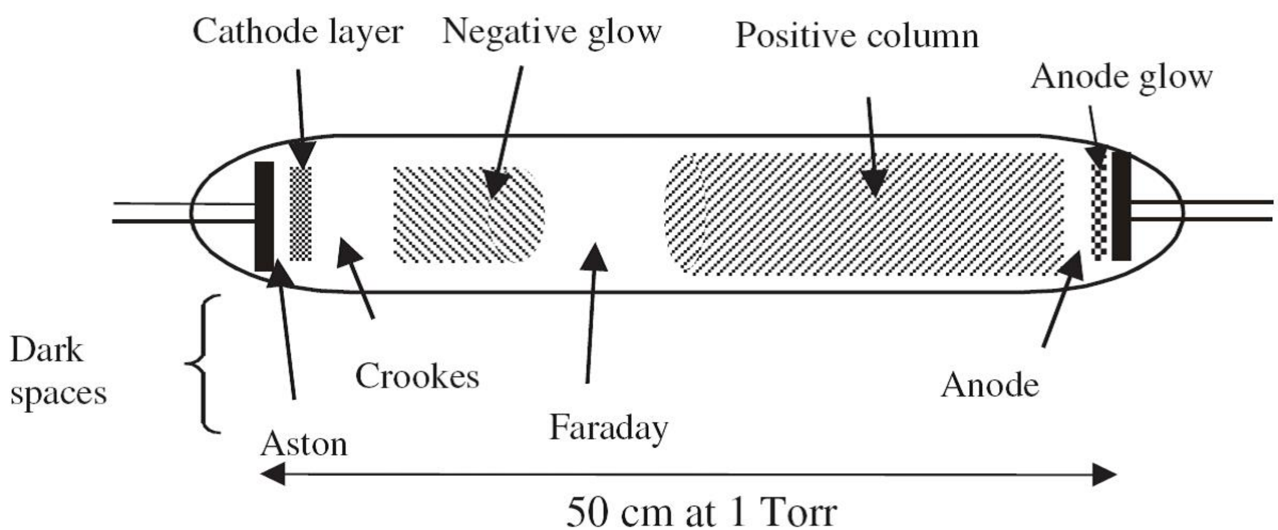

Plasma Sources Sci. Technol. **12** (2003) 295–301

Potentials along the Tube

Light intensity

Potential V

Field E

Current

Charge density

Charge density (total)

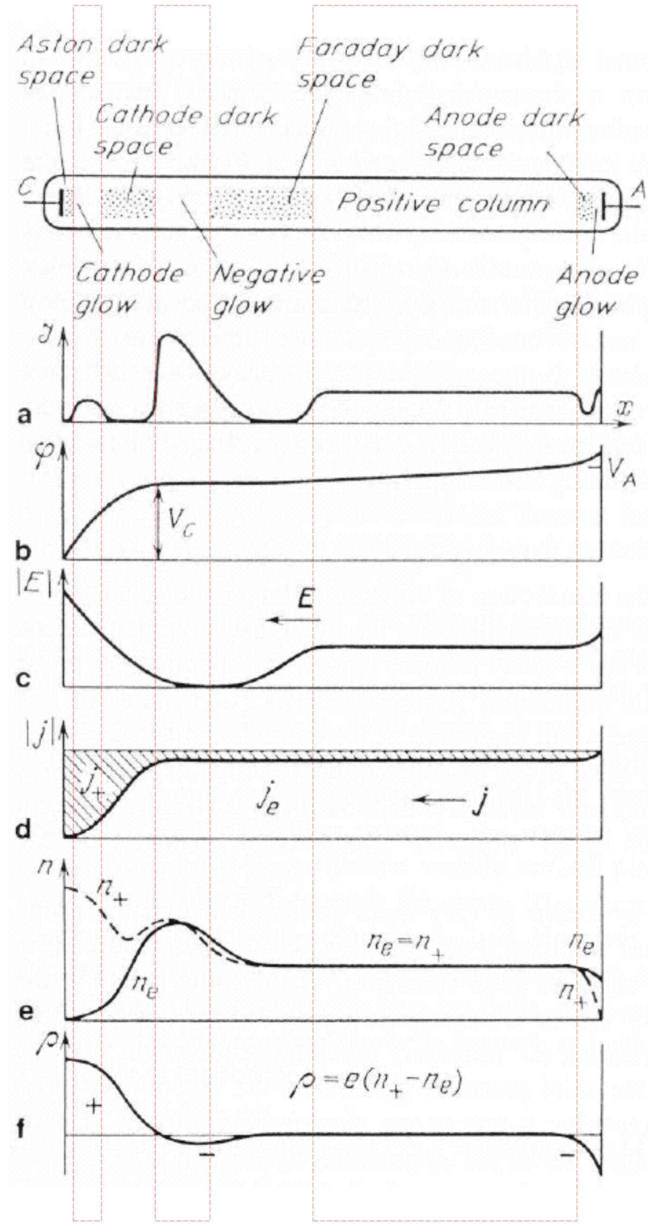

Yu. P. Raizer. Gas Discharge Physics. Springer, Berlin, 1991.

$$\frac{dV}{dx} = -E$$

$$\frac{dE}{dx} = \frac{1}{\varepsilon} q(N^{+} - N^{-})$$

$$N^{+} - N^{-}$$

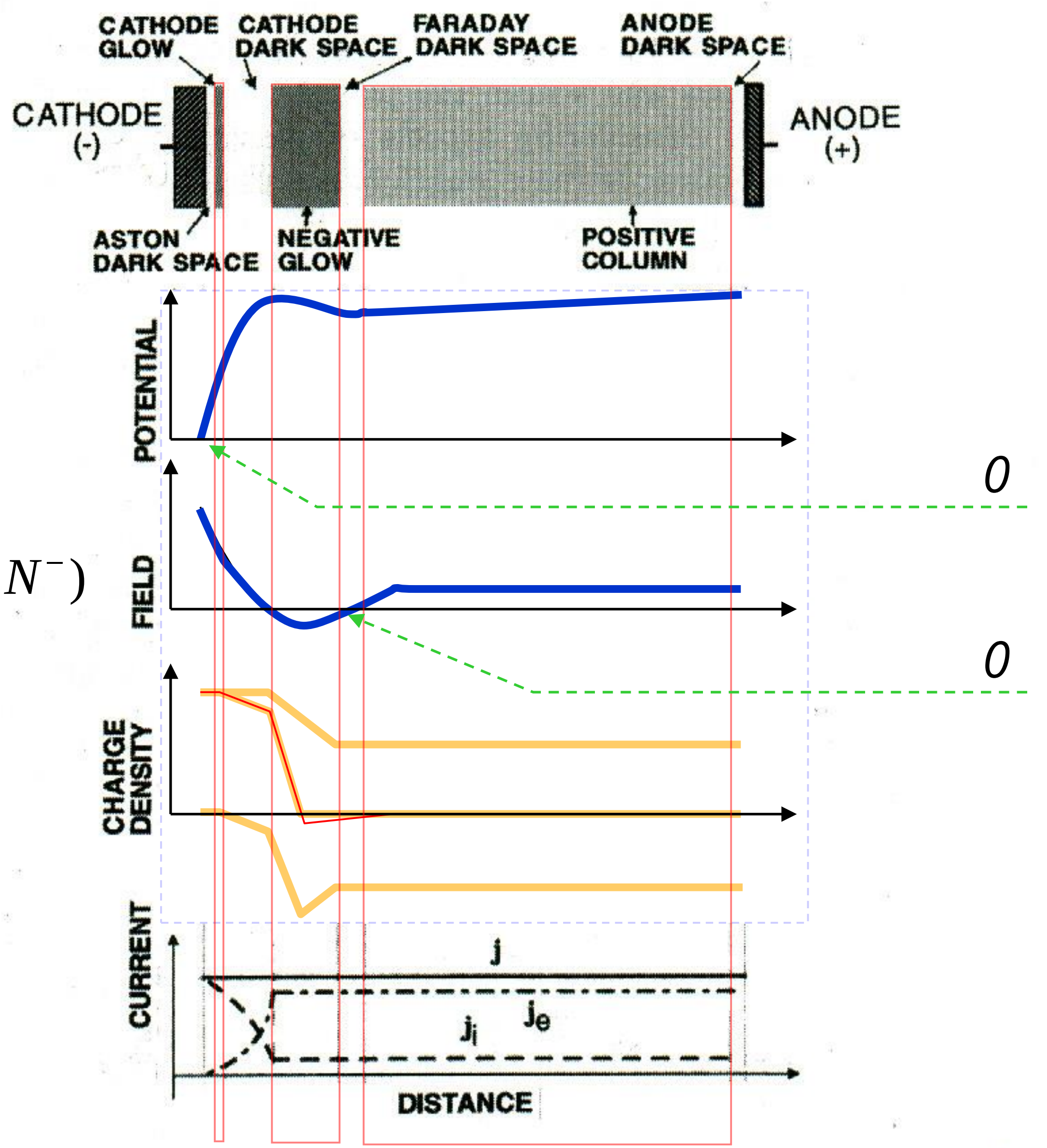

Figure 4-3 Structure of a DC glow discharge with corresponding potential, electric field, charge, and current distributions.

Formation and destruction of $H_3^+(v=0)$ in He/Ar/H_2 microwave discharge

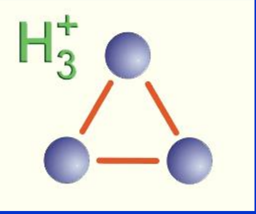

Laser – Single-mode tuneable **diode laser**,
λ = 1470 ± 10nm; P ~ 3 mW
Mirrors – R = 99.994%,

PULSE REGIME

TEST TUBE

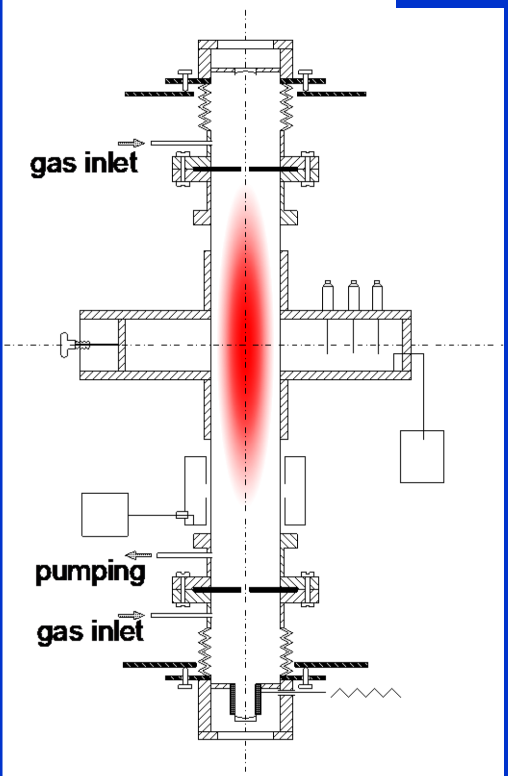

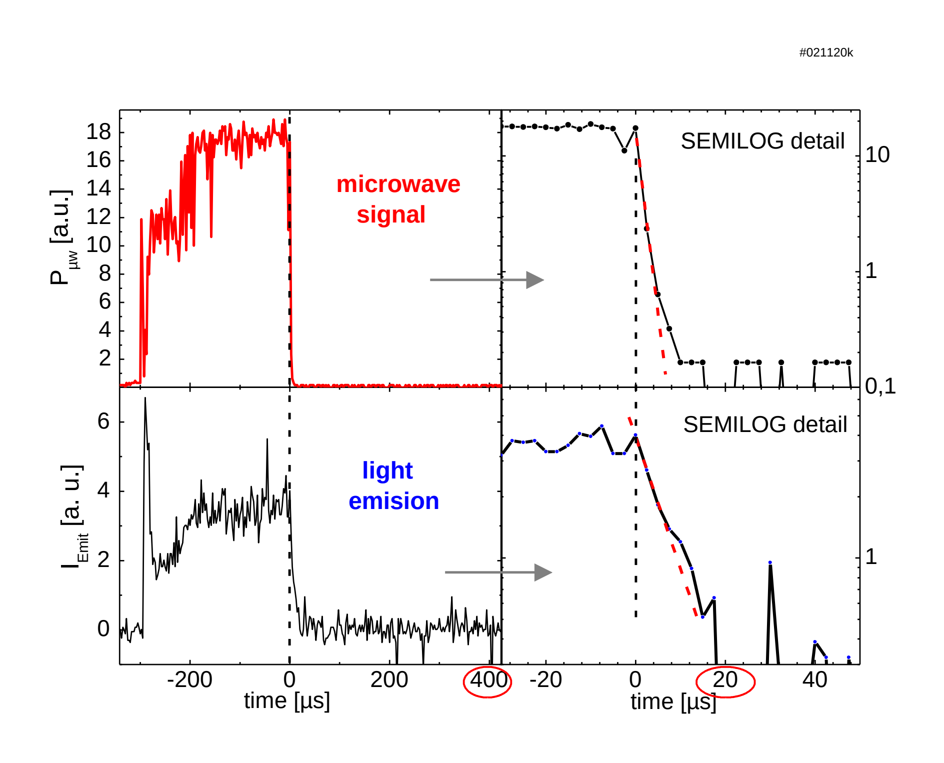

Kinetic temperature of $H_3^+(v=0)$ measured from the Doppler broadening

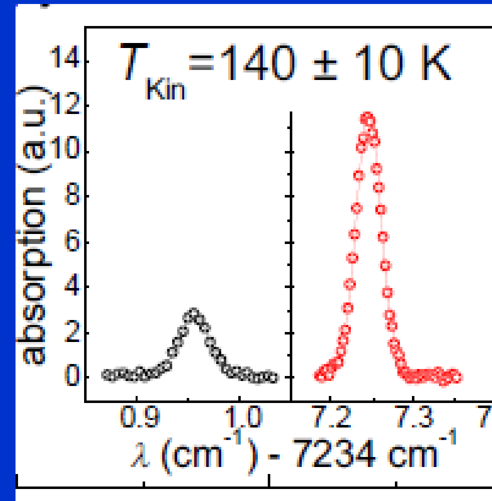

μw PULSES

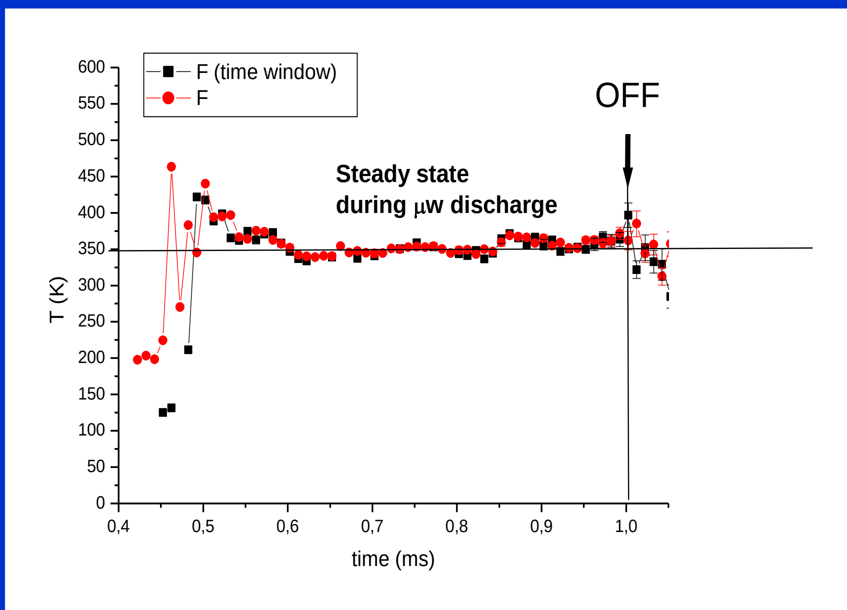

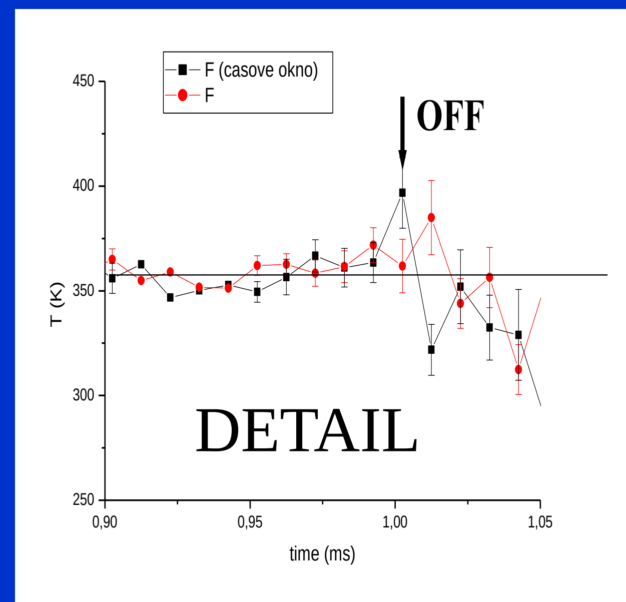

From the spectrum rotational temperature is determined

Recombination of $H_3^+(v=0)$ in He/Ar/H_2 Stationary afterglow

PULSE REGIME

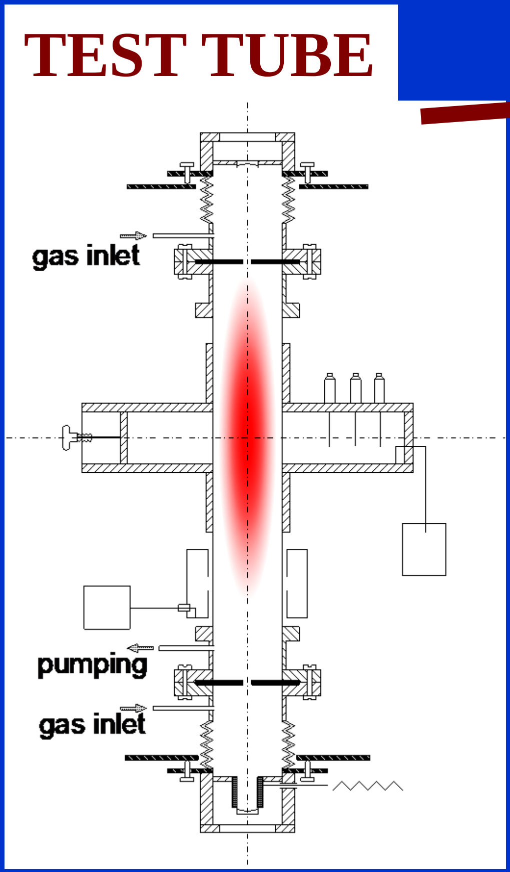

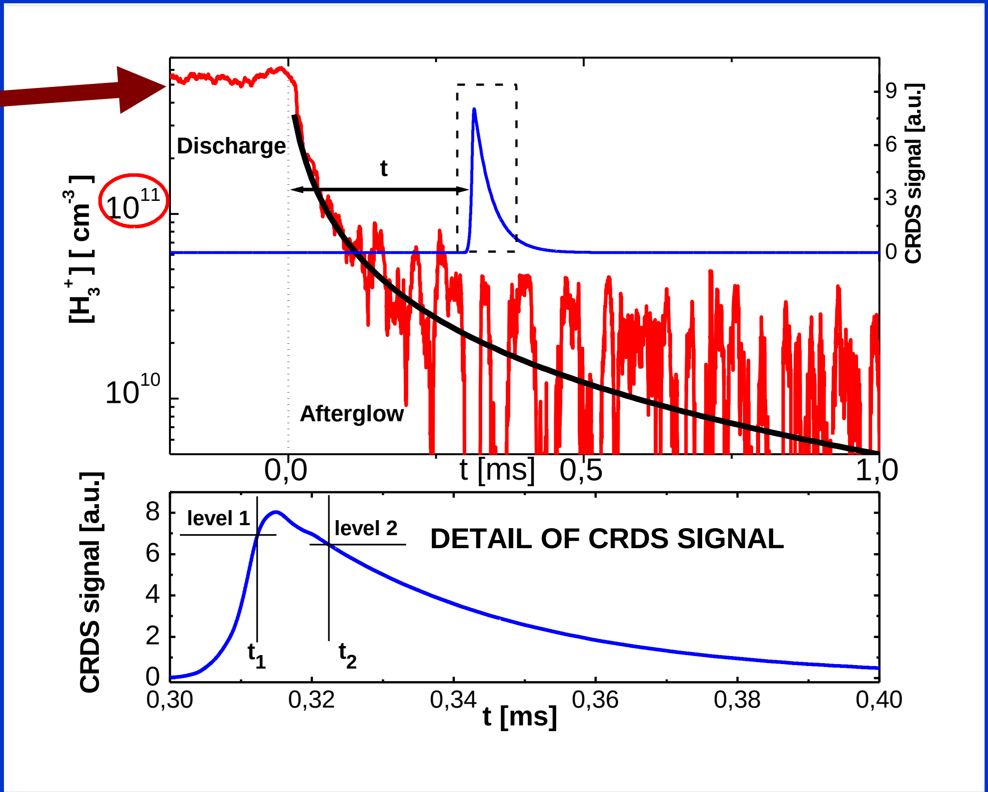

CRDS 2003

Yesterday's results

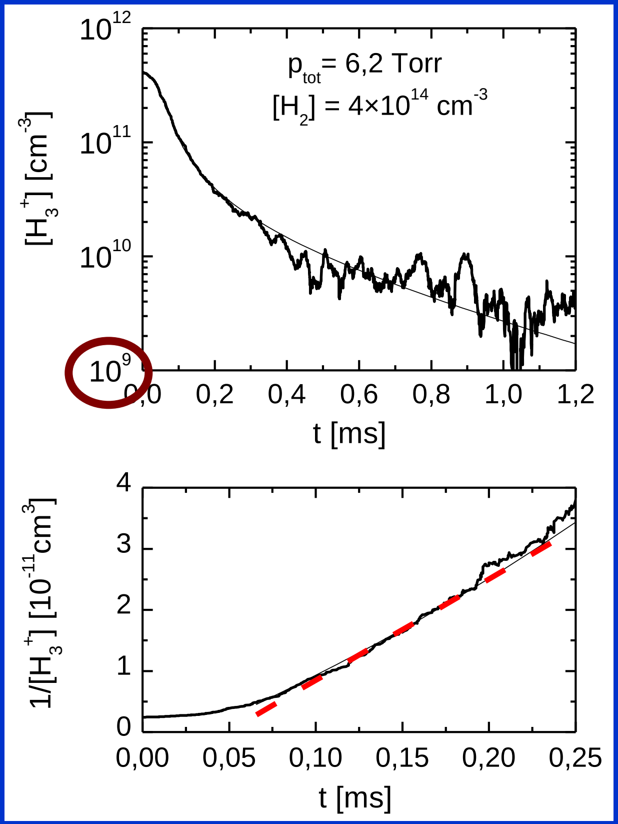

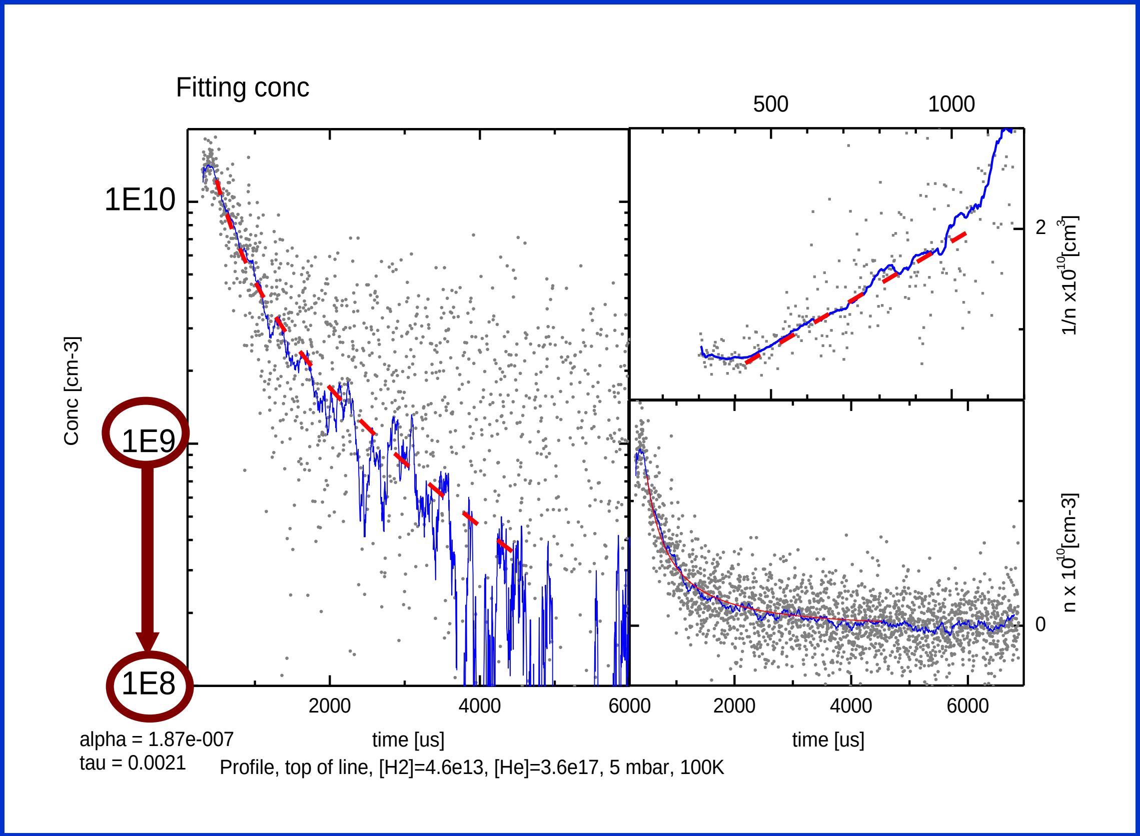

100μs → 1000μs

Decay of $H_3^+(v=0)$ …. iteration

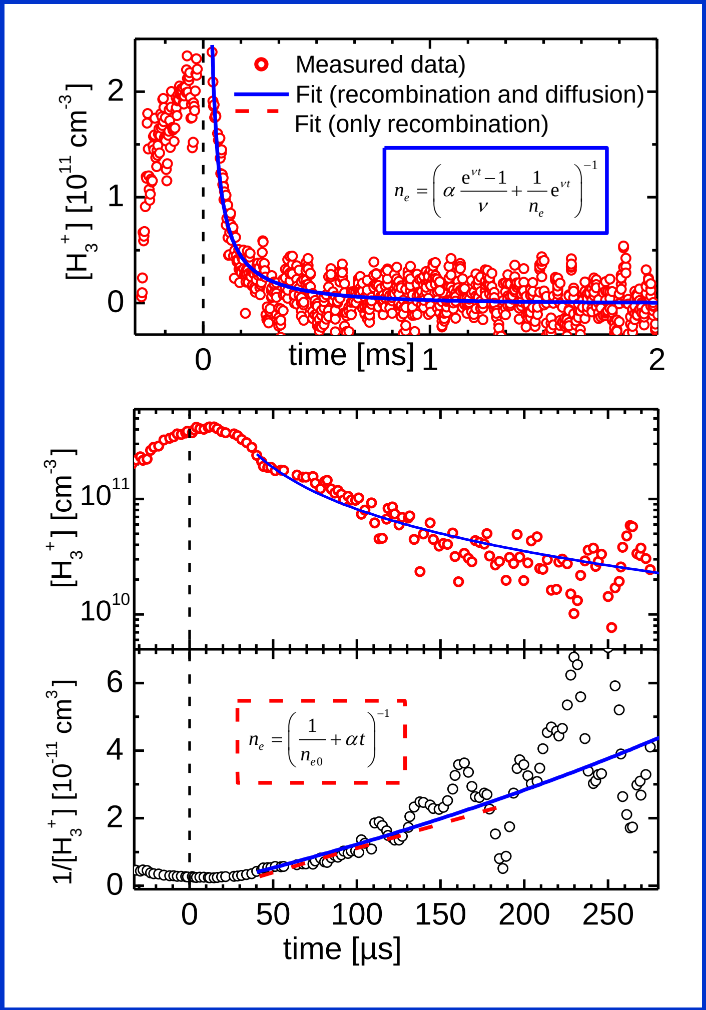

Spectroscopy of discharge in He/Ar/H2

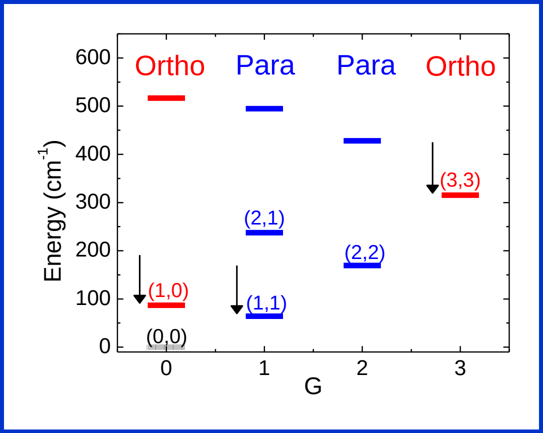

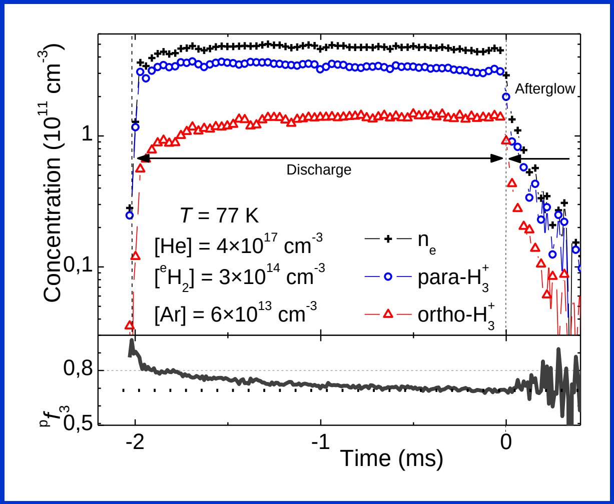

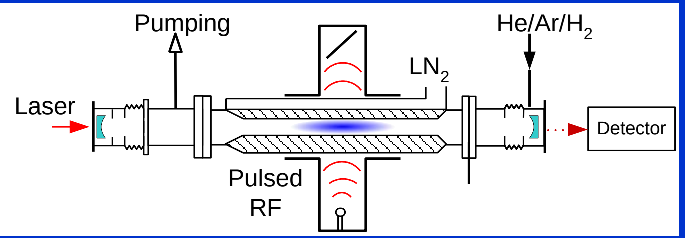

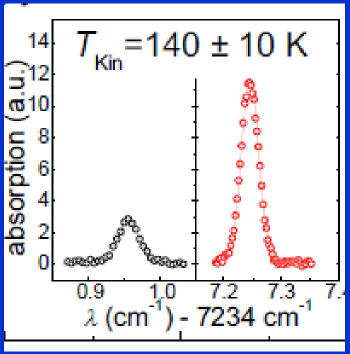

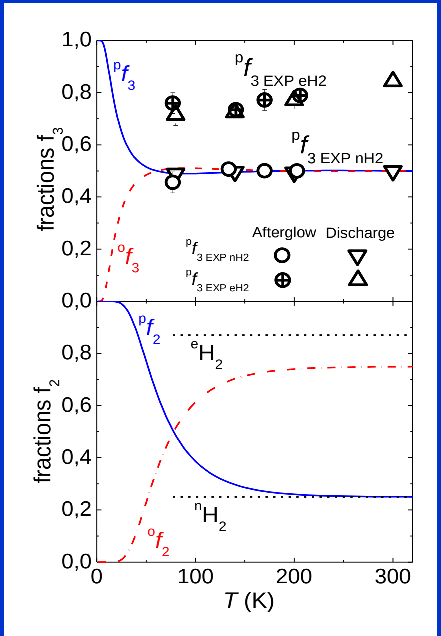

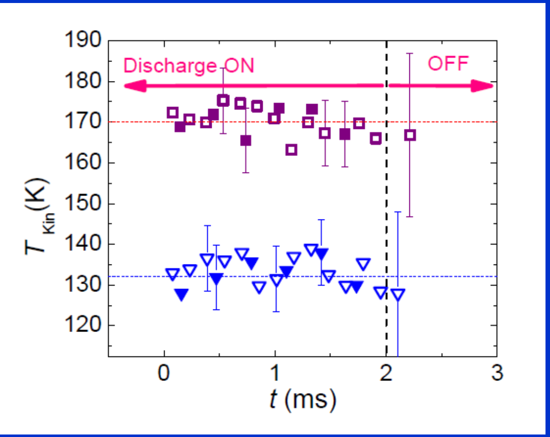

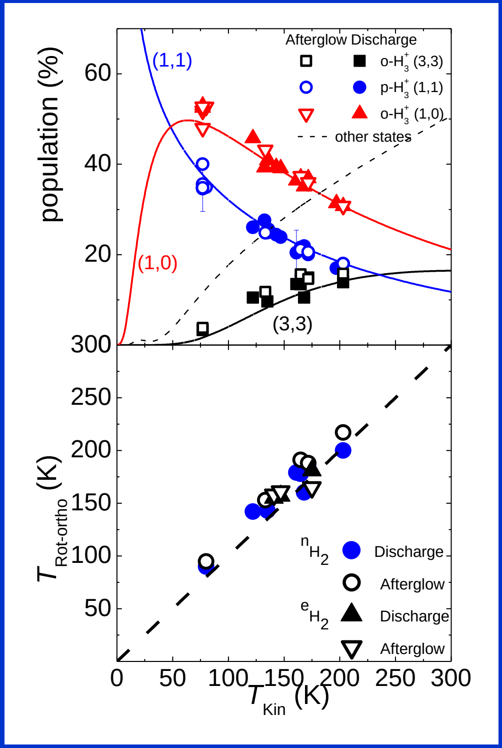

Formation of para-H3+ and ortho-H3+

$$^{\mathrm{p}}\mathrm{H}_3^+ + \mathrm{e}^- \xrightarrow{\ ^{\mathrm{p}}\alpha_{\mathrm{eff}}\ } \text{neutral products}$$

$$^{\mathrm{o}}\mathrm{H}_3^+ + \mathrm{e}^- \xrightarrow{\ ^{\mathrm{p}}\alpha_{\mathrm{eff}}\ } \text{neutral products}$$

$$^{\mathrm{p}}\mathrm{H}_3^+ \underset{\nu_{\mathrm{op}}}{\overset{\nu_{\mathrm{po}}}{\longleftrightarrow}} {}^{\mathrm{o}}\mathrm{H}_3^+$$

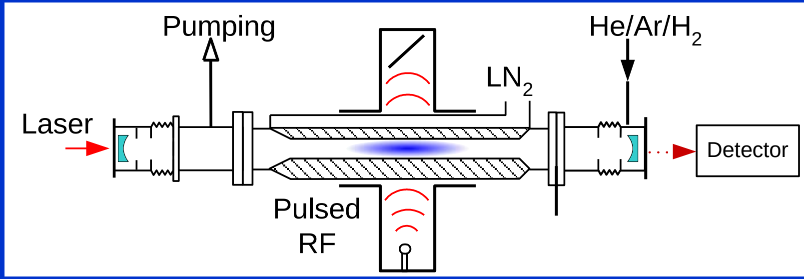

$$\frac{\mathrm{d}[^{p}\mathrm{H}_3^+]}{\mathrm{d}t} = -{}^{p}\alpha_{\mathrm{eff}}[^{p}\mathrm{H}_3^+]n_e - \frac{[^{p}\mathrm{H}_3^+]}{\tau_{\mathrm{D}}} - \nu_{po}[^{p}\mathrm{H}_3^+] + \nu_{op}[^{o}\mathrm{H}_3^+]$$

$$\frac{\mathrm{d}[^{o}\mathrm{H}_3^+]}{\mathrm{d}t} = -{}^{o}\alpha_{\mathrm{eff}}[^{o}\mathrm{H}_3^+]n_e - \frac{[^{o}\mathrm{H}_3^+]}{\tau_{\mathrm{D}}} + \nu_{po}[^{p}\mathrm{H}_3^+] - \nu_{op}[^{o}\mathrm{H}_3^+]$$

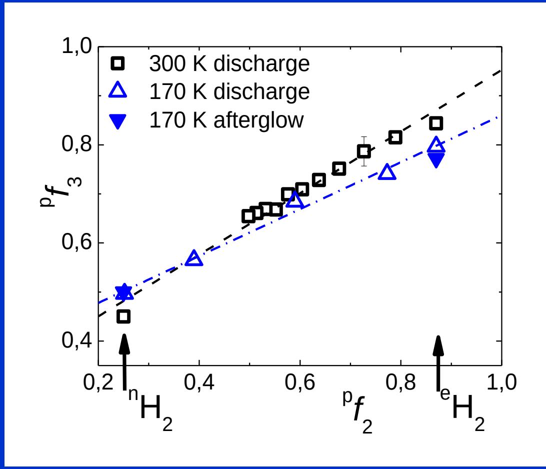

$$\frac{dn_{\mathrm{e}}}{dt} = -({}^{\mathrm{p}}\alpha_{\mathrm{eff}}\,{}^{\mathrm{p}}f_3 + {}^{\mathrm{o}}\alpha_{\mathrm{eff}}\,{}^{\mathrm{o}}f_3)n_{\mathrm{e}}^2 - \frac{n_{\mathrm{e}}}{\tau_{\mathrm{D}}}$$

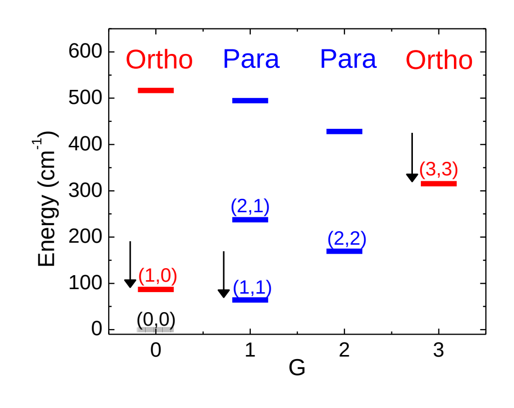

Calculation of avalanche…

Calculation of avalanche…

Calculation of avalanche…

Electric discharges - data

$$\frac{\mathrm{d}j_-}{\mathrm{d}x} = \alpha n_- = \frac{\alpha}{V_-} n_- V_- = \delta j_-$$

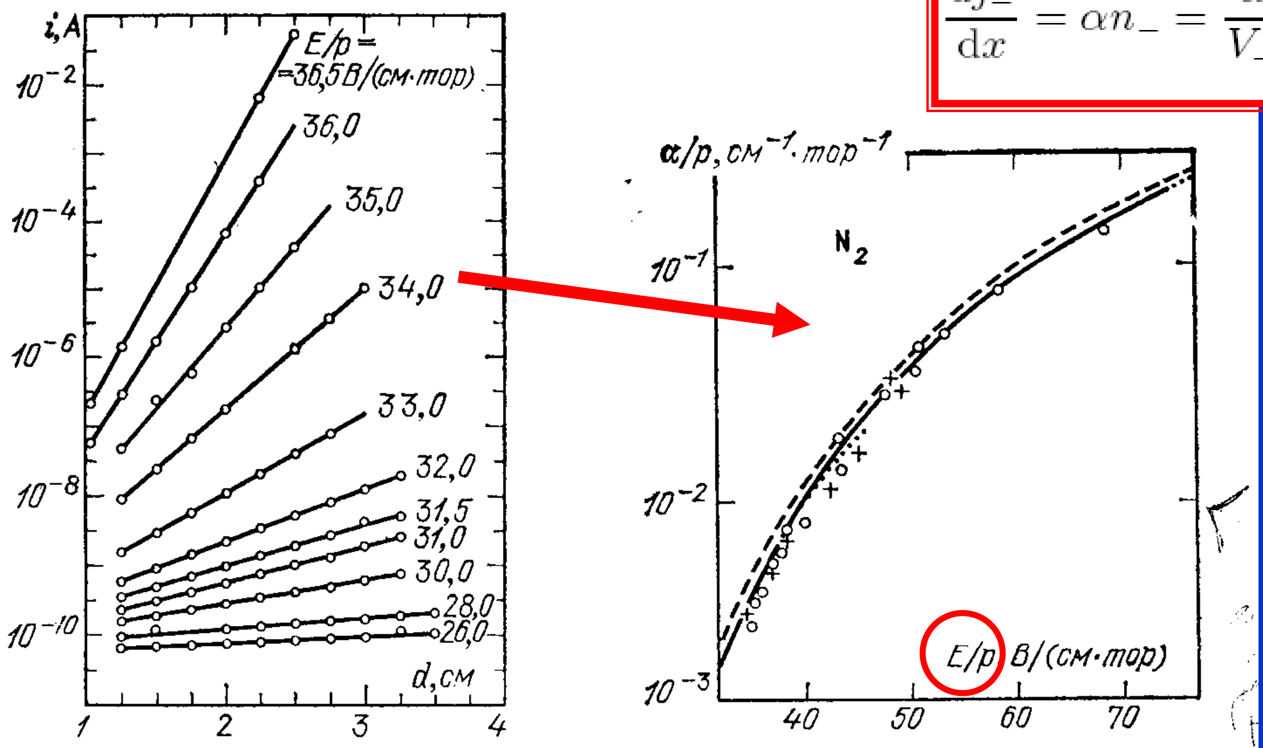

Р и с. 5.3. Экспериментальный график, демонстрирующий постоянство α и экспоненциальный характер нарастания тока в разрядном промежутке; ионизационные коэффициенты определяются наклонами прямых [6]

Р и с. 5.4. Ионизационный коэффициент Таунсенда α в N_2 по разным измерениям

E/N …… 1 Townsend = 1 Td = 10^{-17} Vcm^2 = 10^{-21} Vm^2

E/p at 293 K (cca 20 C)……. 1V/cmTorr=3.034Td, resp. 1 Td = 0,3296V/cmTorr

Electric discharges Townsend avalanche theory

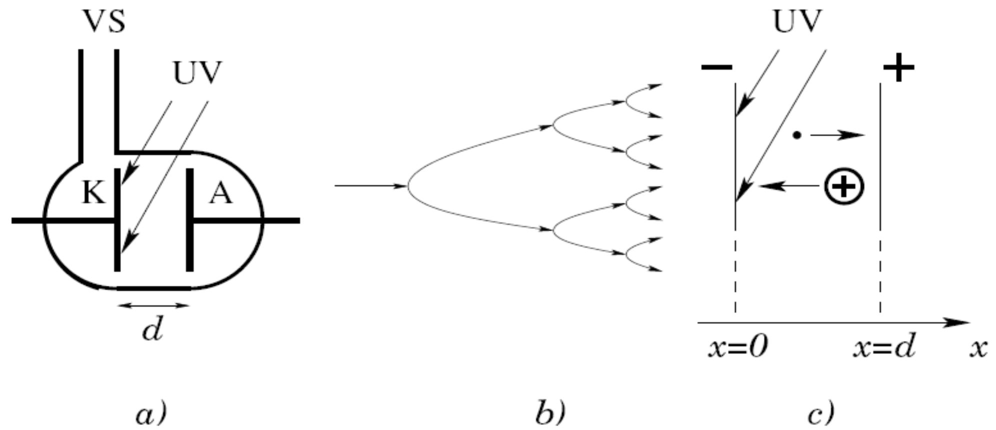

Obr. 5.2: Zapaľovanie výboja: *a*) výbojka na meranie zapaľovacieho napätia: K - katóda, A - anóda, UV - ultrafialové žiarenie zabezpečujúce emisiu primárnych elektrónov, VS - napojenie na vákuový systém; *b*) elektrónová lavína; *c*) označenie polohy elektród

$$\frac{\mathrm{d}j_-}{\mathrm{d}x} = \alpha n_- = \frac{\alpha}{V_-} n_- V_- = \delta j_-$$

medzi elektródami (obr. 5.2 *c*). Povrch katódy K sa nachádza v mieste $x = 0$ a povrch anódy A v mieste $x = d$. Elektróny sa pohybujú smerom k anóde a vytvorené kladné ióny ku katóde, kde zanikajú. Podobne ako v odseku 4.3.1, môžeme napísať rovnicu kontinuity pre elektróny v jednorozmernej geometrii a v ustálenom stave

$$\boxed{\frac{\mathrm{d}j_-}{\mathrm{d}x} = \alpha n_- = \frac{\alpha}{V_-} n_- V_- = \delta j_-}, \tag{5.2}$$

kde V_- je driftová rýchlosť elektrónov v elektrickom poli (v homogénnom poli je konštantná) a $\delta = \alpha / V_-$ je **prvý Townsendov koeficient**. Analogická rovnica platí aj pre kladné ióny

$$\frac{\mathrm{d}j_+}{\mathrm{d}x} = \alpha n_- = \delta j_- \,. \tag{5.3}$$

Townsendov výboj

Prvý Townsendov koeficient δ má rozmer m^{-1} a označuje počet ionizácii, ktoré vykoná jeden elektrón v smere elektrického poľa na jednotkovej dráhe (na rozdiel od ionizačnej frekvencie α udávajúcej počet ionizácií za jednotku času). Ak rovnice odčítame, dostaneme

$$\frac{\mathrm{d}(j_+ - j_-)}{\mathrm{d}x} = 0 \quad \Rightarrow j_+ - j_- = K = \text{ konšt}\,.$$

Potom hustota elektrického prúdu medzi elektródami $i = e(j_+ - j_-) = eK$ je taktiež konštantná, napriek tomu, že hustoty toku elektrónov a iónov sa menia s polohou x.

V homogénnom poli je Townsendov koeficient δ konštantný a preto môžeme rovnice kontinuity ľahko integrovať

$$j_- = C\exp(\delta x)\,; \qquad j_+ = C\exp(\delta x) + i/e\,,$$

kde C je integračná konštanta. Hodnota tejto integračnej konštanty sa dá určiť z hustoty toku elektrónov na katóde: $C = j_-(0)$. Potom

$$j_- = j_-(0)\exp(\delta x)\,; \qquad j_+ = j_-(0)\exp(\delta x) + i/e\,. \tag{5.4}$$

Problém určenia hustoty toku $j_-(0)$ spočíva v tom, že okrem primárnych elektrónov emitovaných z katódy ultrafialovým žiarením (ich hustotu toku označíme j_0), elektróny emitujú aj dopadajúce kladné ióny. Tento typ emisie sa nazýva **potenciálová emisia**.

Potenciálová emisia

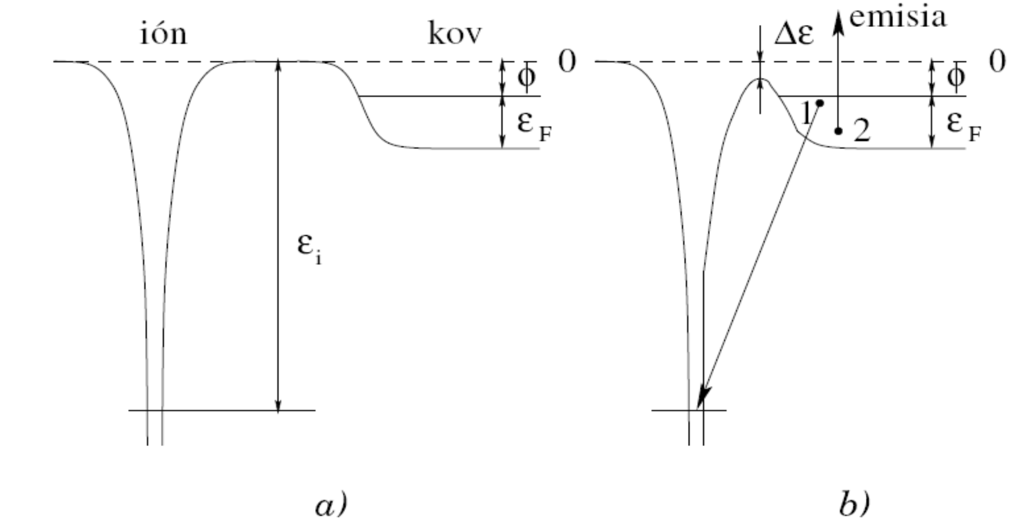

Obr. 5.3: Emisia elektrónu pri dopade kladného iónu na povrch kovu: *a*) ión je ďaleko od povrchu: ε_i - ionizačná energia atómu, Φ - výstupná práca kovu a ε_F - Fermiho energia; *b*) kladný ión pri dopade na povrch kovu: 1 - elektrón prechádza na neobsadenú hladinu v ióne, 2 - emitovaný elektrón preberá prebytočnú energiu **Augerova emisia**

plynu. Ak však vypneme ultrafialové žiarenie, hustota primárnych elektrónov i_0 klesne na nulu a potom tiež $i = 0$. Lavínová ionizácia sa teda samostatne neudrží. Preto tento typ výboja nazývame **nesamostatný výboj** alebo tiež **Townsendov výboj**. Townsendov výboj je teda predprierazovým štádiom. Pri dostatočne silných poliach sa začne

lovej emisie opúšťajú povrch elektróny s hustotou toku γj_+. Koeficient γ reprezentuje výťažok elektrónov pri emisii, ktorý sa často (nelogicky) nazýva koeficient sekundárnej emisie. V teórii zapaľovania výboja sa zvykne nazývať **druhý Townsendov koeficient** (v staršej literatúre aj tretí Townsendov koeficient). Obvykle nadobúda hodnoty 0,1 – 10^{-3} (pre ióny veľkých organických molekúl až 10^{-10}).

Electric discharges

Teraz sa vrátime k rovniciam (5.4). Hustotu toku $j_-(0)$ možno totiž napísať ako súčet toku primárnych elektrónov a elektrónov od potenciálovej emisie

$$j_-(0) = j_0 - \gamma j_+(0)\,.$$

Záporné znamienko pred hustotou toku kladných iónov súvisí s orientáciou súradníc, pretože $j_-(x) \geq 0$, $j_0 > 0$ a $j_+(x) \leq 0$. Z (5.4) vyplýva $j_+(0) = j_-(0) + i/e$, čo umožní napísať výslednú hustotu toku elektrónov na katóde

$$j_-(0) = \frac{j_0 - \gamma i/e}{1+\gamma}\,.$$

Týmto vzťahom už máme určený súvis medzi hustotami toku nabitých častíc a hodnotami j_0 a hustotou prúdu i. Pripomeňme, že z orientácie osi x vyplýva $i \leq 0$. Kladné ióny – na rozdiel od elektrónov – sa pohybujú smerom ku katóde. Smerom k anóde ich hustota toku by mala klesať. Vzhľadom na to, že anóda neemituje kladné ióny zo svojho povrchu, hustota toku kladných iónov na anóde je nulová: $j_+(d) = 0$. Potom postupne dostaneme nasledujúce vzťahy

$$j_+(d) = j_-(0)\exp(\delta d) + \frac{i}{e} = \frac{j_0 - \gamma i/e}{1+\gamma}\exp(\delta d) + \frac{i}{e} = 0\,.$$

Z posledného vzťahu možno vypočítať hustotu elektrického prúdu

$$i = \frac{i_0 \exp(\delta d)}{1 - \gamma[\exp(\delta d) - 1]}\,, \qquad (5.5)$$

Electric discharges

$$i = \frac{i_0 \exp(\delta d)}{1 - \gamma[\exp(\delta d) - 1]}\,, \tag{5.5}$$

V slabom elektrickom poli elektróny nezískavajú dostatočnú energiu na ionizáciu, preto $\delta = 0$. Vtedy $i = i_0$ – prúd medzi elektródami prenášajú len primárne elektróny od ultrafialového žiarenia. Ak elektrické pole zosilňujeme, zväčšuje sa aj prvý Townsendov koeficient δ a prúd i začne rýchlo narastať. Tento nárast súvisí s lavínovou ionizáciou plynu. Ak však vypneme ultrafialové žiarenie, hustota primárnych elektrónov i_0 klesne na nulu a potom tiež $i = 0$. Lavínová ionizácia sa teda samostatne neudrží. Preto tento typ výboja nazývame **nesamostatný výboj** alebo tiež **Townsendov výboj**. Townsendov výboj je teda predprierazovým štádiom. Pri dostatočne silných poliach sa začne

$$\gamma\,[\exp(\delta d) - 1] = 1\,, \tag{5.6}$$

hustota prúdu i diverguje a stáva sa nezávislá od hodnoty i_0. Preto práve túto podmienku považujeme za kritérium zapálenia výboja. Hovoríme tiež, že nesamostatný výboj prechádza na **samostatný výboj**. Vtedy totiž kladné ióny dopadajúce na katódu emitujú dostatočný počet elektrónov, ktoré nahradia primárne elektróny od ultrafialového žiarenia. Preto výboj sa už udrží aj vtedy, keď katódu prestaneme ožarovať ultrafialovým žiarením. V samostatnom výboji koncentrácia nabitých častíc prudko narastie, takže priestorový náboj sa začne uplatňovať. Preto vzťah (5.5) už za týchto podmienok neplatí. V niektorých typoch výboja existujú oblasti, kde je aj naďalej prítomná lavínová ionizácia; treba ju už ale opísať rovnicami, ktoré zohľadňujú prítomnosť priestorového náboja.

Electric discharges

Paschenov zákon

E/p

$$\gamma\,[\exp(\delta d) - 1] = 1\,, \tag{5.6}$$

Podmienka (5.6) ešte nie je priamo použiteľná na určenie zápalného napätia. Táto veličina je totiž schovaná v prvom Townsendovom koeficiente. Preto musíme sa teraz zaoberať problémom závislosti prvého Townsendovho koeficientu δ od intenzity elektrického poľa. Exaktné odvodenie je jedine možné pomocou kinetickej rovnice, k čomu treba ale poznať detailnú závislosť prierezov pre pružné zrážky a pre ionizáciu molekúl elektrónmi. Jednoduchší prístup využíva možnosť priameho merania δ od intenzity elektrického poľa s využitím rovnice (5.5). Prv než uvedieme poloempirické vzťahy, nájdeme zákony podobnosti pre prvý Townsendov koeficient.

Ak vyjadríme frekvenciu ionizácie α pomocou (4.16) a driftovú rýchlosť elektrónov pomocou pohyblivosti $V_- = \mu_- E$, prvý Townsendov koeficient sa dá napísať v tvare

$$\delta = \frac{\alpha}{|V_-|} = \frac{n_g \langle \sigma_i v_- \rangle}{|\mu_- E|}\,.$$

Formálne môžeme vykonať nasledujúce úpravy

$$V_- = \mu_- E = n_g \mu_- \boxed{\frac{E}{n_g}}\,,$$

kde koeficient $n_g \mu_-$ nezávisí od koncentrácie molekúl plynu n_g

Paschen law

kde koeficient $n_g\mu_-$ nezávisí od koncentrácie molekúl plynu n_g (pozri odsek 3.4.3). Stredná hodnota $\langle\sigma_i v_-\rangle$, ktorá určuje schopnosť elektrónov ionizovať molekuly plynu, závisí od energie, ktorú elektrón nadobudne tesne pred zrážkou od elektrického poľa. Táto energia je úmerná práci $e|E|\langle\lambda_-\rangle$, ktorú vykoná elektrické pole na strednej voľnej dráhe elektrónu $\langle\lambda_-\rangle$, čo formálne môžeme zapísať (F_2 je zatial neurčená funkcia)

$$\langle\sigma_i v_-\rangle = F_2(e|E|\langle\lambda_-\rangle) = F_2\left(en_g\langle\lambda_-\rangle\frac{|E|}{n_g}\right) .$$

Výrazy $n_g\mu_-$ a $en_g\langle\lambda_-\rangle$ nezávisia od koncentrácie molekúl n_g a teda aj od tlaku plynu. Je zrejmé, že veličiny V_- a α/n_g závisia od E a n_g prostredníctvom pomeru $|E|/n_g$, takže prvý Townsendov koeficient možno napísať

$$\frac{\delta}{n_g} = \Phi\left(\frac{|E|}{n_g}\right) ,$$

kde Φ je zatial neurčená funkcia. Pomer $|E|/n_g$ je významnou veličinou vo fyzike elektrických výbojov, ktorej rozmer je Vm^2. Na praktické meranie je to však príliš veľká jednotka. Preto sa zaviedla jednotka **Townsend**

$$1\ \text{Townsend} = 1\ \text{Td} = 10^{-17}\ \text{Vcm}^2 = 10^{-21}\ \text{Vm}^2 .$$

Pomocou pomeru $|E|/p_0$ možno vyjadriť δ v tvare

$$\frac{\delta}{p_0} = F\left(\frac{|E|}{p_0}\right) , \tag{5.7}$$

Electric discharges

$$\frac{\delta}{p_0} = F\left(\frac{|E|}{p_0}\right)$$

$$\delta = \frac{\alpha}{|V_-|} = \frac{n_g\langle\sigma_i v_-\rangle}{|\mu_- E|}.$$

so zatiaľ neznámou funkciou F. Ak si označíme ako δ_z hodnotu prvého Townsendovho koeficientu, ktorý spĺňa podmienku (5.6) (platí $\delta_z d = \ln(1 + 1/\gamma)$), môžeme formálne vyjadriť intenzitu elektrického poľa $|E_z|$ potrebného na zapálenie výboja

$$\frac{|E_z|}{p_0} = F_{inv}\left(\frac{\delta_z}{p_0}\right) = F_{inv}\left[\frac{\ln\left(1+\frac{1}{\gamma}\right)}{p_0 d}\right],$$

kde F_{inv} je inverzná funkcia k funkcii F. Z hodnoty elektrického poľa potrebného na zapálenie výboja už ľahko vypočítame aj zápalné napätie

$$\boxed{U_z = d|E_z| = p_0 d F_{inv}\left[\frac{\ln\left(1+\frac{1}{\gamma}\right)}{p_0 d}\right]}. \tag{5.8}$$

Z tohoto výsledku možno formulovať uzáver vo forme zákonitosti:

Paschenov zákon – Zápalné napätie U_z je pre daný plyn funkciou súčinu redukovaného tlaku p_0 a vzdialenosti elektród d.

Electric discharges

Na aproximáciu experimentálnych hodnôt sa často používa poloempirický vzťah

$$\frac{\delta}{p_0} = A \exp\left(-\frac{Bp_0}{|E|}\right), \tag{5.9}$$

kde hodnoty konštánt možno najsť v tabuľke 5.1 pre rôzne plyny. Tiež je uvedený rozsah hodnôt $|E|/p_0$ pre ktoré je aproximácia (5.9) použiteľná. Inverznou funkciou k funkcii

$$F(x) = A \exp\left(-\frac{B}{x}\right)$$

je funkcia

$$F_{inv}(x) = \frac{B}{\ln(A/x)}.$$

Electric discharges

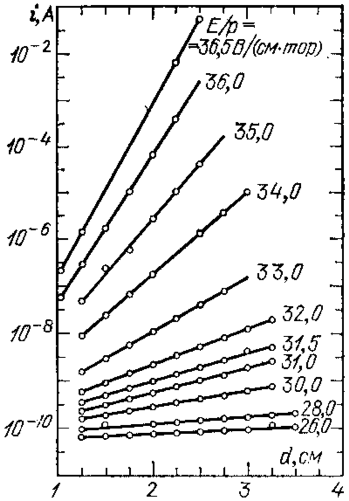

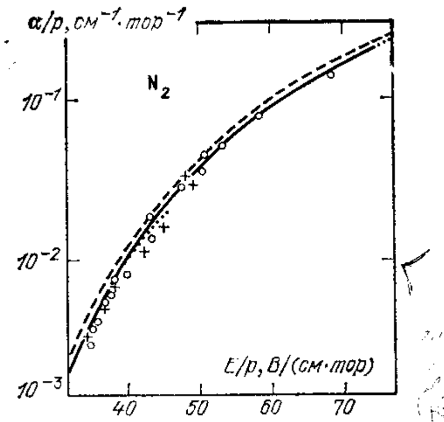

Р и с. 5.3. Экспериментальный график, демонстрирующий постоянство α и экспоненциальный характер нарастания тока в разрядном промежутке; ионизационные коэффициенты определяются наклонами прямых [6]

Р и с. 5.4. Ионизационный коэффициент Таунсенда α в N_2 по разным измерениям

ниям

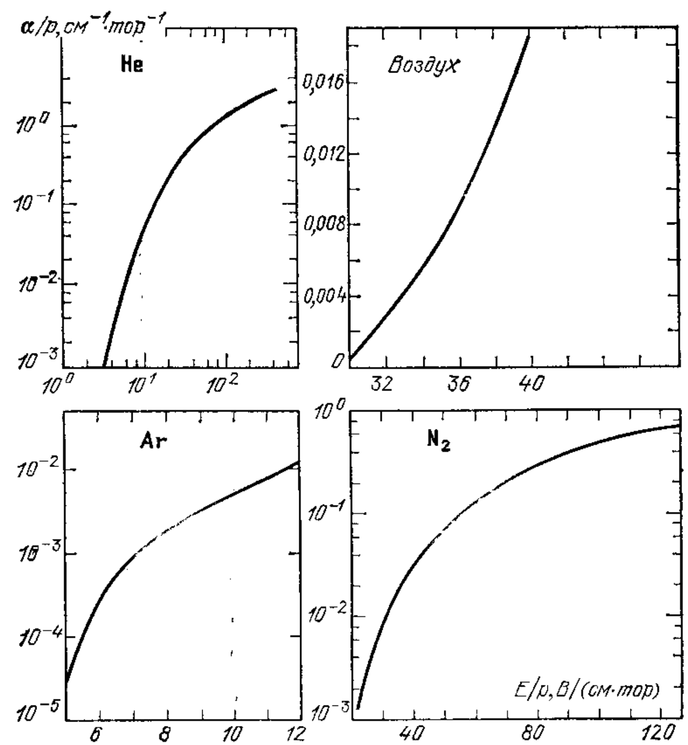

Р и с. 5.5. Ионизационный коэффициент в He, воздухе, Ar, N_2 [26]

Data for Paschen law

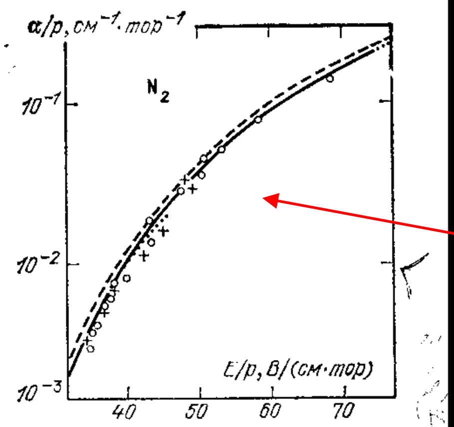

…, демонстрирующий постоянство α и экс-
…тока в разрядном промежутке; ионизацион-
…еляются наклонами прямых [6]

…ент Таунсенда α в N_2 по разным измере-
…ниям

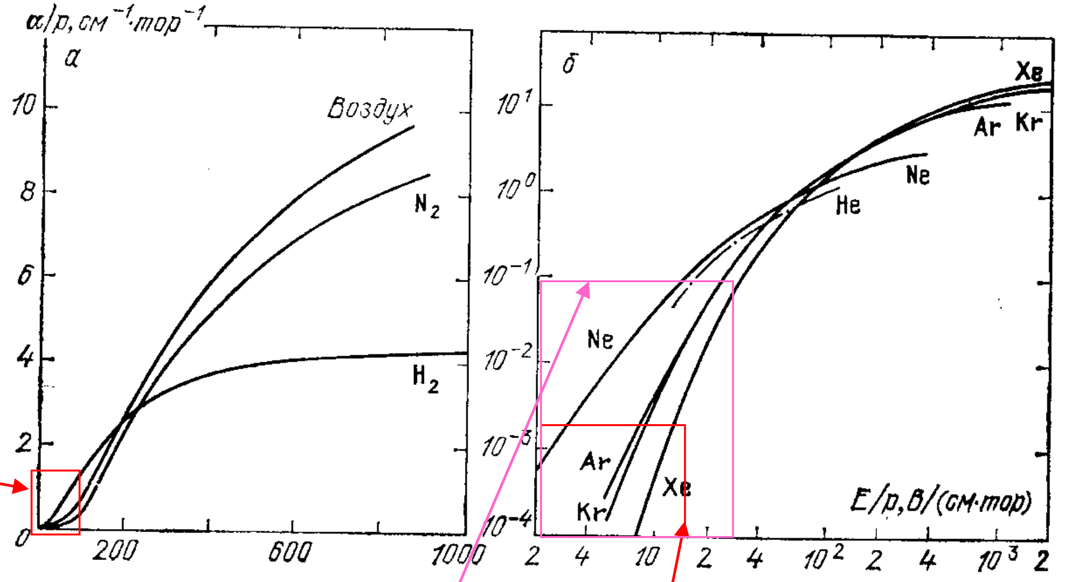

Р и с. 5.6. Ионизационный коэффициент в широком диапазоне E/p: *а* — в H_2, N_2 и в воздухе, *б* — в инертных газах [6]

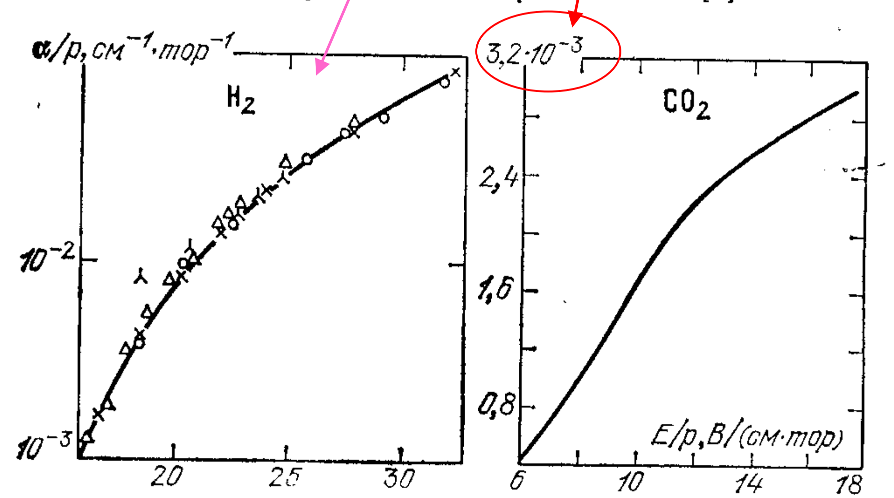

Р и с. 5.7. Ионизационный коэффициент в H_2 [26] и CO_2 [6]

Paschen law – data gama

$$i = \frac{i_0 \exp(\delta d)}{1 - \gamma[\exp(\delta d) - 1]}, \qquad (5.5)$$

V důsledku emise opouští povrch katody elektrony s hustotou toku γj_+

$E/p \sim 30$—40 В/(см·тор), характерных для пробоя плотных газов, в

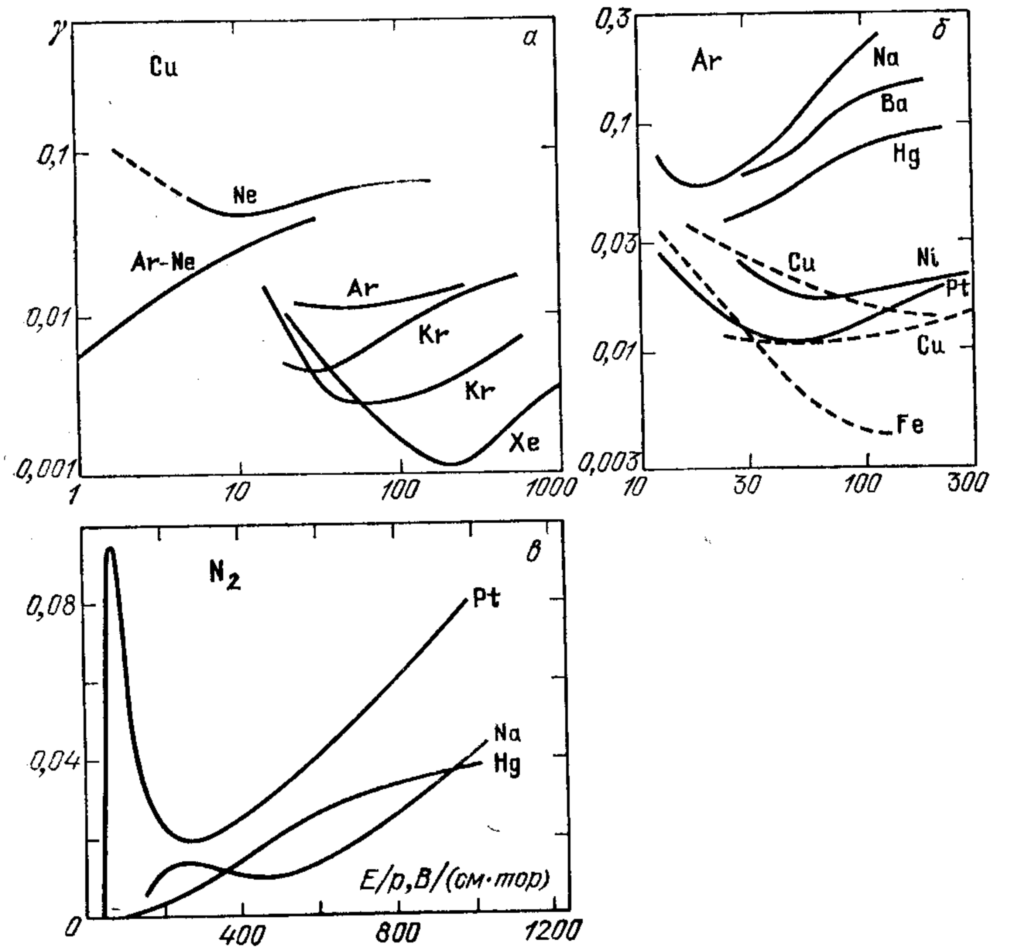

Р и с. 6.13. Коэффициент ионно-электронной эмиссии, определенный из разрядного эксперимента (п. 4.1): *а* — медный катод в инертных газах; *б* — различные металлы в Ar; *в* — различные металлы в N_2 [6]

Electric discharges

Na aproximáciu experimentálnych hodnôt sa často používa poloempirický vzťah

$$\frac{\delta}{p_0} = A \exp\left(-\frac{B p_0}{|E|}\right), \tag{5.9}$$

kde hodnoty konštánt možno najsť v tabuľke 5.1 pre rôzne plyny. Tiež je uvedený rozsah hodnôt $|E|/p_0$ pre ktoré je aproximácia (5.9) použiteľná. Inverznou funkciou k funkcii

$$F(x) = A \exp\left(-\frac{B}{x}\right)$$

je funkcia

$$F_{inv}(x) = \frac{B}{\ln(A/x)}\,.$$

Electric discharges

Tabu*l*ka 5.1: Koeficienty A a B pre poloempirický vzťah (5.9) podľa [19]. Posledný stĺpec označuje rozsah hodnôt $|E|/p_0$, v ktorom možno aproximáciu použiť

Plyn	A $[\mathrm{cm}^{-1}\mathrm{Torr}^{-1}]$	B $[\mathrm{Vcm}^{-1}\mathrm{Torr}^{-1}]$	oblasť $|E|/p_0$ $[\mathrm{Vcm}^{-1}\mathrm{Torr}^{-1}]$
He	3	34	20 – 150
Ne	4	100	100 – 400
Ar	14	180	100 – 600
Kr	17	240	100 – 1000
Xe	26	350	200 – 800
vzduch	15	365	100 – 800
H_2	5	130	150 – 600
N_2	12	342	100 – 600
CO_2	20	466	500 – 1000
H_2O	13	290	150 – 1000
Hg	20	370	200 – 600

Použitím tejto funkcie vo vzťahu (5.8) dostaneme

$$U_z = \frac{Bp_0d}{\ln(Ap_0d) - \ln[\ln(1 + 1/\gamma)]} \tag{5.10}$$

Electric discharges

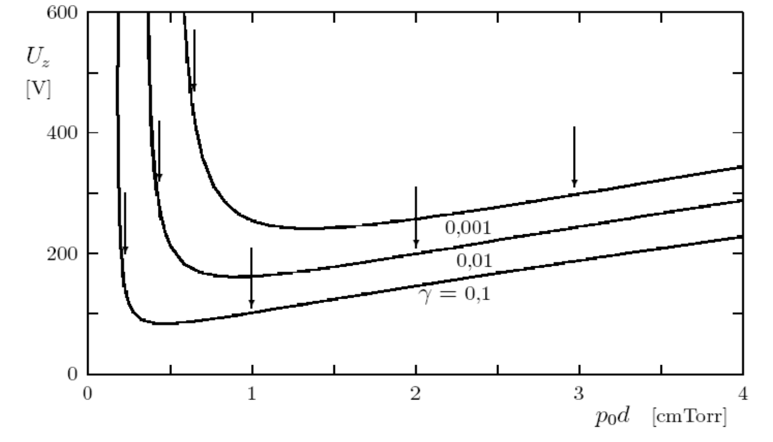

Obr. 5.5: Zápalné napätie U_z výboja v argóne ako funkcia súčinu $p_0 d$ pre rôzne hodnoty druhého Townsendovho koeficientu γ. Medzi zvislými šípkami sa nachádza oblasť hodnôt E/p_0 z tab. 5.1, v ktorej platí vzťah (5.9)

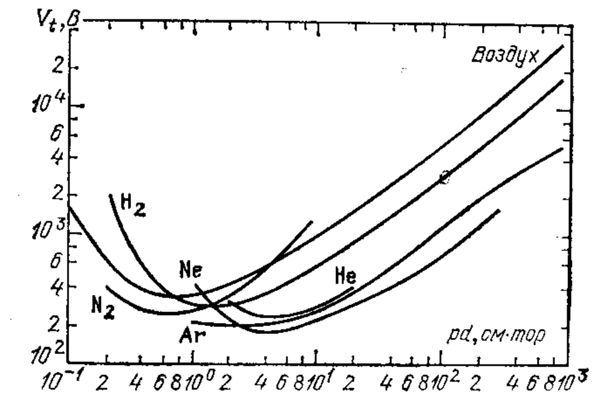

Р и с. 13.2. Потенциал зажигания в различных газах в широком диапазоне *pd* (кривые Пашена)

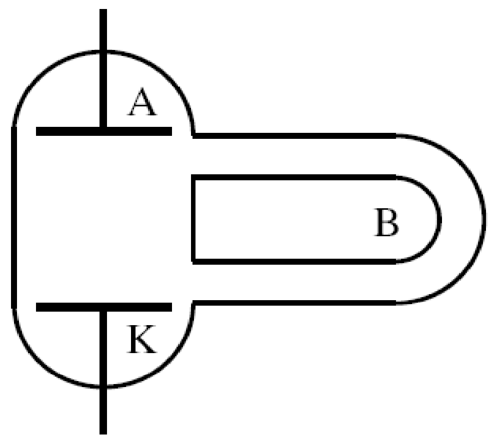

Obr. 5.6: Výbojka s bočnou dráhou B na demonštráciu nestability nízkotlakovej vetvy Paschenovej krivky

Paschen law curves

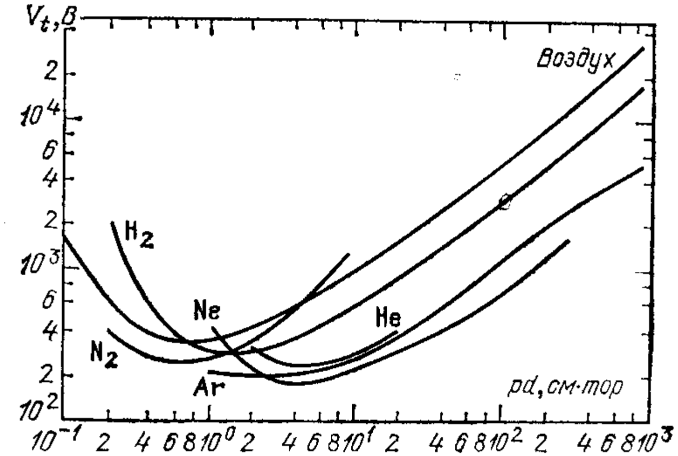

Р и с. 13.2. Потенциал зажигания в различных газах в широком диапазоне pd (кривые Пашена)

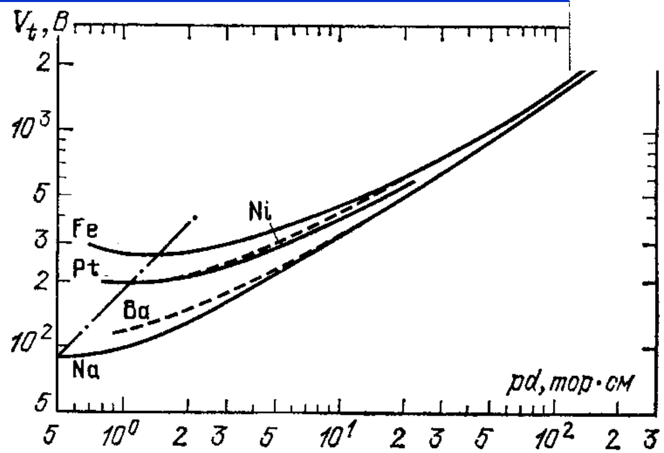

Р и с. 13.3. Влияние материала катода на напряжение пробоя аргона. Штрих-пунктирная прямая соединяет точки минимума. Ее наклон 45° соответствует независимости $(E/p)_{\min}$ от материала катода [6]

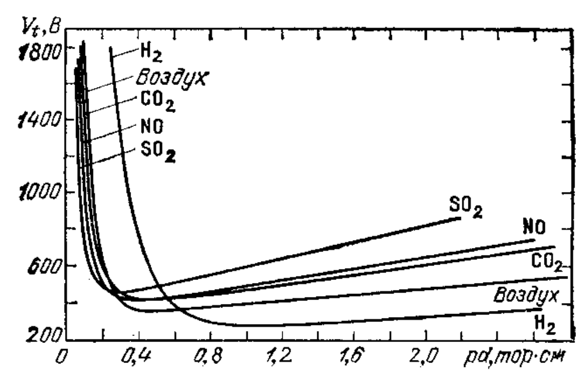

Р и с. 13.4. Кривые Пашена в укрупненном масштабе [6]

Electric discharges – electron attachment versus ionization

$$dN_e/dx = (\alpha - a) N_e, \quad N_e \sim \exp[(\alpha - a) x],$$

указывают, что $\alpha_{эф} \to 0$ при $(E/p)_1 \approx 35$ В/(см·тор), что как раз соответствует $(E/p)_{пред} \approx 26$ кВ/(см·атм). При $E/p < (E/p)_1$ размножение

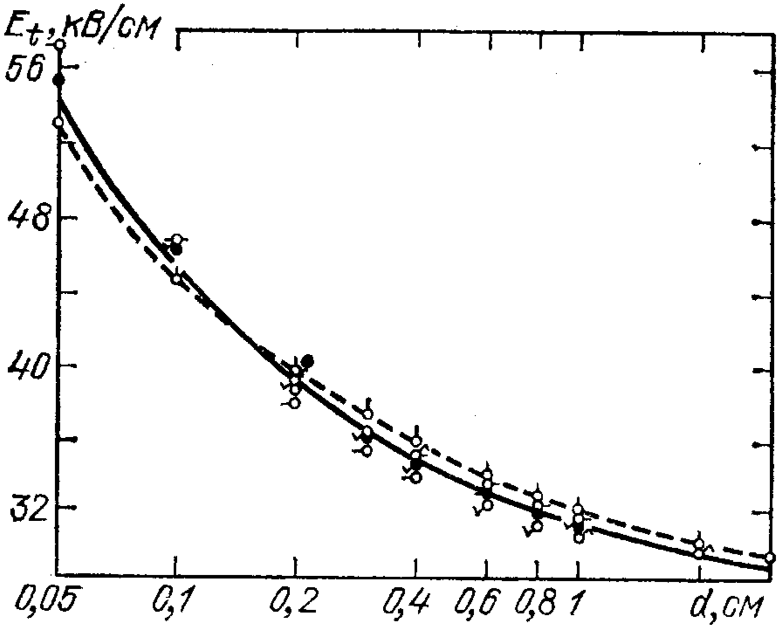

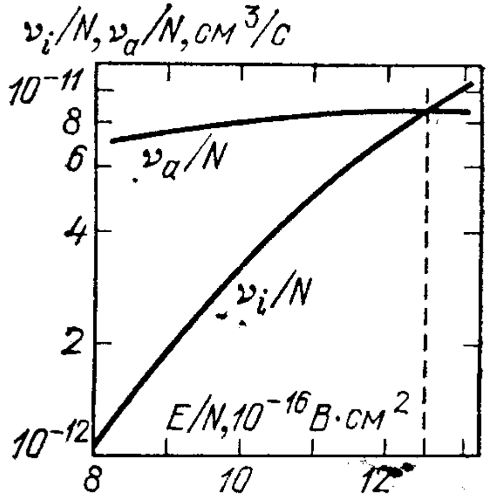

Рис. 13.5. Пробивающие поля в плоском воздушном промежутке длины d при $p=1$ атм по данным разных авторов [21]

Рис. 13.6. Частоты ионизации и прилипания в воздухе, рассчитанные на основе решения кинетического уравнения. Пересечение при $E/p=41$ В/(см·тор) [10]

Paschen low curves

Таблица 13.1. Ориентировочные пороги пробоя газов при высоких давлениях

Газ	Постоянное поле, недлинные промежутки, $p \sim 1$ атм		СВЧ, $p \sim 100$—300 тор
	E_t/p, кВ/(см·атм)	E_t/p, В/(см·тор)	E_t/p, В/(см·тор)
He	10	13	3
Ne	1,4	1,9	3—5
Ar	2,7	3,6	5—10
H_2	20	26	10—15
N_2	35	46	$\sim$25
O_2	30	40	35
Воздух	32	42	$\sim$30
Cl_2	76	100	
CCl_2F_2 *)	76	100	
CSF_8	150	200	
CCl_4	180	230	
SF_6 **)	89	117	

*) Фреон
**) Элегаз

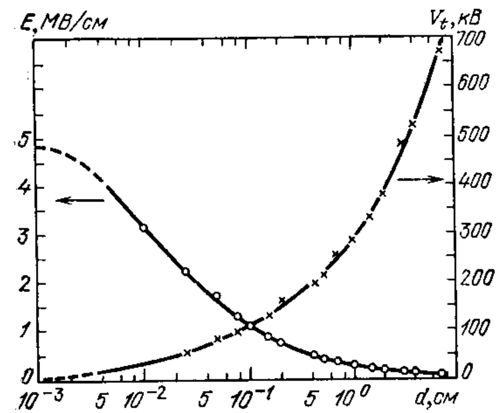

Рис. 13.7. Напряжение и поле пробоя вакуумного промежутка между шаром диаметром 2,5 см и диском диаметром 5 см из стали в зависимости от длины промежутка [3]

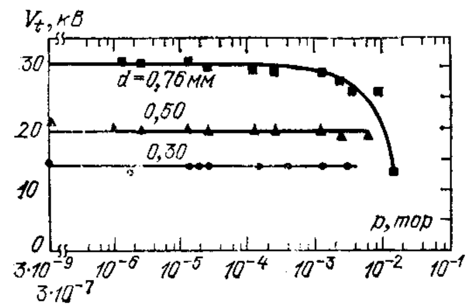

Рис. 13.8. Напряжения пробоя коротких промежутков d между стальными электродами в зависимости от давления заполняющего их водорода. Независимость от p свидетельствует о вакуумном характере пробоя. Загиб вниз верхней кривой соответствует переходу к левой ветви кривой Пашена [15.3]

RF discharges

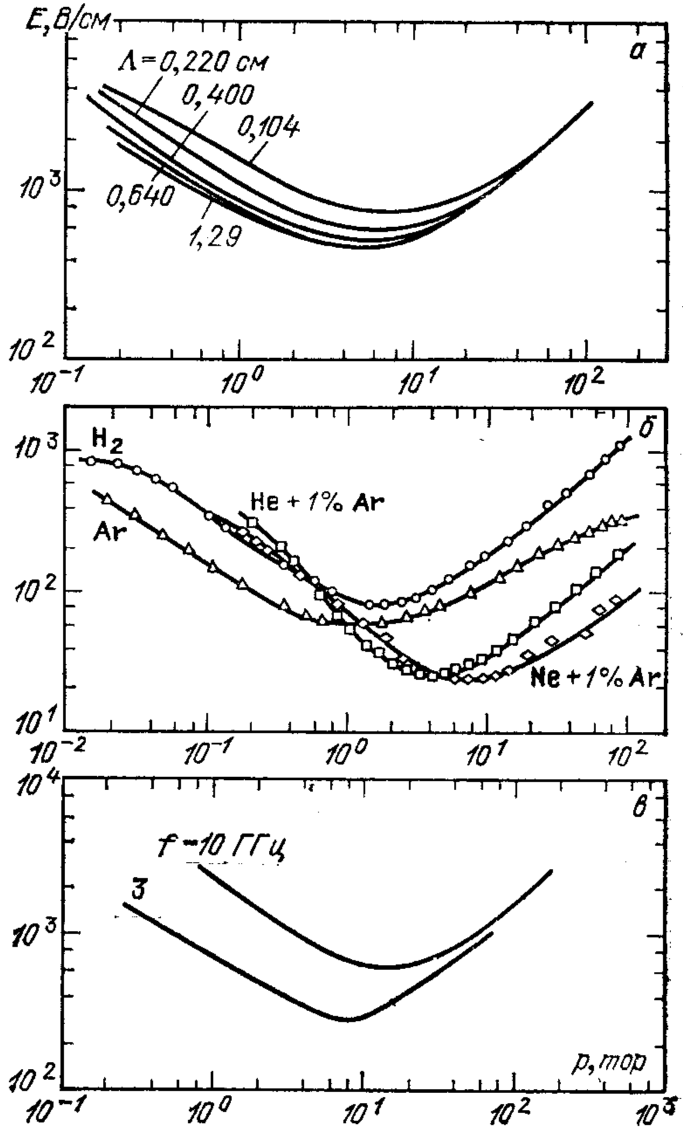

Р и с. 13.10. Измеренные пороги СВЧ пробоя: *а* — воздух, частота $f=9{,}4$ ГГц, около кривых указаны диффузионные длины Λ; *б* — несколько газов, $f=0{,}99$ ГГц, $\Lambda=0{,}63$ см; *в* — Heg-газ (гелий с добавкой паров ртути), $\Lambda=0{,}6$ см [24]

Electric discharges

Table 4.3. Cross sections of photoionization of atoms and molecules from the ground state close to the threshold

Gas	$\hbar\omega = I$, eV	λ, Å	σ_ν, 10^{-18} cm^2
H	13.6	912	6.3
He	24.6	504	7.4
Ne	21.6	575	4.0
Ar	15.8	787	35
Na	5.14	2412	0.12
K	4.34	2860	0.012
Cs	3.89	3185	0.22
N	14.6	852	9
O	13.6	910	2.6
O_2	12.2	1020	~ 1
N_2	15.58	798	26
H_2	15.4	805	7

Electric discharges

7.3.2 Ionization Kinetics Equation

When oscillation displacements are small, electron densities obey an equation of type (2.44):

$$\partial n_{\mathrm{e}}/\partial t = D\nabla^2 n_{\mathrm{e}} + (\nu_{\mathrm{i}} - \nu_{\mathrm{a}})n_{\mathrm{e}} \,, \quad D \equiv D_{\mathrm{e}} \tag{7.6}$$

(electrons diffuse freely in breakdown). If the condition $\omega \gg \nu_{\mathrm{m}}\delta$ (Sect. 5.5.2) holds (it is satisfied for microwave frequencies), the electron energy distribution is quasisteady and the ionization and attachment frequencies, ν_{i} and ν_{a}, are determined by the root-mean-square field E. The dependencies $\nu_{\mathrm{i}}(E)$, $\nu_{\mathrm{a}}(E)$ are much stronger than $D_{\mathrm{e}}(E)$, so that $D_{\mathrm{e}}(E) \approx$ const. For simplification, assume that the field is spatially homogeneous, and hence, ν_{i} and ν_{a} are independent of coordinates. Averaging (7.6) over the volume, we obtain, in accord with the results of Sect. 4.5, an equation for the mean density, or (which is equivalent) for the total number of electrons, N_{e}, in the discharge volume:

$$dN_{\mathrm{e}}/dt = (\nu_{\mathrm{i}} - \nu_{\mathrm{a}} - \nu_{\mathrm{d}})N_{\mathrm{e}} \,, \quad \nu_{\mathrm{d}} = D/\Lambda^2 \,, \tag{7.7}$$

where ν_{d} is the frequency of diffusion losses of electrons. This equation describes the ionization kinetics of the gas.

Calculation of avalanche…

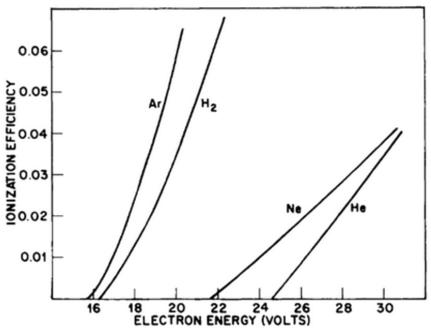

Fig. 4. Efficiency of ionization in hydrogen, argon, neon, and helium.

where P is a net production or loss rate. Generally this will be written $n\nu_i$ where ν_i is the net ionization rate per electron. Combining the above equations, we obtain

$$(\partial n/\partial t) = \nabla^2(Dn) + n\nu_i. \tag{2}$$

This equation has many solutions depending on the initial and boundary conditions, but one of the most useful can be written

$$n = n_0 \exp[(\nu_i - D/\Lambda^2)t], \tag{3}$$

where Λ is the characteristic diffusion length which is determined by the boundary conditions. For a right circular cylinder of length L and radius R, for example, it is given by

$$1/\Lambda^2 = (\pi/L)^2 + (2.405/R)^2.$$

(d) *Attachment* When an electron becomes attached to an ion in a microwave discharge, the net effect is the same as though it were lost from the region in which the field acts. This is so because the negative ion which replaces the electron is at least two thousand times as heavy and so will be accelerated so little during a cycle of the field that energy transfer to it will be negligible. The attachment rate is significant in oxygen and in air and so is of much importance in breakdown phenomena in the atmosphere. There has been considerable work done on attachment in oxygen and much less on attachment rates in air. (Burch and Geballe, 1957; Schulz, 1962; Craggs *et al.*, 1957; Buchel'nikova, 1959; Bradbury, 1933; Harrison and Geballe, 1953.)

valid. The definition of the characteristic diffusion length for the right circular cylinder given earlier,

$$\frac{1}{\Lambda^2} = \left(\frac{\pi}{L}\right)^2 + \left(\frac{2.405}{R}\right)^2,$$

gives an indication of the dimensions for which the nonuniformity of the field is important. If the second term is large enough so that it significantly

4. Magnetic Fields

The introduction of a dc magnetic field changes the motion of the electrons because the acceleration term changes from $(e/m)\mathbf{E}$ to $(e/m)(\mathbf{E} + \mathbf{v} \times \mathbf{B})$, where $\mathbf{B}$ is the magnetic induction. The electrons move in spiral fashion changing the mode of diffusion differently in different directions so that diffusion is no longer isotropic. When the modified force term is put into Eqs. (4)–(8) the analysis is very complicated and leads to a modified expression for the effective electric field:

$$E_{eb}^2 = \frac{E^2 \nu_m{}^2}{2}\left[\frac{1}{\nu_m{}^2 + (\omega - \omega_b)^2} + \frac{1}{\nu_m{}^2 + (\omega + \omega_b)^2}\right], \tag{23}$$

where ω_b is equal to eB/m. Assuming that the collision frequency ν_m is independent of energy, the effect of the magnetic field on energy transfer is taken account of by replacing E_e by E_{eb} in all equations. Because the electron paths are changed by the magnetic forces, the diffusion rates are also changed. The analysis, which in general leads to a second-order tensor diffusion coefficient, will not be reproduced here. For the simple case of a magnetic field applied along the axis of a right circular cylinder, the characteristic diffusion length Λ can be replaced by Λ_b, where

$$\frac{1}{\Lambda_b{}^2} = \frac{1}{\Lambda_r{}^2}\left(\frac{\nu_m{}^2}{\nu_m{}^2 + \omega_b{}^2}\right) + \frac{1}{\Lambda_z{}^2}, \tag{24}$$

where Λ_r and Λ_z are, respectively, $R/2.405$ and L/π. Thus the diffusion in directions perpendicular to the magnetic field is reduced by an amount equivalent to increasing the dimension by a factor

$$\left(\frac{1 + \omega_b{}^2}{\nu_m{}^2}\right)^{1/2}$$

Lax *et al.* (1950) made measurements in Heg gas in S-band microwave fields and with the magnetic fields applied both transverse and parallel to the electric field. Figure 6 shows both experimental data and the theoretical prediction based on the breakdown as in Eq. (18) with the effective field and diffusion length modified as in Eqs. (23) and (24). The cyclotron resonance, the reduced breakdown field caused by the magnetic field, and the excellent agreement between theory and experiment are evident from the figure.